NASA TECHNICAL MEMORANDUM

NASA TM X- 68009

NASA-TM-X-68009

ENGINE SELECTION FOR TRANSPORT AND COMBAT AIRCRAFT

by James F. Dugan, Jr.
Lewis Research Center
Cleveland, Ohio

TECHNICAL PAPER proposed for presentation at Conference on Aircraft Performance - Prediction Methods and Optimization sponsored by Advisory Group on Aeronautical Research and Development Brussels, Belgium, April 24-28, 1972

ENGINE SELECTION FOR TRANSPORT AND COMBAT AIRCRAFT

by James F. Dugan, Jr.

National Aeronautics and Space Administration
Lewis Research Center
Cleveland, Ohio

E-6783

INTRODUCTION

The purpose of this paper is to illustrate the procedures that are used to select engines for transport and combat aircraft. In general, the problem is to select the engine parameters including engine size in such a way that all constraints are satisfied and airplane performance is maximized. This is done for four different classes of aircraft: a long haul conventional takeoff and landing (CTOL) transport, a short haul vertical takeoff and landing (VTOL) transport, a long range supersonic transport (SST), and a fighter aircraft. For the commercial airplanes the critical constraints have to do with noise while for the fighter, maneuverability requirements define the engine. Generally, the resultant airplane performance (range or payload) is far less than that achievable without these constraints and would suffer more if nonoptimum engines were selected.

NEXT GENERATION CTOL TRANSPORT

The next generation of CTOL transport is likely to use the supercritical wing proposed by Whitcomb (ref. 1). It offers the potential for delaying the transonic drag rise experienced by present-day jet transports as Mach 1 is approached. The supercritical wing can be exploited in several ways. A new airplane with this wing could cruise at higher speeds than current airplanes with little or no penalty in lift-drag ratio (L/D). (Symbols are listed in appendix A.) Alternatively, at lower speed (e.g., around Mach 0.9) the supercritical wing will permit less sweepback, more thickness, and higher aspect ratio. Used in this way, the supercritical wing would result in higher cruise L/D or less wing weight for the same L/D. In this part of the paper where design cruise speed was varied from a maximum of Mach 0.98 down to Mach 0.90, wing weight fraction remained constant but L/D increased as design speed was reduced. At Mach 0.98 the L/D was near that of the Boeing 747 cruising at Mach 0.86. At Mach 0.90, the L/D is postulated to be slightly above that obtained with the Boeing 707-320B designed to cruise at Mach 0.80. The material is taken from references 2, 3, and 4.

A sketch of a conceptual advanced tri-jet transport is shown in figure 1. It uses the supercritical wing and has three acoustically treated turbofan engines (fig. 2). The objective of the study was to identify the engine parameters which maximized airplane performance while satisfying desired engine noise goals during takeoff and approach.

Total perceived noise has two components: jet noise from the two jet streams and fan turbomachinery noise. Jet noise, measured in PNdB, was calculated by standard methods described by the Society of Automotive Engineers in references 5 and 6. Jet noise is primarily a function of the exit velocities of the two flow streams, but is also affected by the gas flow rates and the flow areas. These variables were calculated at both Mach 0.23 (152 knots) after lift-off at full thrust and with thrust cut back to the level required during the 3^{o} approach at Mach 0.203 (135 knots).

Fan turbomachinery noise, also measured in PNdB, is a function of spacing between rotor and stator, number of rotor and stator blades, rotor tip speed, number of stages, fan pressure ratio, thrust, and amount of nacelle acoustic treatment. It was assumed that the engines would be built in such a way as to minimize noise generation. Curves presented in reference 7 relate machinery perceived noise level to fan pressure ratio at a fixed thrust and distance for both one- and two-stage fans. These curves were scaled from a total airplane net thrust of 400 000 newtons (90 000 lb) and a measuring-point distance of 305 meters (1000 ft) to both the sideline and approach conditions of this study. In addition to logarithmic thrust and distance-squared scaling, extra air absorption due to a change in slant range (ref. 5) was included. The curves which result for the sideline condition are shown in figure 3 for a total airplane net thrust of 508 000 newtons (114 000 lb). The curves which result for the approach condition are also shown in figure 3 for a total airplane net thrust of 160 000 newtons (36 000 lb). These thrust levels are typical for airplanes having a takeoff gross weight of 175 000 kilograms (386 000 lb), as was the case in the first part of the study where range was used as the figure of merit. At a given fan pressure ratio, the two-stage noise is about 8 dB higher than the one-stage noise. More recent investigations indicate the difference to be about 6 decibels and the matter is still under investigation.

In order to determine the total perceived noise from both the jets and the fan turbomachinery, the jet and machinery sound pressure levels (SPL) in each octave were added antilogarithmically. (This procedure is described in ref. 5 for the addition of core and fan jet noise.)

Noise calculations were made for two measuring points, both of which are specified in Federal Air Regulation Part 36. They were:

(1) Sideline noise measured on the ground at the angle of maximum noise immediately after lift-off on a 463-meter (1520-ft) sideline for three-engine airplanes (650-m sideline for four-engine airplanes)

(2) Approach noise, when the airplane is 1850 meters (1 n. mi.) from the runway threshold, measured on the ground directly under the glide path at the angle of maximum noise.

The airplanes of this study were assumed to be at an altitude of 113 meters

(370 ft) at this measuring station.

For airplanes with TOGW's of interest, FAR Part 36 specifies a noise limit of 106 EPNdB for both of the above measurements. A third measurement specified by this regulation should be made at a point 6.48×10^3 meters (3.5 n. mi.) from the start of takeoff roll on the extended runway centerline. If the airplane altitude at this measuring point exceeds 305 meters (1000 ft), the thrust may be reduced to that required for a 4 percent climb gradient or to maintain level flight with one engine out, whichever thrust is greater. The noise limit at this measuring station for the TOGW's considered here is 102 to 104 EPNdB. This noise measurement was ignored in this study because insufficient low-speed aerodynamic data were available to investigate the tradeoffs involved in minimizing noise at this point. The tradeoffs involved are between constant Mach number climb to maximum altitude and maximum acceleration to 305 meters (1000 ft) before thrust is reduced. For the three-engine airplanes which meet a sideline noise goal, it is felt that little difficulty will be involved in meeting the 6.48×10^3 meters (3.5 n. mi.) "takeoff" goal since the sideline noise is measured at 463 meters (1520 ft). With four-engine airplanes, the 6.48×10^3 meters (3.5 n. mi.) goal might be more difficult to meet, however, because the sideline measurement is specified at 650 meters (2126 ft) and is therefore easier to meet. The 6.48×10^3 meters (3.5 n. mi.) measurement might thus be more of a constraint for four-engine airplanes.

The noise calculations made in this study are in units of PNdB. The FAR Part 36 requirements, however, are stated in terms of EPNdB. The EPNdB scale (where E stands for effective) is a modification of the PNdB scale where a correction is made to account for subjective response to the maximum pure tone and duration of the noise heard by the observer. These modifications to the PNdB scale were not made in this study since the amount of information known about the maximum tones and directivity of the noise from the parametric engines is limited. It is thought that the error introduced by ignoring these modifications is less than the error that might occur by making further assumptions about the noise sources.

In any study of future airplanes, it is well to consider noise levels lower than those specified in FAR 36 since it is quite likely that in future years the required noise levels will be lower. Already it has been suggested that noise levels should be lowered 10 decibels every 10 years until the background noise level is reached. In this study noise levels as much as 20 decibels below the FAR Part 36 levels are considered.

Engine Cruise Performance

In any engine-airplane study it is necessary to generate engine performance over the range of important flight conditions (especially cruise, takeoff, and landing) for a family of engines whose design parameters (turbine temperature (T_4), overall pressure ratio (OPR), fan pressure ratio (FPR), and bypass ratio (BPR)) have been systematically varied.

Depending on the purpose of the study, an appropriate degree of sophistication is used to estimate engine performance (thrust, specific fuel consumption (SFC), weight, size). Of course, this presumes that we are starting from scratch with an unrestricted choice of paper engines. The approach would be different if we were limited to existing engines.

For the airplane being considered, typical cruise conditions are Mach 0.98 and 12 200 meters (40 000 ft).

A plot of cruise performance is shown in figure 4 for an FPR of 1.50 and a cruise T_4 of 1370 K (2460° R). Although not shown, similar plots were made for other values of FPR and T_4. Figure 4 shows that SFC can be reduced by increasing BPR with OPR fixed or by increasing OPR with BPR fixed. Unfortunately, both changes reduce cruise specific thrust which means that if cruise sizes the engine, engine airflow must be increased to overcome the cruise drag. Higher airflow increases the engine diameter which in turn increases both drag and weight. In addition, increasing the OPR by itself tends to increase engine weight since more compressor stages are required.

Using the BPR = 4, OPR = 24 point of figure 4 as a reference, the effects of changes in cruise T_4, OPR, BPR, and FPR are shown in figure 5. Increasing cruise T_4 causes an increase in both SFC and specific thrust, a mixed blessing. Increasing OPR up to about 36 causes a small decrease in SFC and only a slight reduction in specific thrust. A higher BPR decreases the SFC at a considerable drop in specific thrust. Increasing FPR, however, has a favorable effect on both SFC and specific thrust and is one of the keys to better engine performance. Since the other engine parameters improve one performance parameter at the expense of the other, an overall measure of airplane performance such as range must be examined in order to find those engine design parameters yielding an optimum balance between SFC and engine weight.

Engine Selection

In order to calculate airplane range, it is necessary to know something about the airplane and more about each engine to be considered. Starting with the cruise performance of a particular engine defined by its cruise values of T_4, OPR, FPR, BPR, and component efficiencies, component maps are selected which are expected to characterize the engine. Using procedures such as those presented in reference 8, engine performance at takeoff and approach is calculated. An explanation of this procedure is presented in appendix B. There are many ways of computing engine weight. One convenient way (which was utilized in refs. 2 to 4) is described in reference 9 (see appendix C). The additional weight for installation (including inlet nacelle and nozzle) was assumed to be 3.13 times the total airflow at takeoff and was based on empirical data for existing high-bypass-ratio engines used in large commercial transport.

Considering now the airplane, the weight breakdown for an airplane

with particular engines is shown below. Those items which remained fixed when other engines were installed are noted as "(fixed)."

Weight Statement

	kg	lb
Airframe weight, (fixed)	81 700	180 000
Engine weight	18 100	40 000
Payload, (fixed)	27 200	60 000
Climb fuel, (fixed)	9 070	20 000
Cruise fuel	29 400	64 920
Descent fuel, (fixed)	907	2 000
Reserve fuel, (0.18 total fuel)	8 650	19 080
Takeoff gross weight, (fixed)	175 027	386 000

In this study the only other information on the airplane that was needed was its cruise L/D which was 16.8 when engine diameter was 2.03 meters (80 in.). (It rose to 17.5 for 1.52 m (60 in.) engines and dropped to 15.75 for 2.79 m (110 in.) engines.) The cruise L/D of course is needed to calculate cruise range

$$R = V \frac{L/D}{SFC} \ln \left(\frac{\text{Weight at start of cruise}}{\text{Weight at end of cruise}} \right)$$

Because of the fixed weights indicated above cruise range is calculated from:

$$R_{cr} = 561 \frac{L/D}{SFC} \ln \frac{366\ 000}{268\ 000 + 0.82\ W_{eng}}$$

The total range was assumed to be 648×10^3 meters (350 n. mi.) greater than the cruise range (370×10^3 m climb and 278×10^3 m letdown). Thus each engine defined by its cruise parameters leads to a specific value of airplane range.

Having selected design values for FPR and T_4 cruise, a "thumbprint" plot similar to the sketch of figure 6(a) can be made for a spectrum of design values of BPR and OPR with contours of constant range. A thrust limiting line is shown below which takeoff performance will be unsatisfactory. Broken lines of constant sideline jet noise are also shown, with the lowest lines representing the highest noise levels. (Total noise is not shown as it depends on the amount of noise suppression which is defined in a later step.) Engines A, B, C, and D (selected because they produce maximum range at the selected levels of sideline jet noise) are singled out for further analysis.

In figure 6(b), approach noise is plotted against sideline noise for lines of constant suppression and BPR. A noise goal represented by point X is postulated such that approach and sideline noise are equal.

By interpolation, the noise goal can be achieved with about 16 PNdB of turbomachinery noise suppression. The range can now be found from figure 6(c) where the ranges from figure 6(a) have been reduced due to suppression (more suppression results in heavier engines and less fuel). In this manner then, the engine which maximizes range and the required suppression can be found for any desired noise goal.

Low Noise Engines for a Mach 0.98 Transport

Using the procedure discussed in the previous section, engines were identified which maximized airplane range when various noise constraints were imposed. Figure 7 shows the results for engines without a jet noise suppressor and with a cruise T_4 of 1150° C (2100° F). With no noise constraint, range maximizes for an FPR of 3.0. For the Federal Air Regulation Part 36 requirement of 106 PNdB, FPR must be 2.9 or less. At 96 PNdB, allowable FPR is about 2.1 and falls to 1.7 for 86 PNdB.

Similar results are shown in figure 8 for engines having a 10 PNdB jet noise suppressor. The attainable range for a given noise level is higher because a higher FPR can be used.

The range/noise tradeoff for engines having a cruise T_4 of 1150° C (2100° F) is shown in figure 9 with specific engine characteristics shown in figure 10. Curve A is for engines having a maximum of 15 PNdB machinery noise suppression and no jet noise suppressor. Curve B is for engines without jet noise suppressors but with up to 40 PNdB of machinery noise suppression. Curve C has up to 40 PNdB of machinery noise suppression and a weightless jet noise suppressor which reduces jet noise by 10 PNdB.

The most significant comparisons to be made from figure 9 are summarized in figure 10. From figures 9 and 10 it can be seen that a range penalty of 926×10^3 meters (500 n. mi.) is entailed in meeting a noise goal of 106 PNdB using curve A which represents current technology. The major reason for this is that FPR had to be reduced from 3.0 to 1.7. If curve B applies, then allowable FPR is 2.9 and the range penalty is only 139×10^3 meters (75 n. mi.). At lower noise goals, allowable FPR drops and the range penalty becomes large. At these lower noise goals, an effective lightweight jet noise suppressor would help considerably. Using curve C and a noise goal of 96 PNdB, an FPR of 2.72 can be used and the range penalty is only 167×10^3 meters (90 n. mi.).

In preliminary design work, the range and payload are fixed by route and market considerations so that airplane gross weight becomes the criteria of merit. The most commonly used economic criteria of merit is direct operating cost, DOC. It is expressed as cents per seat mile and accounts for the expenses of buying, maintaining, and insuring the airplane, paying the crew, and buying the fuel and oil. All of these expenses are dependent on the airplane design. In the preliminary design stage, DOC is a useful criteria of merit since the best designs will have the lowest DOC. DOC was calculated using the methods described in

reference 10. The results of figure 9 were used to calculate airplane TOGW and DOC values for a fixed range of 5560×10^3 meters (3000 n. mi.). In addition some optimum engines were defined which used full coverage film cooling for cruise temperatures up to 1540° C (2800° F). These results are shown in figure 11. Using current noise technology, a noise level 10 PNdB below FAR 36 can be achieved for a 4 percent increase in DOC. Using advanced noise technology, a noise level 20 PNdB below FAR 36 causes DOC to increase 9 percent. This penalty drops to 8 percent when both advanced noise technology and advanced turbine technology are available.

Having determined the optimum engine for a particular application based on specific input assumptions, the analyst should consider the effects of changes in the inputs. This will indicate what will happen if components do not function as expected and what benefits will accrue for various improvements in technology. The studies can also indicate the effects of lowering OPR to satisfy a pollution criterion or lowering turbine temperature to increase blade life. For the CTOL transport, a sensitivity study was done for a reference engine having a BPR of 4.8, an FPR of 1.7, an OPR of 31, and a T_4 of 1260° C (2300° F). This is the optimum engine for a noise goal of 106 PNdB if 15 PNdB of machinery noise suppression is used. The bar graph in figure 12 shows the range increases for a 0.01 change in each of the variables. Also shown is the range increase for a 10-percent decrease in bare engine weight. By far the most sensitive of these parameters was the duct nozzle gross thrust coefficient. A one-percent change in it produced a 185×10^3 meters (100-mile) change in range. Somewhat less sensitive parameters were inlet pressure recovery and bare engine weight. It is obvious from the bar graph that care will have to be given to the inlet, duct, and duct nozzles when treating for noise since these areas are the most sensitive.

Low Noise Engines for Mach 0.90 to Mach 0.98 Transports

In this section the procedures discussed in previous sections are used to select engines for transports that cruise from Mach 0.90 to 0.98. Fan machinery noise suppression up to 20 PNdB is used. This is offered as a reasonable goal which hopefully can be met by 1978, the postulated year of first flight.

Figure 13 summarizes the results for a cruise FPR of 1.70. Range with a penalty included for the weight of the turbomachinery noise suppression is plotted against the total combined noise at either the sideline or the approach condition, whichever is greater. Three curves are shown - one for each of the cruise Mach numbers considered. The right-hand end of each curve represents the optimum cycle meeting the thrust constraint and results in a noise level of about 114 PNdB. As the noise goal is reduced, the design BPR is increasing and more acoustic treatment is being added. At the left-hand end of the curves, 27 to 30 PNdB of turbomachinery noise suppression is required. With 20 PNdB suppression, noise goals from 93 to 96 PNdB can be met at this design FPR.

Figure 14 shows the effects of various amounts of turbomachinery noise suppression for engines with a cruise FPR of 2.25. With no suppression, noise levels of about 126 PNdB are obtained. Approach noise exceeded the sideline noise at all levels of suppression considered in this plot. Unlike the case with an FPR of 1.70, BPR is not increased as the noise goal is reduced. It was found that with an FPR of 2.25 the range decreased as BPR was increased without a significant reduction in total noise. (Total noise was generally dominated by machinery noise, which is unaffected by BPR.) Hence, the best tradeoff was to keep the engine cycle parameters fixed as more machinery noise treatment was added. With 20 PNdB of suppression, goals of 106 to 108 PNdB can be obtained, depending on design cruise Mach number. If the trades of FAR 36 are permitted, the goals that are met can be said to be 2 PNdB lower than these values since noise measured at the sideline station is more than 2 PNdB less than the approach noise.

In figure 15(a) range is plotted against cruise Mach number for noise goals of 106 and 96 PNdB. Data for the 106 PNdB curve is for the two-stage fans with an FPR of 2.25 while that for the 96 PNdB curve is for the single-stage fan with an FPR of 1.70. Figure 15(a) emphasizes the increase in range possible by reducing the cruise speed from Mach 0.98 to 0.90. The range increase is 926×10^3 meters (500 n. mi.) for the 106 PNdB noise goal and 1480×10^3 meters (800 n. mi.) for the 96 PNdB noise goal. It is also apparent that there is a range penalty involved in reducing the noise from 106 to 96 PNdB. This range penalty decreases from 741×10^3 meters (400 n. mi.) at Mach 0.98 to less than 185×10^3 meters (100 n. mi.) at Mach 0.90.

The remaining parts of figure 15 show the optimized engine parameters as a function of cruise speed and noise level. From figure 15(b), BPR optimizes at 4 for all values of M_{cr} for the 106 PNdB noise goal and at about 6 for the 96 PNdB noise goal. In figure 15(c) the optimum cruise overall compressor pressure ratios are shown to vary from 32 to 36 for the 106 PNdB noise goal and from 36 to 41 for the 96 PNdB noise goal. OPR is not a strong optimum and can be reduced to the vicinity of 30 without a significant adverse effect on range. This reduction may be required to curtail nitrogen oxide emissions. OPR optimized at rather high values in this study because of the advances that were assumed to occur in engine weight technology by the year 1978. Higher OPR's, therefore, did not cause great increases in engine weight. More conservative engine weight assumptions would have caused engine weight to rise faster with increasing OPR so that the optimum OPR's would have been lower.

In figure 15(d) it is shown that the takeoff thrust-to-gross-weight ratio increases from the minimum of 0.24 for the lower cruise speeds to values as high as 0.31 for a cruise speed of Mach 0.98 and a noise goal of 96 PNdB. In this study the cruise T_4 was adjusted with the takeoff T_4 fixed at 1260° C (2300° F) to obtain an $(F_n/W_g)_{sls}$ of not less than 0.24. (The three-engine Boeing 727-200 has this value when fully loaded.) The fact that $(F_n/W_g)_{sls} > 0.24$ for the Mach 0.98 cruise case reflects

that the cruise T_4 has been adjusted upward to its maximum permissible value of 1200° C (2200° F) for a takeoff T_4 of 1260° C (2300° F). To have obtained values of $(F_n/w_g)_{sls}$ closer to 0.24 would have required raising the cruise T_4 beyond 1200° C (2200° F) making the climb thrust too marginal as cruise is approached.

The cruise T_4's that optimized performance are plotted against Mach number in figure 15(e). For the 106 PNdB noise goal, it is seen that the cruise T_4 rises linearly from 1070° C (1965° F) at Mach 0.90 to 1200° C (2200° F) at Mach 0.98. For the 96 PNdB noise goal, the cruise T_4 optimizes at 1050° C (2100° F) at Mach 0.90 and increases linearly to 1204° C (2200° F) at Mach 0.94 where it meets the aforementioned constraint for thrust margin. Beyond Mach 0.94, the cruise T_4 is restricted to 1204° C (2200° F) although range would probably have improved if higher temperatures had been allowed.

Figure 15(f) shows the sea-level-static corrected airflow required for each of the optimized engines with airplane TOGW fixed at 175 000 kilograms (386 000 lb). For the 106 PNdB noise goal, these airflows varied from 381 to 432 kilograms per second (840 to 950 lb/sec). Airflows from 468 to 618 kilograms per second (1030 to 1360 lb/sec) were required to meet the 96 PNdB noise goal. The corresponding maximum engine diameters are shown in figure 15(g). For the optimum engines meeting the 106 PNdB goal, the maximum diameter is about 1.78 meters (70 in.). To meet the 96 PNdB goal the maximum engine diameter must be increased to 2.03 to 2.29 meters (80 to 90 in.).

Figure 15(h) shows the variation of both sideline and approach noise with M_{cr} for the two noise goals. The solid curves represent sideline noise and the broken curves approach noise. The figure shows that at the nominal 106 PNdB goal, the approach noise ranges from 106 to 108 PNdB while sideline noise varies from 100 to 102 PNdB. (As previously discussed, the ground rules of FAR Part 36 permit an excess of up to 2 PNdB at one measuring station if a corresponding reduction can be obtained at another measuring station.) For the 96 PNdB goal there was very little difference between the sideline and approach noises.

DOC is plotted against cruise Mach number in figure 16 for noise goals of 96 and 106 PNdB. The best DOC's are obtained at cruise speeds of about Mach 0.94. At Mach 0.94 the DOC increases by only 0.00871 cents per seat-kilometer (0.014 cents per seat-statute-mile) when the noise goal is reduced from 106 to 96 PNdB. If the cruise speed is increased to Mach 0.98, the DOC increases by 0.0143 cents per seat-kilometer (0.023 cents per seat-mile) for the 96 PNdB noise goal. For the 106 PNdB noise goal, the economic penalty of increasing the cruise speed to Mach 0.98 is not nearly as great. Here, the increase in DOC is only 0.00404 cents per seat-kilometer (0.0065 cents per seat-statute-mile).

The engine cycles which were previously optimized on a range basis were reevaluated in terms of TOGW for a fixed range of 5560 kilometers

(3000 n. mi.) and a fixed payload of 300 passengers. Airframe weight was assumed to be a constant percentage of the TOGW. Engine airflows, diameters, and weights were recomputed on the basis of the different thrust levels required at the lower TOGW's. In figure 17 TOGW is plotted against cruise Mach number for noise goals of 106 and 96 PNdB. TOGW increases markedly when cruise speed is increased from Mach 0.94 to 0.98, especially for the 96 PNdB noise goal. At the lower Mach numbers there is only a modest rise in TOGW for a noise goal of 96 PNdB as opposed to 106 PNdB. At Mach 0.98, however, the weight increase is appreciable.

In figure 18, DOC is plotted against cruise Mach number for noise goals of 96 and 106 PNdB. These 5560 kilometer (3000-mile) DOC curves are analogous to the TOGW curves of figure 17. For comparison, the DOC curves for a constant TOGW and variable range (fig. 16) have been replotted in figure 18 as the broken curves. By comparing the two sets of curves it is seen that the reduction in TOGW that was accomplished by fixing the range at 5560 kilometers (3000 n. mi.) lowered the level of DOC generally and accentuated changes resulting from increments in cruise Mach number or noise goal reduction.

The large difference between the solid curves and the broken curves at Mach 0.94 and below results from the fact that TOGW was calculated to be more than 4540 kilograms (100 000 lb) less when range was fixed at 5560 kilometers (3000 miles). The DOC's of both sets of curves appear to minimize near the middle of the range of cruise speeds studied. For the fixed range of 5560 kilometers (3000 miles), the DOC minimized at Mach 0.94 for the 106 PNdB goal and Mach 0.92 for the 96 PNdB goal. But very little increase in DOC is introduced by raising the cruise speed to Mach 0.94 for the 96 PNdB noise goal and Mach 0.95 for the 106 PNdB noise goal. At these speeds, DOC is increased by only about 0.0124 cents per seat-kilometer (0.02 cents per seat-statute-mile) when the noise goal is reduced from 106 to 96 PNdB. This does not seem to be a very large economic penalty to pay for a 10 PNdB reduction in noise. If the cruise speed is increased to Mach 0.98, the DOC increases by about 0.0497 cents per seat-kilometer (0.08 cents per seat-mile) at the 96 PNdB noise goal but by only 0.0187 cents per seat-kilometer (0.03 cents per seat-mile) for the 106 PNdB goal.

DOC, of course, does not present the entire economic picture. It does not, for instance, show how load factor might be affected by the introduction of competing airplanes designed for higher cruise speeds. Hence, although the lowest DOC's occur at design speeds between Mach 0.92 and 0.94, a faster airplane having a slightly higher DOC but a higher load factor (because of its lower block time) might be more profitable for an airline to operate. The range from New York to San Francisco, 4140 kilometers (2235 n. mi.) represents a long range domestic flight. The block time difference between Mach 0.94 and 0.98 at this range is only about 8 minutes. When block times are considered, however, it does seem worthwhile to increase the design speed to a point just to the right of the "bucket" of the DOC curves of figure 18 since so little penalty in DOC is involved by so doing. Using this criterion, a good cruise speed

selection might be Mach 0.95 for the 106 PNdB noise goal and Mach 0.94 for the 96 PNdB noise goal.

VTOL TRANSPORT

Vertical takeoff and landing aircraft are currently under study as a means for improving short-haul intercity air transportation. VTOL can relieve airport congestion and reduce air time delays, and can service communities currently without air transportation. A number of VTOL transports have been studied in the U.S. and abroad. Various aircraft configurations and various means of providing vertical lift (e.g., rotors, tilting propellers, and high-bypass-ratio lift fans) were studied (refs. 11, 12, and 13). None was outstandingly superior so that there is still interest in many of the concepts.

In reference 14 the requirements and problem areas of low-pressure ratio lift fan propulsion systems are reviewed. The lift fan system has a number of features that qualify it for civilian VTOL transports. These are: (1) good potential for meeting reduced noise limitations, (2) provision for safe management of failure of power plant or thruster, (3) good passenger and airline appeal for resulting aircraft, (4) capability of high cruise speed approaching that of conventional jet transports, (5) direct use of available gas turbine technology, and (6) elimination of mechanical transmissions. Two general types of lift-fan systems are currently being worked on, the integral system and the remote system. The integral system is similar to a high-bypass ratio turbofan in which the fan is powered by a coaxially mounted gas turbine engine. In the remote type, the fan and its drive turbine are separately located from the powerplant, and the working fluid is delivered through ducts to the turbine mounted at the tips of the fan blades. The remote system wherein hot gas from a turbojet engine is delivered to the tip turbine has been under investigation for a number of years (ref. 15) by the General Electric Company and was used in the XV-SA VTOL aircraft (ref. 16).

A second remote system uses a gas turbine driven fan (air generator) to supply compressed air to a burner upstream of the remote tip turbine. During cruise, the lift fans are inoperative and air from the air generator is exhausted in the conventional manner so that the air generator operates as a conventional turbofan engine. The present study is concerned solely with a particular air generator-lift fan VTOL system currently being considered at the Lewis Research Center (ref. 17).

This system consists of four 66 700 newtons (15 000 lb thrust) remote lift fans and eight 33 400 newtons (7500 lb thrust) lift fans driven by gas generated just upstream of the tip turbines in auxiliary burners fed by four low bypass ratio, high fan pressure ratio air generators. Cross ducting is provided between each pair of air generators so that the thrust loss with one air generator out can be minimized. During cruise, the lift fans are inoperative and the fan exhaust is exhausted through cruise nozzles.

The objective of the study is to optimize the parameters of the air generator and remote tip-turbine lift fan. For the air generator, turbine-inlet temperature was varied from 1040° to 1370° C (1900° to 2500° F), overall pressure ratio from 12 to 21 and fan pressure ratio from 2.73 to 4.37. Bypass ratio was a dependent variable to produce the air required by the auxiliary burner which operated at 780° C (1440° F) and supplied working fluid to the 33 400 and 66 700 newtons (7500 and 1500 lb thrust) remote lift fans. Specific values of the air generator parameters were selected based on weight, dimensions, and specific fuel consumption.

The parameters of the remote tip-turbine lift fan were selected by performing a preliminary mission analysis. The propulsion systems examined were installed in a particular airplane which cruised at Mach 0.75 and 7620 meters (25 000 ft). Range was 804 kilometers (500 statute miles) and included 5 minutes of hover to account for two takeoffs and two landings. Gross weight was calculated from consideration of emergency conditions so payload varied as tip-turbine pressure ratio varied from 2.5 to 4.0, lift fan pressure ratio varied from 1.15 to 1.35, and cruise lift to drag ratio from 8 to 12. Takeoff noise was also calculated to illustrate the payload-noise characteristics of the propulsion systems.

Method of Analysis

Propulsion system requirements. - The mission selected to evaluate the propulsion system is as follows:

Stage length	804 km (500 statute miles)
Cruise Mach number	0.75
Cruise altitude	7620 m (25 000 ft)
Nominal takeoff noise goal @ 152 m (500 ft), PNdB	95
Hover time for two takeoffs and two landings, min	5

The type of VTOL transport assumed in this study is shown in figure 19. There are four large lift fans mounted in the high wing, each capable of producing 66 700 newtons (15 000 lb) of lifting thrust at sea level on a 32° C (90° F) day. At the wing tips and the forward and aft fuselage stations, there are eight half-size lift fans producing an additional 267 000 newtons (60 000 lb) of lift thrust. The four air generators are mounted in pairs on the wing. Each air generator supplies two of the full-size lift fans or four of the half-size lift fans. Air generators are interconnected so that there is no one-to-one correspondence between fans and air generators. During lift off and landing, the core flow is deflected downward to provide additional lift thrust (the level varying slightly depending on the design of the air pump). The nominal value of total lifting thrust on a 32° C (90° F) day was 570 000 newtons (128 000 lb).

The gross weight of the VTOL transport was calculated for normal operation, operation with one air generator out, and operation with two full-size lift fans out. The least of these values was taken to be the

transport gross weight for the nominal mission. For normal operation, a vertical thrust to gross weight ratio of 1.1 was assigned and a control thrust to weight ratio of 1.25 giving a gross thrust to weight ratio of 1.375. For the air generator out and full-size lift fan out cases, vertical thrust to weight ratio was 1.05 and control thrust to weight ratio 1.125. The air-generator out case was critical and resulted in a gross weight of 40 300 kilograms (88 700 lb).

Simplifying assumptions were made concerning the operating weight empty less propulsion system weight (50% of gross weight) and the transport aerodynamics (cruise L/D was varied parametrically from 8 to 12). Reserve fuel was assigned to be 3.5 percent of gross weight and fuel to accelerate and climb to cruise conditions from transition was assigned to be 3 percent of gross weight. The airplane fractional weights that varied with propulsion system design were (a) propulsion system weight, (b) fuel for two takeoffs and landings (5 min of hover), and (c) fuel to cruise the 471 kilometers (293 statute miles) of the nominal 804 kilometers (500 statute miles) total range (333 km (207 statute miles) were allotted for climb and letdown).

Propulsion system. - The two major elements of the air generator/lift fan propulsion system are shown in figure 20, the remote drive lift fan and the air generator.

Air enters the air generator through an acoustically treated inlet. All of the air is compressed by the low-pressure compressor, or fan. The air delivered by the low compressor is split: part of it is collected in a scroll to form the delivered air supply, the ultimate product of the air generator. The remaining air goes through the high-pressure compressor, burner, and high pressure turbine. These three components make up the so-called high spool of the air generator which is, in reality, a gas generator for the low pressure turbine. This turbine drives the low pressure compressor, and these two components along with the connecting shaft constitute the low pressure spool. The shafts for the two spools are concentric. The exhaust from the low pressure turbine is ducted through an exhaust system which turns the flow through ninety degrees to produce a vertical thrust or lift for takeoff and landing.

The computer prog m of reference 18 provides a design point configuration for the air generator. The thermodynamic performance, including the discharge thrust, is completely described, along with the dimensions and weight. Detailed thermodynamic performance, size, and weight are also calculated for the principal components (the weight and size equations are those presented in ref. 19, see appendix D).

The length and weight of the inlet acoustic treatment and the exhaust system calculated by this computer program are appropriate for the configuration shown in figure 20. However, the actual inlet and exhaust systems used may differ from those shown. It was assumed in this study that the sonic inlet would suppress forward propagating turbomachinery noise to a level low enough that it would contribute a negligible amount to the total

propulsion system noise.

The computer program of reference 20 provides a preliminary design and analysis tool for an entire tip-turbine-driven lift fan assembly. This program is particularly adaptable to parametric studies of the effect of changes in the principal design variables of both the fan and turbine on the performance of the entire assembly. Considerable attention is given to the scroll which delivers the working fluid to the tip turbine. In the propulsion systems considered herein, the cold ducts that deliver the low pressure compressor discharge air from the air generator to the lift fan are interconnected and just upstream of the scroll inlet to each lift fan is an auxiliary burner with a maximum outlet temperature of 780° C (1440° F).

The computer program for the design and performance of an air generator has considerable inherent flexibility in that no less than 44 independent parameters may be specified for any one air generator design. For all air generators, ambient pressure was 101 000 N/m^2 (2116 lb/sq ft) and ambient temperature 32° C (90° F). Total pressure recovery of the inlet was 0.95.

For each air generator considered, the size was determined to be that required to supply two full-size lift fans each of which delivered 66 700 newtons (15 000 lb) of thrust at liftoff. The low-pressure compressor was designed with a constant hub radius and 3 to 5 stages with a corrected tip speed at the compressor inlet to 366 meters per second (1200 ft/sec) and a design point polytropic efficiency of 0.895. Average axial inlet Mach number was 0.6 and inlet hub-tip radius ratio was 0.5 for the first rotor. Diffusion through the compressor was regulated by selecting axial velocity ratio across the compressor to be 0.75. Average aspect ratio of the first two stages (which affects both length and weight of the low compressor) was 3. The design value of low compressor pressure ratio was varied between 2.73 and 4.37 to provide a tip-turbine pressure ratio of 2.5 to 4.0 (assuming a pressure loss through the ducts and scrolls of 8.4%).

The scroll diameter, corresponding to the maximum flow area in the scroll, was sized by the scroll Mach number of 0.3 and a selected configuration wherein the two delivery ducts are contiguous.

Most of the parameters required to describe the high compressor were used in the same manner as for the low compressor. The similar parameters are:

Flow path	constant hub
Number of stages	6 or 7
Corrected tip speed, m/sec (ft/sec)	335 (1100)
Efficiency	0.895
Axial velocity ratio	0.75
Overall pressure ratio	12 to 20

Four input parameters were required to establish the performance and geometry of the combustor. The reference burner inlet velocity was fixed at 18.3 meters per second (60 ft/sec) so that the resultant flow area, or radial height, of the burner was a dependent variable. Burner length was determined from this height and the prescribed ratio of burner length to height, 3. A lower heating value of 42 800 kilojoules per kilogram (184 000 Btu/lb) of JP fuel and a burner efficiency of 0.98 were used to compute fuel-air ratio.

One of the most significant parameters in the performance of the air generator is the stator inlet temperature to the high turbine. In this study it was varied from 1040° to 1370° C (1900° to 2500° F). Rotor cool-ign air (as a percent of high compressor discharge airflow) was scheduled to be 5.7 to 14.7 percent to reflect current technology in turbine-blade material and cooling airflow to maintain blade integrity. A high turbine loss coefficient ξ of 0.4 was used to calculate efficiency of the one-stage turbine (see appendix D of ref. 20).

The large work extraction from the low turbine reduces the density of the working fluid so that a large flow area is required at the turbine exit. Flow area together with an assigned exit hub-tip radius ratio of 0.6 permitted turbine exit diameter to be calculated. The loss factor for the low turbine was assigned to be 0.4 and resulted in a turbine efficiency of 0.88 to 0.89.

The exhaust system on the core of the air generator includes both a duct and an adjustable nozzle which deflects the core flow to produce lift during takeoff and thrust during cruise. In order to provide control on the jet noise, the exhaust velocity from the nozzle was specified to be 198 meters per second (650 ft/sec). Exhaust system losses were accounted for through the use of a duct pressure loss coefficient of 0.125 which was multiplied by the square of the axial Mach number out of the turbine and by assigning a nozzle discharge velocity coefficient of 0.98.

During cruise the air pump is employed as the cruise thrusting engine to overcome airplane drag. To get the required variation of specific fuel consumption with thrust setting on a standard day + 31° F (17.2° C), the procedures described in reference 8 were employed. Maximum thrust was assigned to be that corresponding to a turbine inlet temperature 111° C (200° F) less than takeoff turbine temperature. The exhaust nozzle discharge velocity coefficient was 0.98.

Each of the full-size lift fans was sized to produce 66 700 newtons (15 000 lb) of thrust at takeoff on a 32° C (90° F) day at sea level. The program described in reference 20 was used to compute dimensions, weight, and performance of single-stage lift fans having design pressure ratios of 1.15 to 1.35. The single-stage tip-turbine pressure ratio was varied from 2.5 to 4.0.

The temperature into the scroll was set at 780° C (1440° F) so that the scroll could be constructed of conventional alloys. Inlet duct pressure ratio was 0.95 while fan inlet Mach number was 0.55 and fan hub-tip

radius ratio was 0.4. For each tip-turbine driven lift fan, turbine exit axial Mach number was 0.3.

Some pertinent parameters are listed below:

Turbine pressure ratio	2.5	3.0	3.5	4.0
Air generator exit temperature, ^{o}C	410	427	446	463
Fan tip speed, m/sec	251	283	283	314
Fan efficiency (for fan pressure ratio of 1.25)	0.831	0.840	0.840	0.843
Tip-turbine lift fan weight (for 66 700 N thrust), kg	484	465	447	442

The total perceived noise is made up of jet noise from the fan air generators, jet noise from the twelve lift fans, and suppressed turbomachinery noise from the twelve lift fans. Turbine jet noise from the lift fans was assumed to make a negligible contribution to total noise (whether or not this can be achieved in an actual engine remains to be demonstrated). Turbomachinery noise projected out the fan inlets and air generator inlets (which contain choking devices for noise suppression) was also assumed to make a negligible contribution to total noise. The noise rating condition was assigned to be at maximum takeoff thrust.

Jet noise, measured in PNdB, was calculated by standard methods described by the Society of Automotive Engineers in references 5 and 6. At jet velocities below 1000 feet per second, there is some uncertainty as to how overall sound pressure level (OASPL) varies. In this report, the semi-log plot of the curve of OASPL against relative jet velocity shown in figure 1 of reference 6 was extrapolated as a straight line below 305 meters per second (1000 ft/sec). While this technique is not used exclusively throughout the industry, it does agree with recent data published in reference 7.

Fan turbomachinery noise, also measured in PNdB, is a function of many things; for example, number of rotor blades and stator blades, tip speed, spacing between rotor and stator, fan pressure ratio, thrust, and amount of nacelle acoustic treatment. In this study, it was assumed that the engines would be built with optimum stator-rotor spacing and without inlet guide vanes in order to minimize noise generation. Curves developed by the Propulsion Systems Acoustic Branch at NASA-Lewis, and presented in reference 7, relate fan machinery noise to fan pressure ratio for one-stage fans. These noise curves were scaled from a net thrust of 534 000 newtons (120 000 lb) and a distance of 152 meters (500 ft). According to reference 7, acoustic treatment can reduce turbomachinery noise as much as 15 PNdB, the amount of suppression used in the noise calculations of this study. Total noise was obtained by adding anti-logarithmically, the suppressed turbomachinery and jet perceived noise, as described in reference 5.

Results and Discussion

For a propulsion system having a lift fan pressure ratio of 1.20, the effects of the air generator overall pressure ratio and turbine temperature on specific thrust and specific fuel consumption at SLS conditions of the complete propulsion system are shown in figure 21. As overall pressure ratio increases from 12 to 21, specific lift thrust increases 2 percent and specific fuel consumption decreases 4 percent (fig. 21(a)). For an overall pressure ratio of 15, as turbine temperature increases from 1040° to 1370° C (1900° to 2500° F), specific lift thrust increases 2 percent and specific fuel consumption remains constant (fig. 21(b)).

On the basis of the above variations, a nominal air generator was selected with an overall pressure ratio of 15 and a turbine temperature of 1204° C (2200° F). A higher overall pressure ratio and turbine temperature offers small performance, weight, and size improvements but probably at some increase in development cost, original cost, and maintenance cost.

The weight breakdown of the dependent weight fractions is shown in figure 22 for a cruise L/D of 10 and a lift fan pressure ratio of 1.25. As tip-turbine pressure ratio increases, weights of the lift fans and hover fuel decrease, cruise fuel weight increases, and air generator weight stays constant above a tip-turbine pressure ratio of 3.5 (fig. 22(a)). The total of these weights decreases from 13 000 to 12 200 kilograms (28 750 to 27 000 lb) (fig. 22(b)). The weight saving can go into payload (fig. 22(a)). As tip-turbine pressure ratio increases from 2.5 to 4.0, the payload increases from 4440 to 5220 kilograms (9800 to 11 500 lb). At 93 kilograms (205 lb) per passenger and baggage, the tip turbine pressure ratio of 4.0 yields 56 passengers.

The effect of lift fan pressure ratio on the weight breakdown is shown in figure 23 where tip-turbine pressure ratio is 3.5 and cruise L/D is 10. As lift fan pressure ratio increases, cruise fuel stays constant, hover fuel and air generator weight increase and lift fan weight decreases. The summation of these weights increases (fig. 22(b)) so payload decreases as lift fan pressure ratio increases (fig. 22(a)). For a lift fan pressure ratio of 1.15, payload is 57 200 kilograms (126 000 lb) or 62 passengers.

The tradeoff between payload and noise is shown in figure 24. A fan pressure ratio less than 1.15 is required to achieve the noise goal of 95 PNdB. However, a lift fan pressure ratio of 1.15 comes close: noise is 96.2 PNdB while payload for the tip turbine pressure ratio of 4.0 is 57 200 kilograms (12 600 lb). For lift fan pressure ratios less than 1.15, cruise thrust available from the four air generators falls below the drag of an airplane having a lift to drag ratio of 10.

Concluding Remarks

A simplified mission analysis was performed to evaluate the effects of lift fan pressure ratio and tip-turbine PR on the payload and noise of a remote-drive VTOL lift system. This system consisted of four 66 700 newtons (15 000 lb) thrust lift fans, eight 33 400 newtons (7500 lb) thrust lift fans and four air generators which were also used as the cruise engines.

A range of 804 kilometers (500 statute miles) was selected with a cruise Mach number of 0.75 at an altitude of 7620 meters (25 000 ft). The allowable takeoff gross weight, as dictated by the maximum available lift under emergency conditions and control requirements, was found to be about 40 300 kilograms (88 700 lb). Cruise lift-drag ratios of 8 to 12 were assumed in the study. Cruise performance calculations show that the airpump cycle can be used at cruise; with the L/D's assumed in this study, however, all four air generators would be required to provide enough cruise thrust. Cruise SFC was then used in the Breguet equation to calculate the weight of cruise fuel. Finally, payload was obtained by subtracting airframe, engine, and fuel weights from the TOGW.

For the range of tip-turbine PR's and lift-fan pressure ratios examined, a near-maximum payload of 57 200 kilograms (12 600 lb) was obtained with the highest tip-turbine pressure ratio considered (4) and the lowest lift fan pressure ratio considered (1.15). At higher fan pressure ratios, noise increased and payload decreased due to an increase in hover fuel and an increase in air generator weight. Noise at 152 meters (500 ft) was calculated to be 96.2 PNdB. As advances in noise generation and suppression are made, the noise goal of 95 PNdB should be attainable.

These results are quite encouraging and suggest that the air generator lift fan remote propulsion system is an attractive candidate for V/STOL transports.

SUPERSONIC TRANSPORT

The Concorde and TU 144 supersonic transports use conventional kerosene fuel and cruise at about Mach 2. There is incentive to cruise at higher speed since flight efficiency continues to improve at higher speeds. The now defunct Boeing SST was designed to cruise at Mach 2.7. One of the factors that limited its cruise speed to Mach 2.7 was the heat-sink capacity of conventional kerosene-type fuel. Practically all of the heat sink available was used to absorb the heat discharged by the cabin environmental control system and the engine oil cooling system.

Studies by NASA have indicated that liquid methane may prove to be a superior fuel for SST's designed to cruise at Mach 2.7 and higher. Liquid methane has a heat sink capacity, up to seven times as great as that of kerosene, and a heat of combustion 13 percent higher than that of kero-

sene. Since excess cooling capability is available, higher temperature engines may be considered. A methane-air heat exchanger can be built into the engine to cool the compressor discharge air in the turbine cooling circuit.

The purpose of this study is to determine what benefit will be obtained from the high-turbine-inlet temperature permitted by methane fuel. The data are from reference 21. This is done with and without consideration of airport and community jet noise restrictions during airplane takeoff and climb. The method used is to determine the improvement that might be obtained in two overall airplane figures of merit, namely, (1) payload (number of passengers) and (2) direct operating cost in cents per seat-kilometer (cents per seat-statute mile). The airframe is arbitrarily selected as a fixed-sweep, arrow-wing SCAT 15F configuration. The SCAT 15F configuration was developed by the NASA Langley Research Center to have a very high cruise lift-to-drag ratio. It is still under investigation to overcome some low-speed handling problems.

The afterburning turbojet, nonafterburning turbojet, and the duct-burning turbofan are the three engine cycles investigated. The turbine-inlet temperature is varied from 1204° to 1704° C (2200° to 3100° F). The compressor pressure ratio, bypass ratio, and the fan pressure ratio are optimized for each turbine inlet temperature, both with and without airport and community noise restrictions.

Noise restrictions are imposed on the engines because the problem of airport and community noise during airplane takeoff and climb is of major concern to the airports and the public. Approach noise levels are also important, but these restrictions are not considered herein. If approach noise is a problem, it can be solved with a sonic inlet. The so-called airport noise is measured at the start of takeoff roll, 457 meters (1500 ft) from the centerline of the aircraft and at the angle of maximum noise. The noise level at this point should not exceed 116 PNdB. For the community noise, during airplane climb a point on the ground directly beneath the flight path and at a distance of 4.8 kilometers (3 statute miles) from the point of brake release is considered. After the engine power is reduced for a 2.53 meters per second (500 ft/min) rate of climb, the maximum noise at this point should not exceed 105 PNdB. These noise goals were suggested by the Federal Aviation Agency at the time of the study and are less stringent than those of FAR Part 36.

Noise suppression devices of the exhaust jet are not used in order to better emphasize the influence of the primary engine parameters. It is entirely possible that the use of noise suppression devices would change the results of this study. The data presented can be considered as the two extreme cases. The best possible case assumed no airport or community noise restrictions, and the worst possible case assumed noise restrictions without suppression devices. Thus, data obtained by using various degrees of suppression would most likely occur somewhere between the extremes.

Method of Analysis

The effect of increasing turbine-inlet temperature with or without noise restrictions was calculated by analytically flying a fixed-wing airplane over a standard mission profile. The methane-fueled airplane was similar to the one shown in figure 25 and had a ramp gross weight of 209 000 kilograms (460 000 lb). The engine parameters and engine size were optimized to maximize payload both with and without airport and community noise restrictions. The maximum cross-sectional area of the fuselage was fixed while fuselage length was varied in order to accommodate different numbers of passengers. Comparisons were made among the afterburning turbojet, nonafterburning turbojet, and duct burning turbofan engines.

The mission requirements observed were:

Range, km; n. mi.	6482; 3500
Cruise Mach number	3
Maximum sonic boom, N/m^2; lb/ft^2	
Climb	95.8; 2
Cruise	71.8; 1.5
Minimum climb-acceleration thrust-to-drag ratio	1.4
Minimum second segment climb angle, deg	1.7
Maximum lift-off distance, m; ft	1460; 4450

The fuel reserve for the mission allows for (1) an additional 7 percent of the total mission fuel, (2) an extension of 483 kilometers (261 n. mi.) to an alternate airport at cruise altitude and Mach number, and (3) a 30 minute hold at 4570 meters (15 000 ft) altitude at Mach 0.6. An additional fuel allowance was incorporated in the mission fuel for a 25 minute idle prior to takeoff as well as a 1 minute period of maximum augmentation power application prior to takeoff roll.

The aerodynamic parameters were based on wind-tunnel data supplied by the NASA Langley Research Center for the SCAT 15F which is an advanced fixed-sweep, arrow-wing SST configuration similar to the one shown in figure 25. The weights of the major components that comprise the empty weight were estimated by empirically established relations based on preliminary designs for similar configurations.

For each of the three types of engines considered, the performance and weight of each engine was calculated for a range of design variables. The range of variables covered in analytically finding the optimum cycle combination is shown in figure 26. In calculating the design and off-design performance, each engine component was matched to satisfy the relations involving continuity of flow, engine rotational speed, and power balance between the compressor (or fan) and its driving turbine. The procedures used are similar to those discussed in reference 22 (see appendix B). Engine weight was calculated from empirical equations that relate installed engine weight to the type of engine, the design engine airflow, compressor pressure ratio, fan pressure ratio, bypass ratio, and turbine-

inlet temperature. The equations are based on a composite of industry data.

The procedures for calculating jet noise are those outlined by the Society of Automotive Engineers in references 5 and 6. The method accounts for atmospheric absorption, ground attenuation, and multiple engines. The calculations are for noise produced by the jet exhaust only and do not include the noise generated by the fan or compressor.

The direct operating cost calculations were performed in the manner described in reference 10. Airframe price, which is a function of airframe weight, was estimated with development costs included and was based on a production of 200 aircraft. The equation used to calculate the airframe price is as follows:

$$\text{Cost (dollars)} = 19\times10^6 + (\text{WAF} - 69\ 000\ \text{kg})147$$

$$\text{Cost (dollars)} = 19\times10^6 + (\text{WAF} - 150\ 000\ \text{lb})66.7$$

where WAF is weight of the airframe without engines, fuel, and passengers. A one-million dollar cost for electronics was included in the airframe price. Engine price, which is a function of engine type and size, was based on a production schedule of 1200 engines assuming each airplane would eventually require two spare engines. Engine price includes development cost. For the afterburning turbojet:

$$\text{Cost (dollars)} = 1.08\times10^6 + 0.00344(w - 136\ \text{kg/sec})$$

$$\text{Cost (dollars)} = 1.08\times10^6 + 0.00156(w - 300\ \text{lb/sec})$$

For the nonafterburning turbojet:

$$\text{Cost (dollars)} = 1.04\times10^6 + 0.00344(w - 136\ \text{kg/sec})$$

$$\text{Cost (dollars)} = 1.04\times10^6 + 0.00156(w - 300\ \text{lb/sec})$$

For the duct-burning turbofan:

$$\text{Cost (dollars)} = 1.21\times10^6 + 0.00280(w - 136\ \text{kg/sec})$$

$$\text{Cost (dollars)} = 1.21\times10^6 + 0.00127(w - 300\ \text{lb/sec})$$

Liquid methane fuel delivered to the airplane was assumed to cost 2.65 cents per kilogram (1.2 cents/lb).

Results and Discussion

Engine and wing sizing. - Figure 27(a) is a thumbprint map for a series of SCAT 15F airplanes powered by afterburning turbojets having a turbine inlet temperature of 1050° C (2100° F). Each point on a given

contour represents a combination of engine and wing size that will permit a particular number of passengers to be carried over the 6480 kilometer (3500 n. mi.) range when the ramp gross weight is fixed at 209 000 kilograms (460 000 lb). The map shows that the maximum payload that can be carried is 252 passengers, which is obtained at takeoff wing and thrust loadings of approximately 2960 newtons per square meter (62 lb/ft^2) and 0.27, respectively. These wing and thrust loadings correspond to a wing planform area of 687 square meters (7400 ft^2) and an engine size of 180 kilograms per second (397 lb/sec). When the engine size is increased above 180 kilograms per second (397 lb/sec), payload suffers at the expense of greater engine weight. With smaller engines, payload decreases in spite of less engine weight because of excessive fuel consumption. When the engines are too small, acceleration is reduced and climb to cruise altitude takes longer. Thus, more fuel is used during climb. Cruise fuel is higher because more afterburning (higher SFC) is required to produce the required cruise thrust.

Among the performance criteria that can be critical in the design of the airplane are lift-off distance and velocity, transonic acceleration thrust margin, and sonic boom at the beginning of cruise. For the engine and wing combination that maximized payload, the required lift-off distance was 3050 meters (9000 ft) with a velocity of 104 meters per second (203 knots) (fig. 27(b)). The angle of attack at lift-off was not allowed to exceed 11° in order to prevent the tail of the airplane from dragging on the runway. A 1370 meter (4500 ft) lift-off distance is considered to be a reasonable design criteria when hot-day conditions, one engine out performance, and clearance of a 9.14-meter (30-ft) obstacle at the end of a 305-meter (10 000-ft) runway are considered. Using takeoff lift coefficients of 0.5 and 0.6, the 1370 meter (4500 ft) lift-off distance lines are shown in figure 27(b). Corresponding lift-off velocity scales are shown as auxiliary abscissa scales. The desired lift-off speed is 82.2 meters per second (160 knots). No firm minimum transonic thrust-drag F/D requirements exist today, but many authorities believe it should be at least 1.4 on a standard day. An F/D of 1.5 limiting line has also been superimposed on the thumbprint map. The third auxiliary abscissa scale is for initial cruise sonic boom. It decreases at lower wing loading because large wings result in higher cruise altitude and sonic boom decreases as distance increases.

With the limiting lines superposed on the thumbprint, it is obvious that the wing and engine combination which maximized payload does not result in a satisfactory airplane. Using a takeoff lift coefficient of 0.5, a good design point would have a takeoff wing loading of 2390 newtons per square meter (50 lb/ft^2), a takeoff thrust to gross weight ratio of 0.32, and a resulting payload of 201 passengers. Lift-off velocity would be about 87 meters per second (169 knots) and lift-off distance 1360 meters (4450 ft). Transonic F/D would be 1.94 and initial cruise sonic boom about 73.6 newtons per square meter (1.54 lb/ft^2).

If high lift devices allow a takeoff lift coefficient of 0.6, then a

better airplane results. In this case, a good selection would be a 208 kilograms per second (460 lb/sec) engine and 2870 newtons per square meter (60 lb/sq ft) wing loading. Passengers would increase 9 percent from 201 to 219 and lift-off velocity would decrease from 87 to 83.6 meters per second (169 to 163 knots). Transonic F/D would decrease slightly and cruise sonic boom would increase slightly although neither change is very significant.

Effect of engine design variables. - The afterburning turbojet, the nonafterburning turbojet, and the duct burning turbofan were considered separately to determine the engine design parameters that would enable the aircraft to carry the greatest number of passengers. The effect that design turbine inlet temperature had on engine design parameters, payload, and DOC was considered with and without takeoff and community noise limits.

Figure 28(a) shows the passenger carrying capability of an SST as a function of design turbine inlet temperature when the SST is powered by four afterburning turbojet engines. Without noise constraints, the number of passengers increases by 12.1 percent as turbine temperature is increased from 1204° to 1704° C (2200° to 3100° F). Overall pressure ratio increased from 10 to 19 (fig. 28(b)). Engine airflow decreased 11.1 percent (fig. 28(c)) but engine weight changed only slightly (fig. 28(d)) as a result of the combined effects of overall pressure ratio, airflow, and turbine temperature.

The results obtained when takeoff noise limits were imposed are also shown in figure 28 by the dashed lines. In meeting the noise restriction, a 10.4 percent payload penalty resulted at a design turbine-inlet temperature of 1204° C (2200° F) (fig. 28(a)). A significant increase in engine weight and size was the cause of the payload decrease. It was necessary to increase the design engine airflow by 57 percent (fig. 28(c)). This more than offset the effect of a lower overall pressure ratio (fig. 28(b)) to increase engine weight by 62.2 percent (fig. 28(d)).

In figure 29, which uses airport sideline noise and community noise as coordinates, the 161 kilograms per second (353 lb/sec) airflow allowed the aircraft to carry maximum payload (point (a)). This engine produced sufficient thrust to meet the lift-off distance and climb-acceleration constraints for the mission. However, these engines produced 122.3 PNdB airport sideline noise and 110.3 PNdB community noise levels, which were considerably over the maximum limits.

The jet noise was reduced by operating the engine at reduced thrust without afterburning and at a reduced turbine inlet temperature, 957° C (1755° F). To make up the thrust loss, engine size was increased to 251 kilograms per second (553 lb/sec). This engine satisfied the noise and lift-off distance constraints (point (b), fig. 29). In fact, community noise at the 4.8 kilometer (3 mile) point after power cut back was 102.5 PNdB. If engine thrust were increased until the limiting noise of

105 PNdB is reached, rate of climb at the 3-mile point would be 381 meters per second (1250 ft/min) which is well above the minimum requirement of 152 meters per second (500 ft/min).

With noise restrictions, the payload decreased by 5.6 percent (fig. 28(a)) as the turbine-inlet temperature increased to 1704° C (3100° F). Overall compressor pressure ratio increased from 8 to 12 (fig. 28(b)) and engine airflow increased 1.5 percent (fig. 28(c)). The combination of the effects of increasing turbine-inlet temperature, compressor pressure ratio, and engine size resulted in an installed engine weight increase of 13.5 percent (fig. 28(d)).

As the turbine inlet temperature of the afterburning turbojet was increased with noise restrictions, the payload decreased because the engine weight increased faster than the fuel weight decreased. Engine performance improvement with increasing turbine inlet temperature was offset by the engine weight as a result of the large engine size required to meet the noise and lift-off distance constraints. In fact, the oversized engines in some cases cruised while using no afterburning and with turbine-inlet temperature reduced below design values. Therefore, little use was made of the high design turbine inlet temperature capability.

The results for the nonafterburning turbojet are shown in figure 30. Without noise restriction, payload increased 17.4 percent as design turbine-inlet temperature was increased from 1204° to 1704° C (2200° to 3100° F) (fig. 30(a)). Design compressor pressure ratio increased from 8.4 to 19 (fig. 30(b)) while engine airflow decreased by 27 percent. This latter trend resulted because engine size was dictated by the minimum climb acceleration thrust to drag ratio. The trends in turbine temperature, compressor pressure ratio, and engine size caused installed engine weight to decrease 13.2 percent (fig. 30(d)). The engine weight increase that normally would result as the design compressor pressure ratio is raised was offset by the large engine airflow reduction.

Imposing noise constraints lowered the payload only 1.3 percent for a turbine inlet temperature of 1204° C (2200° F) (fig. 30(a)) because airflow had to be increased only 4.7 percent (fig. 30(b)) to meet the noise and lift off distance requirements. As the design turbine inlet temperature was increased from 1204° to 1704° C (2200° to 3100° F), payload decreased 4 percent. Optimum compressor pressure ratio increased from 8 to 12 (fig. 30(b)) and engine airflow increased 1.5 percent (fig. 30(c)) duplicating the trends for the afterburning turbojet. The trends in turbine temperature, compressor pressure ratio, and engine size caused installed engine weight to increase 21 percent (fig. 30(d)).

The results for the duct burning turbofan are shown in figure 31. Without noise restrictions, payload increases 8.2 percent as turbine inlet temperature is increased from 1204° to 1704° C (2200° to 3100° F) (fig. 31(a)). Engine noise at the airport increased from 117.9 to 121.7 PNdB. Compressor pressure ratio increased somewhat (fig. 31(b)), bypass ratio stayed constant at a value of 1.0 (fig. 31(c)), fan pres-

sure ratio increased (fig. 31(d)), and design engine airflow decreased 11.5 percent (fig. 31(e)). The above trends resulted in an installed engine weight decrease of 8.4 percent (fig. 31(f)).

When airport and community noise limits were imposed on the duct burning turbofan powered SST, payload decreased 2.1 percent at 1204° C (2200° F) turbine inlet temperature. The decrease again was the result of a trade-off of a larger heavier engine that is capable of producing more thrust at maximum power, which, in turn somewhat decreased the fuel required to fly the mission. As turbine inlet temperature increased from 1204° to 1704° C (2200° to 3100° F), payload increased 4.3 percent (fig. 31(a)). Design compressor pressure ratio increased from 9.4 to 11 (fig. 31(b)). The tendency of higher turbine inlet temperature to increase primary stream noise was counteracted by increases in bypass ratio (fig. 31(c)) and fan pressure ratio (fig. 31(d)). Design engine airflow decreased 2 percent (fig. 31(e)). All the above trends combined to decrease installed engine weight by 4.3 percent (fig. 31(f)).

A comparison of the number of passengers the methane-fueled SST could carry when the afterburning turbojet, nonafterburning turbojet, or duct burning turbofan engines were used is shown in figure 32. Without noise restrictions, the number of passengers increases by 11 percent as turbine-inlet temperature is increased from 1204° to 1704° C (2200° to 3100° F). Although the effect of cycle was not great, the duct burning turbofan was superior at lower values and the nonafterburning turbojet was superior at the higher values of turbine inlet temperature. With takeoff and community noise restrictions, the duct burning turbofan did significantly better than either turbojet at all temperatures considered. By increasing design turbine inlet temperature, the number of passengers for the duct burning turbofan powered SST increased by 4 percent. Thus, the benefits of high turbine inlet temperature were markedly affected by the takeoff noise limits. The major difference was the consequence of noise restrictions forcing the use of larger engines operating at part throttle during takeoff. The differences could be minimized (curves without noise restrictions approached) by development of effective jet noise suppressors having little thrust and weight penalty.

Figure 33 shows the effect that increasing the turbine inlet temperature has on direct operating cost. Without noise restrictions, the DOC decreased by 14 percent when turbine inlet temperature was increased from 1204° to 1704° C (2200° to 3100° F). The afterburning turbojet is superior at lower values of turbine inlet temperature, and the nonafterburning turbojet is superior at higher values. The DOC for the duct burning turbofan powered SST was approximately 7 percent greater than that for the afterburning turbojet powered SST because of higher duct burning turbofan engine cost.

Figure 34 is for a different SST, the 340 000 kilogram (750 000 lb) gross weight Boeing 2707. The prototype airplane was to be powered by afterburning turbojets. Range was very adequate but sideline noise was excessive. Using a full afterburner takeoff, sideline noise was 128 PNdB

or 20 PNdB above the FAR 36 requirement of 108 PNdB. Noise could have been lowered by installing larger engines and taking off at part power but this would have resulted in a large range penalty. The other curves are for a nonafterburning turbojet, a duct burning turbofan, and an afterburning turbofan. The afterburning turbofan gives the best results but the range penalty at FAR 36 is still excessive. The dashed curve indicates that if the afterburning turbofan engine is equipped with a jet noise suppressor that gives 6 dB of suppression for a 6 percent thrust loss, the FAR 36 noise requirement can be met with an acceptable range penalty.

FIGHTER AIRPLANE

A fighter pilot able to enter an engagement at a higher energy level than his opponent, and maintain this superiority, will have an offensive maneuvering advantage. The same result can be accomplished with an excess of power, for the pilot who is at a lower energy level but has the greater excess power will quickly ascend to an advantageous energy level. Energy maneuverability (EM) is the name given a process of energy management, whereby comparisons are made of energy and power of competing aircraft; manipulations are also performed to maximize each aircraft's capabilities throughout its speed-altitude envelope.

Specific Excess Power Concept

EM is based on principles of mechanics available since the time of Newton. Major John Boyd, an Air Force tactician, discovered how these relationships could be used to evaluate the maneuvering abilities of competing aircraft (ref. 23). Specific energy is the sum, per unit weight, of potential and kinetic energy. The time rate of change of specific energy is specific excess power (P_S), a quantity that characterizes a system's ability to change energy levels. The equations of flight mechanics put P_S in terms of easily measurable quantities (fig. 35).

In figure 36(a), the 1-g specific excess power overlays compare Lockheed's CL-981 with its F104G's. The contours are lines of constant specific excess power. Note how at every point the CL-981 has some numerical specific excess power advantage over the F104G. A follow on relationship (fig. 36(b)) is then obtained by generating contours of constant differential specific excess power of the two aircraft. These contours show where each airplane has its greatest maneuvering advantage. In combat, a pilot should always attempt to fight an opponent where his differential increment in specific excess power is greatest, and avoid negative regions where his opponent would have the advantage. Even now pilots study energy maneuverability profiles of their airplane and the enemy's, learning which flight regimes give them the advantage and which do not. Simulator studies have shown time and again that the man that has this information in a fight will beat the man that does not.

Engine Optimization

For the fighter aircraft, the specific excess power requirements lead to the selection of engine design parameters including engine size much as noise requirements dictated engine design for the commercial aircraft discussed in previous sections. This is illustrated in the next three figures for a fighter having a TOGW of 18 100 kilograms (40 000 lb) and a takeoff wing loading of 3830 newtons per square meter (80 lb/sq ft).

In figure 37, thrust loading is plotted against bypass ratio with lines of constant mission radius and various P_S requirements specified by Mach number, altitude, g condition, and thrust setting. The P_S for M0.9/30K/5g Mil is the most demanding and if enforced would result in an unacceptable mission radius. The next most demanding P_S requirements are those for M0.9/30K/1g Mil and M0.9/30K/5g Max AB. These can be satisfied if a BPR of about 0.8 is selected. Relative mission radius is seen to be 100.

In figure 38, BPR is 0.8 and turbine inlet temperature is 1316° C (2400° F). Discarding the M0.9/30K/5g Mil P_S requirement, it appears that an overall pressure ratio of 23 or greater will satisfy the second most demanding P_S requirement at M0.9/30K/5g Max AB. Again relative mission radius is about 100.

In figure 34, BPR is 0.8 and OPR is 23. The critical P_S requirement is again for M0.9/30K/5g Max AB and can be satisfied with a turbine inlet temperature of 1316° C (2400° F). The proper engine size is found from the maximum thrust loading for the selected points from the last three figures. By inspection it is 1.1 so that 196 000 newtons (44 000 lb) of thrust are required. The other parameters are: BPR is 0.8, OPR is 23, and turbine inlet temperature is 1316° C (2400° F). If a relative mission radius less than 100 is desired, TOGW and engine size could be decreased.

CONCLUDING REMARKS

In this paper the procedures that are used to select engines for transport and combat aircraft have been reviewed by illustrating the procedures for a long haul CTOL transport, a short haul VTOL transport, a long range SST, and a fighter aircraft. For the CTOL transport, it was shown that advances in noise technology and advanced turbine cooling technology will greatly reduce the airplane performance penalties associated with achieving low noise goals (as much as 20 PNdB below the FAR 36 requirement). A remote lift fan powered by a turbofan air generator was considered for the VTOL transport. In this case, the lift fan pressure ratio which maximized payload also came closest to meeting the noise goal of 95 PNdB at 152 meters (500 ft). High turbine temperature in three different engines was considered for the SST. Without noise constraints it led to an appreciable drop in DOC, but with noise constraints the reduction in DOC was very modest. For the fighter aircraft, it was

shown how specific excess power requirements play the same role in engine selection as noise constraints for commercial airplanes.

APPENDIX A

SYMBOLS

A	area
AR	aspect ratio
BPR	bypass ratio
C	blade chord
D	drag, diameter
D_{ff}	diameter of front flange
D_{rf}	diameter of rear flange
DMOPR	diameter correction for overall pressure ratio
F	thrust
FPR	fan pressure ratio
f	fuel-air ratio
H	height, total enthalpy
IGV	inlet guide vane
KDY	diameter correction for technology level (year)
K_{gg}	ratio of gas generator weight to total weight
KM	Mach number correction factor
KT_3	turbine temperature correction factor
KW_a	airflow correction factor
KY	technology correction factor
KBPR	bypass ratio correction factor
KDUCT	duct correction factor
KIGV	length correction for inclusion/exclusion of fan IGV
KLBPR	length correction for bypass ratio
KLIFE	life correction factor

KLOPR	length correction for overall pressure ratio
KLW_a	length correction for airflow size
KLY	length correction for technology level (year)
KOPR	overall pressure ratio correction factor
L	axial length, lift
M	Mach number
N	number of stages, rings; rotational speed
OPR	overall pressure ratio
P	pressure
PNdB	perceived noise decibels
R	range, gas constant
S	axial spacing; clearance
SFC	specific fuel consumption
SLS	sea level static
SPL	sound pressure level
T	temperature
TOGW	takeoff gross weight
TBO	time between overhaul
U	wheel speed
V	velocity
W	weight
W_{tot}	total weight of engine
w	weight flow rate
w_a	airflow of gas generator
w_o	total fan face airflow
δ	corrected pressure

θ corrected temperature

ξ loss coefficient, energy loss to ideal energy ratio

σ solidity

Subscripts:

A controls and accessories

a air

B burner

bare bare engine

C compressor

CMD constant mean diameter

cr cruise

D fan duct

d duct

e engine

F fan

f fuel

h hub

L acoustic lining

M mean

max maximum

R rotor

r splitter ring

ref reference

S stage; structure

s stator

T turbine

t tip

VMD varying mean diameter

w wall

x axial

0 free stream

1 inlet; compressor inlet

2 outlet, compressor outlet

3 turbine inlet

4 turbine outlet

Superscript:

$\bar{}$ average

APPENDIX B

CALCULATION OF ENGINE PERFORMANCE

In order to calculate engine performance at design and off design conditions, it is necessary to specify design point parameters (airflow, turbine temperature, pressure ratio, bypass ratio, fan pressure ratio, component efficiencies and pressure drops) and have available component performance maps.

Before the advent of computers, matching of components was done graphically to obtain off-design performance (ref. 22). The example discussed here is for a simple turbojet (fig. B1). The relations which must be satisfied deal with continuity of flow, rotational speed, and power. The relations are:

Continuity	Speed	Power
$w_C = w_T = w$	$N_C = N_T = N$	$w\,\Delta H_C = w\,\Delta H_T$
$\frac{w\sqrt{\theta_1}}{\delta_1}\,\frac{N}{\sqrt{\theta_1}}\,\frac{1}{\frac{P_2}{P_1}\,\frac{P_3}{P_2}} = \frac{wN}{\delta_3}$	$\frac{(N/\sqrt{\theta_1})^2}{(N/\sqrt{\theta_3})^2} = \frac{T_3}{T_1}$	$\frac{\Delta H_C}{N^2} = \frac{\Delta H_T}{N^2}$

To facilitate matching, the compressor and turbine performance are plotted as shown in figure B2. When the maps are overlaid and the axes alined, each point represents a match point satisfying the relations of continuity, speed, and power. The turbine temperature ratio can be calculated from the speed relation. The other parameters can be obtained from auxiliary plots. For example, compressor airflow can be obtained from a compressor plot of $\Delta H_C/N^2$ against $(w\sqrt{\theta}/\delta)$, for lines of constant $N/\sqrt{\theta_1}$. The information obtained from component matching yields the pumping characteristics shown in figure B3. If an engine operating condition is specified (e.g., T_3 = 1089° C (2000° F) and $N = N_{design}$) and a flight condition (e.g., $M_0 = 2$ and Alt = 15 200 m (50 000 ft)), the thrust and specific fuel consumption of the engine can be calculated. Engine operation and flight condition permit T_3/T_1 and $N/\sqrt{\theta_1}$ to be calculated. The rest of the information needed to calculate thrust and specific fuel consumption is then obtained from the pumping characteristics.

The off-design performance calculations can be done much faster using digital computers. Reference 8 describes a digital computer program which is capable of running both design and off-design points for turbojet and turbofan engines. Component performance maps are reduced to tabular form to provide a base for calculating component performance. The design point is run first and map correction factors are calculated to scale the components to the desired performance. These correction factors are then applied to the component performance maps at off-design points. Initially, when the program is running at an off-design point,

the components are not matched (do not satisfy the continuity, speed, and power relations) and errors (for example, work required by the compressor minus work supplied by the turbine) are generated. Small changes in each engine independent variable (for example, compressor speed) then produce small changes in the errors and these differential changes are loaded in a matrix. The matrix is then solved for the set of independent variables which result in zero errors, thus matching the components. This process may be repeated several times before matching occurs because there is a nonlinear relation between the independent variables and the errors.

APPENDIX C

CALCULATION OF ENGINE WEIGHT AND DIMENSIONS

The material in this appendix is a summary of the approach presented in reference 9.

Weight

Semiempirical correlations of engine weights and dimensions were developed using data for over 350 engines spanning the 1940 to 1980 time period. Corrections were made for parameters such as airflow, bypass ratio, pressure ratio, turbine temperature, design flight Mach number, and technology level (year) to normalize the weights and dimensions. The resulting correlations have proved to be very useful for performing engine/airplane optimization analyses.

Ratio of gas generator weight to total weight. - Certain engine design variables such as overall pressure ratio and turbine inlet temperature affect the gas generator section of the engine only and have a negligible effect on the fan section of the engine. In reference 9, the fan section of the engine was assumed to consist of the fan and fan casing, turbines required to drive the fan, and the fan spool shafts and bearings. All remaining weight (including that of any low pressure compressor stages on the fan spool) was assigned to the gas generator section. The ratio of gas generator weight to total weight was defined as K_{gg}.

The variation of K_{gg} with bypass ratio was determined from weight breakdowns obtained for 14 different engine designs. The resulting variation of K_{gg} with bypass ratio is shown in figure C1.

Overall compressor pressure ratio. - Overall compressor pressure ratio (defined as compressor exit total pressure divided by fan face total pressure) primarily affects the weight of the compressor, burner, and high pressure turbine sections of an engine. The predominant effects of increasing compressor pressure ratio are increases in the number of compressor and turbine stages and increases in pressure and temperatures throughout most of the gas generator section of the engine. Therefore, as pressure ratio increases, casing and structural weights increase as a result of higher working pressures and necessary material substitutions in the higher temperature areas. Shafting and bearing weights also tend to increase. Figure C2 shows the pressure ratio correction factors which give the best statistical fit of the data. Straight line relations between KOPR and OPR were used over most of the pressure ratio range. However, it was found that a flattening of the slope of KOPR at the low pressure ratios gave a better fit to the statistical data. Rationalizations which could explain this are as follows: (1) As pressure ratio is reduced below a certain point, increased combustor volume (weight) begins to significantly counteract the decrease in weight due to the reduction

in compressor stages, and (2) when the point is reached where a single stage high pressure turbine can drive the compressor, further reductions in pressure ratio will not significantly reduce HP turbine weight (and may even increase it as annulus area increases). The lower slope of KOPR against OPR for low values of OPR was further confirmed by the results of several lift engines design studies by the engine manufacturers.

Turbine inlet temperature. - A general trend of increasing turbine inlet temperature (T_3) with time has been observed as shown in figure C3. This is as would be expected since one of the main efforts of engine manufacturers is to design engines with higher values of T_3 because of the improvements this gives to several important engine characteristics. The higher thermal stresses and lower allowable stresses which accompany this temperature increase would be expected to result in increases in engine weight. However, significant advances have been made over the years in the development of materials and blade cooling techniques which have enabled T_3 to increase without penalizing weight as much as might be expected. In this correlation, a representative line was plotted through the data on the T_3 against year curve (labeled T_{3R} in fig. C3). This was taken as the reference value of T_3 for a given year at which there will be no penalty on engine weight.

However, at any given state of technological development, represented by a given year of first flight, it should be expected that as design T_3 increases, engine weight will also increase due to lowered material allowables, higher thermal stresses, and the requirement for more complex cooling schemes. A rate of change of gas generator specific weight of 3 percent per 55.6° C (100° F) increment in T_3 was found to give the best fit of the statistical data. This is represented in figure C4 as KT_3 against $(T_3 - T_{3R})$.

Gas generator scaling. - Engine weights are generally scaled by airflow (or thrust which is the same, assuming constant nozzle velocity for any thrust size). Therefore, for any given engine design, the following gas generator weight scaling expression may be applied:

$$\frac{WT}{WT_{ref}} = \left(\frac{w_a}{w_{a_{ref}}}\right)^n$$

where "ref" relates to the airflow size at which the engine design was actually laid out. The schedule chosen for the weight correlation (fig. C5) was influenced to a large extent by the manufacturers' data but was also adjusted to give the best fit with the statistical data. The curve for $w_a > 69$ kg/sec (150 lb/sec) corresponds to a scaling exponent of 1.2.

Scaling with total airflow. - A survey of data from several of the engine manufacturers indicated that fans tend to scale with an exponent

in the order of n = 1.3. This value is currently used in the correlation. For the purpose of the correlation, all engines were scaled to a primary airflow size of 68 kilograms per second (150 lb/sec), and a separate correction, KBPR, was applied to normalize the engines to a common bypass ratio of 0. Performing the airflow scaling at constant bypass ratio made it possible to represent the fan section scaling in terms of primary airflow. According to the assumed scaling law

$$\frac{(WT_{\text{fan section}})_2}{(WT_{\text{fan section}})_1} = \left(\frac{w_{02}}{w_{01}}\right)^{1.3} = \left(\frac{w_{a2}}{w_{a1}}\right)^{1.3}$$

$$KW_0 = \frac{(WT_{\text{fan section}})_2/w_{02}}{(WT_{\text{fan section}})_1/w_{01}} = \left(\frac{w_{a2}}{w_{a1}}\right)^{1.3-1.0} = \left(\frac{w_{a2}}{w_{a1}}\right)^{0.3}$$

Bypass ratio. - Engine specific weight decreases with increasing bypass ratio. This is due to the fact that, as bypass ratio increases the portion of total fan inlet airflow which bypasses the gas generator progressively increases. Thus, the portion of the total airflow which must pass through the relatively heavy (in terms of weight per airflow) primary section of the engine decreases. The variation of engine specific weight with bypass ratio which resulted in the best fit of the statistical data is shown in figure C6.

Year. - It is well known that, due to advances in technology over the years, the engine companies have been able to design and build progressively lighter engines with equivalent cycles. Lighter, stronger materials such as titanium have replaced heavier steels in many engine components. It is now possible to aerodynamically load compressor and turbine stages to higher levels and hence to reduce the number of stages required for a given pressure ratio. Higher wheel speeds available because of improved materials and high Mach blading have also increased pressure ratio per stage. Many other advances have also contributed to the reduction in specific weight. In addition to the effect of year allowed in the turbine inlet correction, a factor KY is applied to the whole engine to account for general advances in the state-of-the-art which affect all areas of the engine design. The trend in KY which gave the best fit to the statistical data is presented in figure C7.

Life. - If all other parameters are held constant, engine weight is a function of design life, with shorter life engines weighing less than longer life engines. For the purpose of the correlation, cruise engines in the data were classified in three general categories: short, medium, or long life. Engines which were known to have been designed for relatively short life, such as drone engines, fighter engines, and lift/cruise engines, were classified as "short life." Engines which were designed for long range cruise application or which were known to have achieved very high TBO's were classified as "long life." Engines in

between these two extremes, and those for which no TBO information was readily available, were classified as "medium life" engines.

The factors for life, KLIFE, which resulted in the best correlation of the statistical data are summarized below:

Engine type	Life correction, KLIFE
Lift engines	0.44
Short life	.90
Medium life	1.00
Long life	1.07

Flight Mach number. - Engines designed to operate at high supersonic flight speeds will tend to be heavier than subsonic and low supersonic designs, primarily due to the higher operating temperatures. The correction for flight Mach number is shown in figure C8. The correction is 1.0 at Mach 2 and below since design conditions which affect engine weight tend to be equivalent between a typical SLS takeoff operating point and a typical Mach 2 operating point.

Fan duct configuration. - Long duct versions of an engine weigh more than short duct versions. The following factors are used in this weight estimation procedure.

Short duct: KDUCT = 1.00

Long duct: KDUCT = 1.07

Calculation of engine weight. - The procedure for using the correlation to predict the weight of an engine with any combination of the variables w_a, BPR, T_3, OPR, etc. is summarized below:

$$W_{tot} = 14W_a(KENG)[K_{gg}(KHP) + (1 - K_{gg})(KLP)]$$

where

$$KENG = (KBPR)(KY)(KLIFE)(KM)(KDUCT)$$

$$KHP = (KT_3)(KOPR)(KW_a)$$

$$KLP = KW_0$$

Dimensions

The procedures used to calculate the bare dimensions of cruise engines are as follows:

$$L_{bare} = \begin{matrix} 2.16 \\ \text{or} \\ 85 \end{matrix} (KLW_a)(KLBPR)(KLY)(KLOPR)(KIGV) \quad \begin{matrix} m \\ \text{or} \\ \text{in.} \end{matrix}$$

where

KLW_a correction for airflow size (fig. C9)

KLBPR correction for bypass ratio (fig. C10)

KLY correction for technology level (fig. C11)

KLORR correction for overall cycle pressure ratio (fig. C12)

KIGV correction for inclusion/exclusion of fan IGV

1.04 with IGV if BPR > 2.5

0.96 without IGV if BPR < 2.5

1.00 otherwise

$$D_{ff} = D \text{ fan tip} + \begin{matrix} 7.62\times10^{-2} \text{ m} \\ \text{or} \\ 3 \text{ in.} \end{matrix}$$

where

D fan tip = f(fan face M, hub/tip, and corrected airflow)

$$D_{rf} = \left[(A)\sqrt{w_a} + \begin{matrix} 7.62\times10^{-2} \text{ m} \\ \text{or} \\ 3 \text{ in.} \end{matrix} \right] \text{ for turbojets and short duct turbofans}$$

where

A = f(BPR), fig. C13

or

$$D_{rf} = \left[(A)\sqrt{w_a} + \begin{matrix} 7.62\times10^{-2} \text{ m} \\ \text{or} \\ 3 \text{ in.} \end{matrix} \right] + C + \begin{matrix} 7.62\times10^{-2} \text{ m} \\ \text{or} \\ 3 \text{ in.} \end{matrix} \text{ for long duct turbofans}$$

where

$A\sqrt{w_a} + \begin{matrix} 7.62\times10^{-2} \text{ m} \\ \text{or} \\ 3 \text{ in.} \end{matrix}$ duct inside diameter

C $D_{do} - D_{di}$: specified by duct corrected flow and Mach number over turbine

M 0.35 for nonduct burning turbofans

  0.16 for duct burning turbofans

D_{max} D_{ff} for short duct turbofans

  greater of D_{ff} or D_{rF} for long duct turbofans

  $(DMOPR)(KDY)\sqrt{w_a}$ for turbojets

where

DMOPR $f(OPR,w_a)$, fig. C13

KDY $f(Y)$, fig. C14

APPENDIX D

EMPIRICAL EXPRESSIONS FOR ESTIMATING LENGTH AND WEIGHT OF AXIAL FLOW COMPONENTS OF VTOL POWERPLANTS

The expressions for estimating the length and weight of axial flow components for use in parametric analysis of powerplants suitable primarily for VTOL transport aircraft presented herein are from reference 19. These expressions were developed from correlated lift and cruise engine data with the aid of simplified component models. Components involved include: fan, fan duct, compressor, burner, turbine, structure, and accessories. Because of differences in reported details as well as in design approaches, considerable variability was noted in the component data. However, when comparisons were made between estimated and actual total engine weight for several representative engines, good agreement was found for nearly all cases considered.

The weight of the fan is calculated from:

$$W_F = K_F(D_t)^{2.7} \frac{N}{(AR)_{X,R}^{0.5}} \left(\frac{\sigma_t}{\sigma_{t,ref}}\right)^{0.3} \left(\frac{U_t}{U_{t,ref}}\right)^{0.3} \tag{D1}$$

where $\sigma_{t,ref} = 1.25$, $U_{t,ref} = 350$ meters per second (1150 ft/sec) and $K_F = 135$ (12 for D_t in ft, W_F in lb). The fans included in the correlation primarily had solid titanium blades. Significant reductions in fan weight may be possible with hollow blade construction or the use of composite materials. In order to reflect these advanced design techniques, adjustments to the value of K_F may be made in the fan weight equations.

The weight of the duct casing was estimated by the simplified expression:

$$W_D = \pi \bar{D}_D L_D \left(\frac{W}{A}\right)_D \tag{D2}$$

where $\bar{D}_D$ is the average diameter (between inlet and outlet) of the duct casing. Values of duct weight per unit surface area, $(W/A)_D$, from engine data varied from 2.4 kilograms per square meter (0.5 lb/ft^2) to 8.3 kilograms per square meter (1.7 lb/ft^2). A value of 3.5 kilograms per square meter (0.72 lb/ft^2) was taken to be representative of current design practice for low pressure lift fans. This corresponds to aluminum (ρ = 2770 kg/m^3, 173 lb/ft^3) with a thickness of 0.13 centimeter (0.05 in.).

Acoustic lining is generally applied to the duct walls as well as to splitter rings concentric to the duct walls. The weight of the acoustic lining is calculated from:

$$W_L = A_L\left(\frac{W}{A}\right)_L \tag{D3}$$

where the area of the acoustic lining, A_L, is a function of length, diameter, and number of splitter rings, N_r:

$$A_L = \pi\left[L_{\substack{\text{inner}\\\text{wall}}}\bar{D}_h + L_{\substack{\text{outer}\\\text{wall}}}\bar{D}_t\right] + \pi\sum_{i=1}^{N_r} L_{r,i}D_{r,i} \tag{D4}$$

and

$$\left(\frac{W}{A}\right)_W = 2.69\ \text{kg/m}^2\ (0.55\ \text{lb/ft}^2) \qquad \text{for the walls}$$

$$\left(\frac{W}{A}\right)_r = 8.55\ \text{kg/m}^2\ (1.75\ \text{lb/ft}^2) \qquad \text{for the splitter rings}$$

The data for the compressor were obtained from compressors with both fixed and variable angle stators, constant hub, mean, and tip flow path designs, as well as both disk and drum construction. In order to estimate compressor length, the ratio of length to inlet mean diameter was correlated with the number of stages and inlet hub-tip diameter ratio to give:

$$\frac{L_C}{D_{M,1}} = 0.2 + \left[0.234 - 0.218\left(\frac{D_h}{D_t}\right)_1\right]N \tag{D5}$$

The number of stages is related to overall compressor pressure ratio and average stage pressure ratio by:

$$\left(\overline{\frac{P_2}{P_1}}\right)_S = \left[\left(\frac{P_2}{P_1}\right)_C\right]^{1/N} \tag{D6}$$

For constant blade loading, the average stage pressure ratio will be a function of the inlet corrected rotor tip speed. Because of reheat effects it will also depend on the overall compressor pressure ratio. An expression relating inlet corrected rotor tip speed to average stage pressure ratio and overall pressure ratio was deduced from simplified compressor aerodynamic considerations.

$$\left(\frac{U}{\sqrt{\theta}}\right)_{C,CMD} = A\left[\left(\overline{\frac{P_2}{P_1}}\right)_S + C(P_2/P_1)_C^{1.8} - B\right] \tag{D7}$$

where the factor A was taken as 466 (or 1530 for $(U/\sqrt{\theta})_{C,CMD}$ in ft/sec). Factor B is used to reflect blade loading level. Two levels were con-

sidered: high and moderate. Corresponding values of B were taken as 0.676 and 0.588, respectively. Factor C was taken as 0.654×10^{-3}. This relation was taken to hold for constant mean diameter compressors.

An adjustment to the average stage pressure ratio was developed to account for the effect of a varying mean diameter design. This adjustment is required because the stage rotor blade speeds (and thus the performance) will be different than for the case of a constant mean diameter compressor with the same inlet tip speed. The average stage pressure ratio for compressors with varying mean diameters was deduced as:

$$\left(\frac{\overline{P_2}}{P_1}\right)_{S,VMD} = \left[0.8\left(\frac{D_{M,2}}{D_{M,1}}\right)_C + 0.2\right]\left[\left(\frac{\overline{P_2}}{P_1}\right)_{S,CMD} - 1\right] + 1 \qquad \text{(D8)}$$

Equations (D7) and (D8) were then combined to give a general expression for inlet corrected tip speed:

$$\left(\frac{U}{\sqrt{\theta}}\right)_C = A\left\{\frac{\left[\left(\frac{\overline{P_2}}{P_1}\right)_S - 1\right]}{\left[0.8\left(\frac{D_{M,2}}{D_{M,1}}\right) + 0.2\right]} + 1 + \frac{\left(\frac{P_2}{P_1}\right)_C^{1.8}}{C}\right\} - B \qquad \text{(D9)}$$

where $(\overline{P_2}/P_1)_S$ is found from equation (D6) and A, B, and C are given with equation (D7).

Compressor weight is calculated from

$$W_C = K_C(D_M)^{2.2}\, N^{1.2}\left[\frac{U_t}{(U_t)_{ref}}\right]^C\left[1 + \frac{(L_C/D_{M,1})}{(L_C/D_{M,1})_{ref}}\right] \qquad \text{(D10)}$$

where

K_C 15.5 (2.5 for D_M in ft) for lift engines

K_C 24.2 (3.9 for D_M in ft) for cruise engines

C 0.5 or less

$(U_t)_{ref}$ 335 m/sec (1100 ft/sec)

The compressor weight is taken to include the rotor blades, disks (or drum), seals, stator blades, and casing.

The burners considered were annular axial-flow or reverse-flow designs. Included in this component are the diffuser (inlet transition) and the outlet transition sections. Burner length is calculated from:

$$L_B = \frac{R}{\pi V_{ref}} \left[\left(\frac{L_B}{H} \right) \left(\frac{wT_1}{P_1 \bar{D}_M} \right) \right] \qquad \text{(D11)}$$

where

V_{ref} 18.3 m/sec (60 ft/sec) for cruise engines

V_{ref} 24.4 m/sec (80 ft/sec) for lift engines

The burner weight includes the inner and outer casing, liner, and fuel nozzles. Burner weight is calculated from:

$$W_B = K_B \bar{D}_M^2 \left[\frac{(L_B/H)}{(L_B/H)_{ref}} \right]^{0.5 \text{ to } 1.0} \qquad \text{(D12)}$$

where

K_B 195 (40 for $\bar{D}_M$ in ft, W_B in lb) for lift engines

K_B 390 (80 for $\bar{D}_M$ in ft, W_B in lb) for cruise engines

$(L_B/H)_{ref}$ 1.6 for left engines and 3.2 for cruise engines

Turbine data were obtained from engines with one, two, and three spools with various flowpath designs. In terms of the average axial chord length and average clearance, the turbine length (excluding possible exit straightening vanes) is given by:

$$L_T = N_T(\bar{C}_{X,R} + \bar{C}_{X,S}) + (2N_T - 1)\bar{S}_T \qquad \text{(D13)}$$

where

$$\bar{C}_X = \frac{\bar{D}_t - \bar{D}_h}{2\overline{AR}_X} \qquad \text{(D14)}$$

and

$$\overline{AR}_X = A + B(\overline{D_L/D_T}) \qquad \text{(D15)}$$

Values for the factors A and B are given in the following table.

CONSTANTS IN TURBINE BLADE ASPECT RATIO EQUATION

Turbine rotor	A	B
Turbofan engines (cruise and lift)		
High and intermediate pressure spool	10.45	-10.00
Low pressure spool[a]	13.36	-11.78
Lift jet engines		
High and low pressure spools	6.1	-5.5

Turbine stator (All engine types)	A	B
High pressure spool	6.45	-5.97
Low and intermediate pressure spool	10.95	-10.9

[a]Note: In this case, AR_X is limited to a maximum value of 6.

The average clearance between blade rows was assumed to be proportional to the average rotor axial chord:

$$\overline{S}_T = a_T \overline{C}_{X,R} \tag{D16}$$

For the turbine data investigated, the proportionality constant was found to vary from 0.2 to 1.0. Since length will be critical for VTOL powerplants, a value of 0.3 or 0.4 can be considered representative for high and low pressure turbines.

The turbine weight includes the rotor disk and blades, stator blades, seals, and casing. Turbine weight is calculated from:

$$W_T = K_T(\overline{D_M})^{2.5} N_T(\overline{U_M})^{0.6} \tag{D17}$$

where

K_T = 4.7 (0.26 for $\overline{D}_M$ in ft, $\overline{U}_M$ in ft/sec) for lift engines

K_T = 7.9 (0.44 for $\overline{D}_M$ in ft, $\overline{U}_M$ in ft/sec) for cruise engines

The use of lightweight materials, such as titanium rotor disks, as well as the reduced design life for lift engines seemed to account for this difference in weight.

Control and accessory weight includes the fuel and control system, oil, and starting systems. Not included are airplane power takeoffs or variable geometry mechanisms for inlets and exhaust nozzles. The relations developed for this weight group were obtained from data for lift engines only. Control and accessory weight was calculated from:

$$W_A = K_A F[1 + A(SFC)] \qquad (D18)$$

where

K_A = 0.0002 (0.002 for F in lb and SFC in lb/hr lb)

A = 13.2 (1.35 for F in lb and SFC in lb/hr lb)

Equation (D18) can be applied to lift system exhaust gas generators by calculating thrust and SFC assuming the exhaust gas is expanded through a nozzle to ambient conditions. Similarly, the thrust and SFC for a lift system air generator can also be found by assuming the generator air as well as the exhaust gas are expanded through a nozzle to ambient conditions. Control and accessory weight for cruise powerplants was found to vary between 9 and 30 percent of the total engine weight compared to a range of from 2 to 10 percent for lift engines.

Structure weight includes the engine mounts, bearings, bearing supports, shafts, inner wall of fan duct (for turbofan engines) and transition sections. Structure weight is calculated from:

$$W_S = K_S \sum W_{components} \qquad (D19)$$

where

K_S = 0.10 for lift engines

K_S = 0.18 for cruise engines

Using the equations presented herein, a total powerplant weight can be determined by summing the estimated component weights including the structure weight. For example, the total weight of a lift turbofan engine may be expressed as:

$$W_{total} = W_F + (W_D + W_L) + W_C + (W_T)_{high} + (W_T)_{low} + W_A + W_S \qquad (D20)$$

REFERENCES

1. Thomas, B. K., Jr.: New Wing Promises Design Breakthrough. Aviation Week and Space Tech., vol. 87, no. 4, July 24, 1967, pp. 25-26.

2. Whitlow, John B., Jr.; Kraft, Gerald A.; and Civinskas, Kestutis C.: Parametric Engine Study for a Mach 0,98 Commercial Air Transport. NASA TM X-52961, 1971.

3. Kraft, Gerald A.; and Whitlow, John B., Jr.: Optimization of Engines for a Mach 0.98 Transport with Low Takeoff and Approach Noise Levels. NASA TM X-67865, 1971.

4. Whitlow, John B., Jr.; and Kraft, Gerald A.: Optimization of Engines for Commercial Air Transports Designed for Cruise Speeds Ranging from Mach 0.90 to 0.98. NASA TM X-67906, 1971.

5. Anon.: Jet Noise Prediction. Aerospace Information Report 876, SAE, July 10, 1965.

6. Anon.: Definitions and Procedures for Computing the Perceived Noise Level of Aircraft Noise. Aerospace Recommended Practice 865, SAE, Oct. 15, 1964.

7. Kramer, James J.; Chestnutt, David; Krejsa, Eugene A.; Lucas, James G.; and Rice, Edward, J.: Noise Reduction. Aircraft Propulsion. NASA SP-259, 1971, pp. 169-209.

8. Koenig, Robert W.; and Fishbach, Laurence H.: GENENG - A Program for Calculating Design and Off-Design Performance for Turbojet and Turbofan Engines. NASA TN D-6552, 1971.

9. Gerend, R. P.; and Roundhill, J. P.: Correlation of Gas Turbine Engine Weights and Dimensions. Paper 70-669, AIAA, June 1970.

10. Anon.: Standard Methods of Estimating Direct Operating Costs of Transport Airlines. Air Transport Assoc. of Amer., Aug. 1960.

11. Anon.: Study on the Feasibility of V/STOL Concepts for Short Haul Transport Aircraft. NASA CR-902, 1967.

12. Marsh, K. R.: Study on the Feasibility of V/STOL Concepts for Short-Haul Transport Aircraft. NASA CR-670, 1967.

13. Fry, Benard L.; and Zabinsky, Joseph M.: Feasibility of V/STOL Concepts for Short-Haul Transport Aircraft. NASA CR-743, 1967.

14. Lieblein, S.: A Review of Lift Fan Propulsion Systems for Civil VTOL Transports. Paper 70-670, AIAA, June 1970.

15. Kutney, J. T.: Propulsion System Development for V/STOL Transports. J. Aircraft, vol. 3, no. 6, Nov.-Dec. 1966, pp. 489-497.

16. Immenschuh, W. T.: XV-SA-A Lift Fan V/STOL Research Aircraft. Verti-Flite, vol. 11, May 1965, pp. 2-9.

17. Dugan, James F., Jr.; Krebs, Richard P.; Civinskas, Kestutis C.; and Evans, Robert C.: Preliminary Study of an Air Generator-Remote Lift Fan Propulsion System for VTOL Transports. NASA TM X-67916, 1971.

18. Krebs, Richard P.: Operational Procedure for Computer Program for Design-Point Characteristics of a Compressed-Air Generator with Through-Flow Combustor for V/STOL Applications. NASA TM X-2422, 1971.

19. Sagerser, David A.; Lievlein, Seymour; and Krebs, Richard P.: Experimental Expressions for Estimating Length and Weight of Axial-Flow Components Used in Analysis of VTOL Powerplants. NASA TM X-2406, 1971.

20. Haller, Henry C.; Lieblein, Seymour; and Auer, Bruce M.: Computer Program for Preliminary Design and Analysis of V/STOL Tip-Turbine Fans. NASA TN D-6161, 1971.

21. Koenig, Robert W.; and Kraft, Gerald A.: Influence of High-Turbine-Inlet-Temperature Engines in a Methane-Fueled SST when Takeoff Jet Noise Limits are Considered. NASA TN D-4965, 1968.

22. Dugan, James F., Jr.: Compressor and Turbine Matching. Aerodynamic Design of Axial-Flow Compressors. Irving A. Johnsen and Robert O. Bullock, eds., NASA SP-36, 1965, pp. 469-508.

23. London, Michael P.: Tactical Air Superiority. Space/Aeronautics, vol. 49, no. 3, Mar. 1968, pp. 62-71.

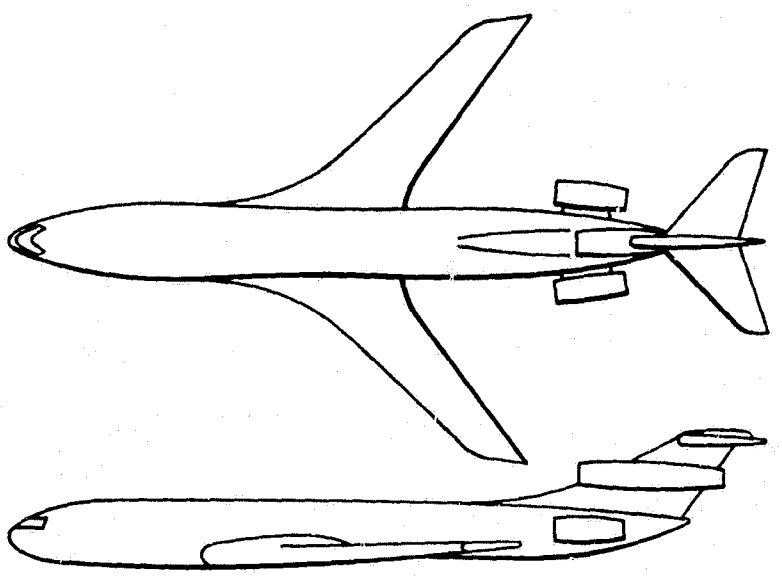

Figure 1. - Conceptual Mach 0.98 transport.

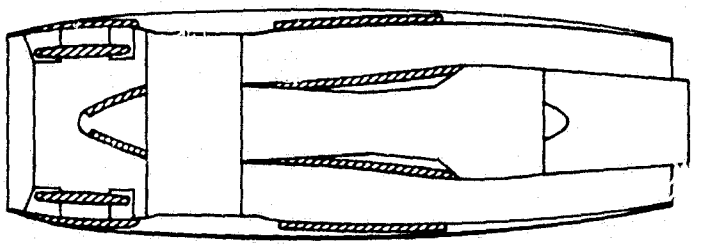

Figure 2. - Turbofan engine with acoustic treatment.

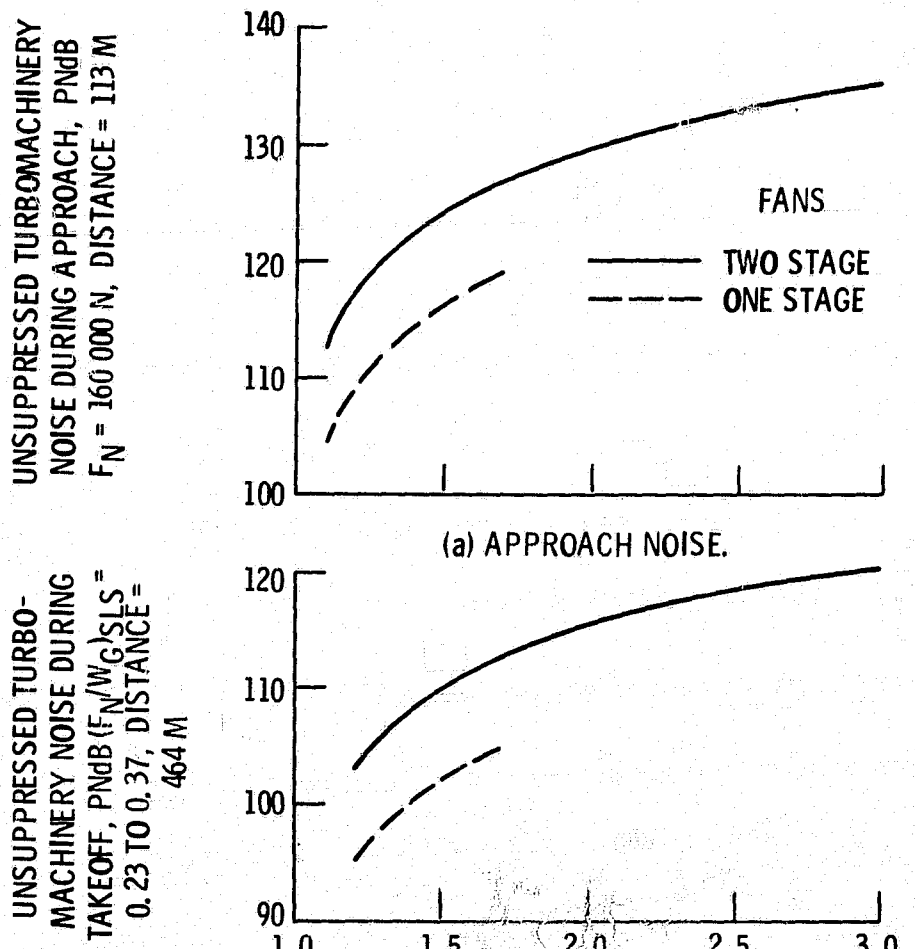

Figure 3. - Unsuppressed turbomachinery noise during approach and takeoff for one and two stage fan engines. Airplane TOGW = 175 000 kg. Noise numbers estimated to be within ±2 PNdB.

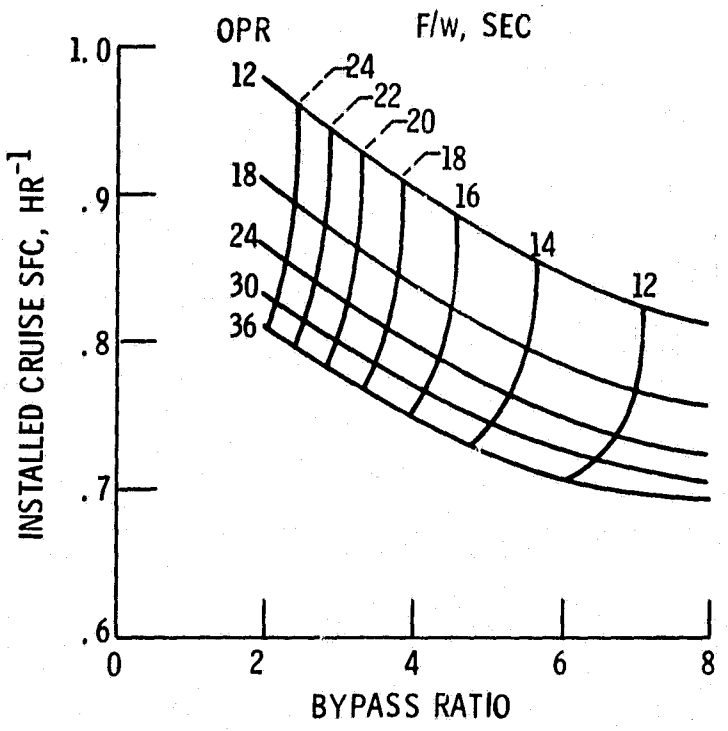

Figure 4. - Performance for cruise at Mach 0.98 and 12 200 m (40 000 ft); FPR = 1.5; T_4 = 1093° C (2000° F).

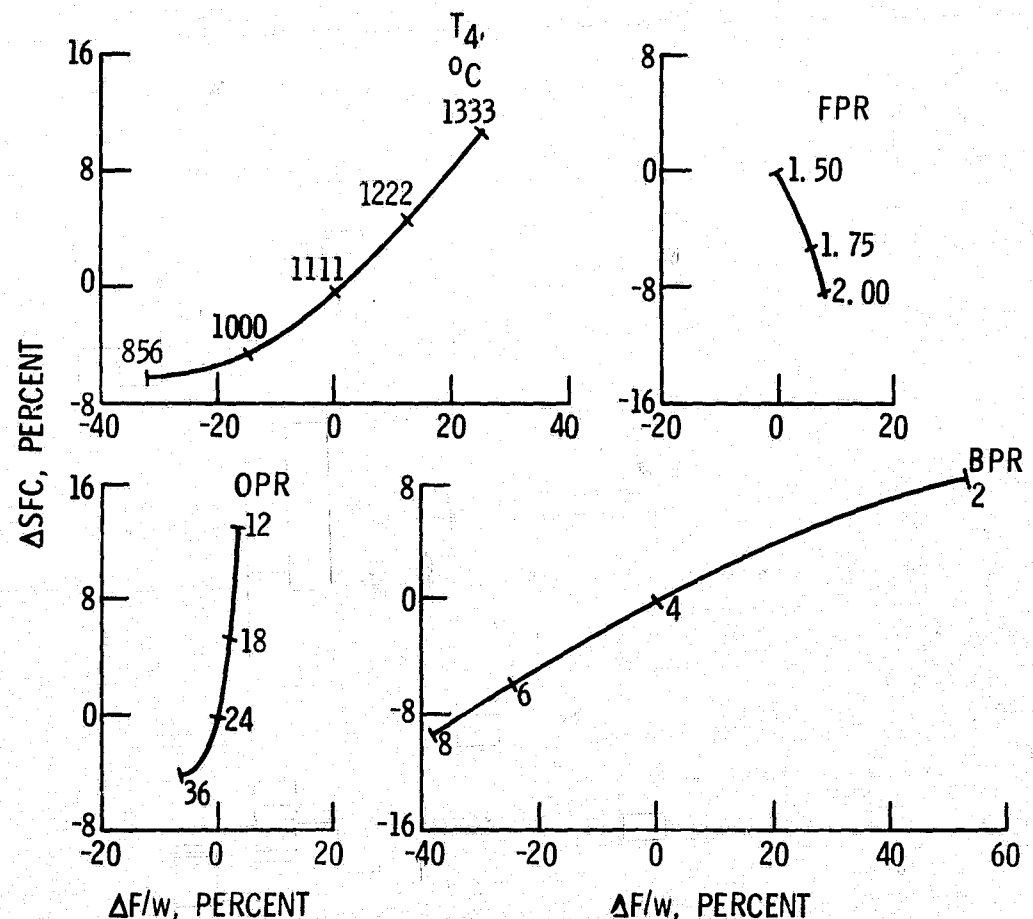

Figure 5. - Effect of engine parameters on cruise performance at Mach 0.98.

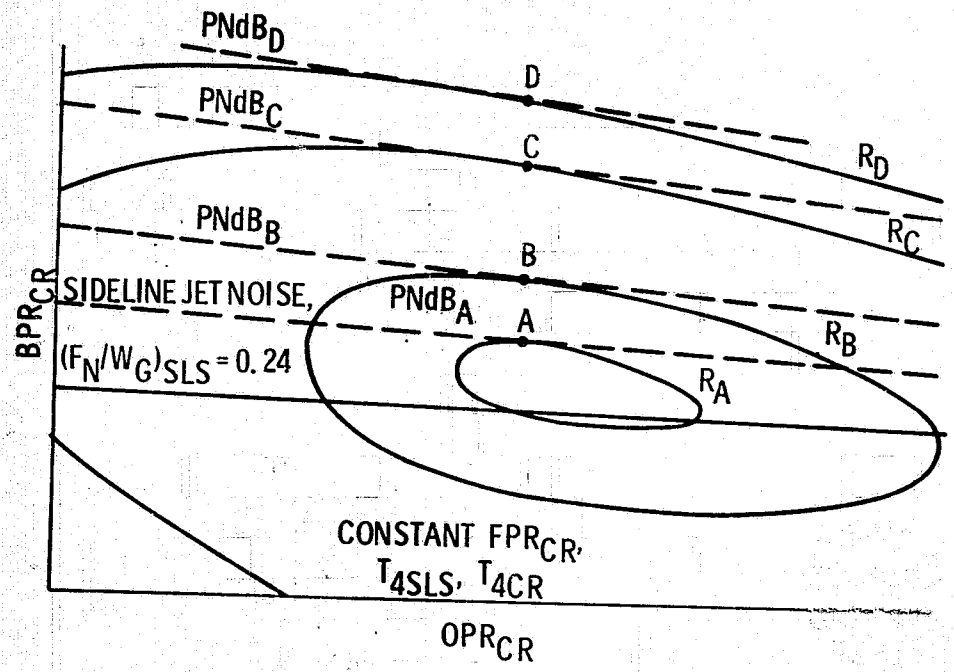

(a) "THUMBPRINT" PERFORMANCE PLOT. NO NOISE SUPPRESSION.

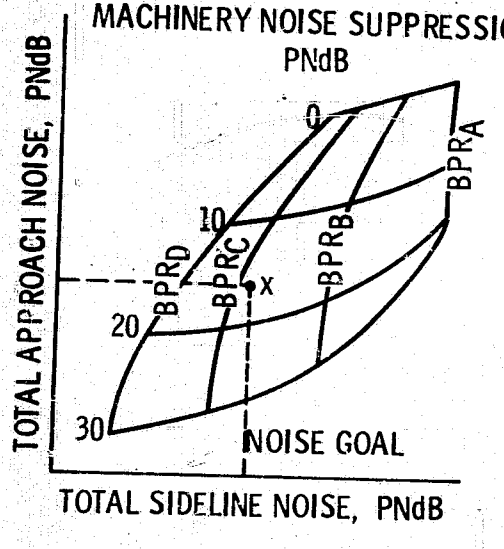

(b) TOTAL SIDELINE AND APPROACH NOISE RELATED TO AMOUNT OF FAN TURBOMACHINERY NOISE SUPPRESSION.

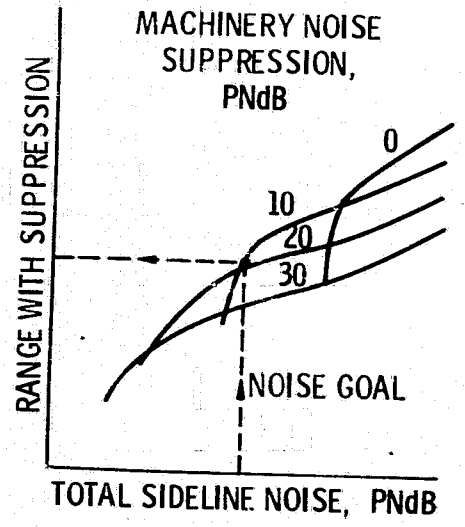

(c) RANGE WITH ACOUSTIC TREATMENT RELATED TO NOISE AND AMOUNT OF SUPPRESSION.

Figure 6. - Illustration of method used to select engine parameters that maximize range for a given noise goal and takeoff thrust constraint. Constant TOGW, PAYLOAD, FPR_{CR}, $T_{4_{SLS}}$, $T_{4_{CR}}$.

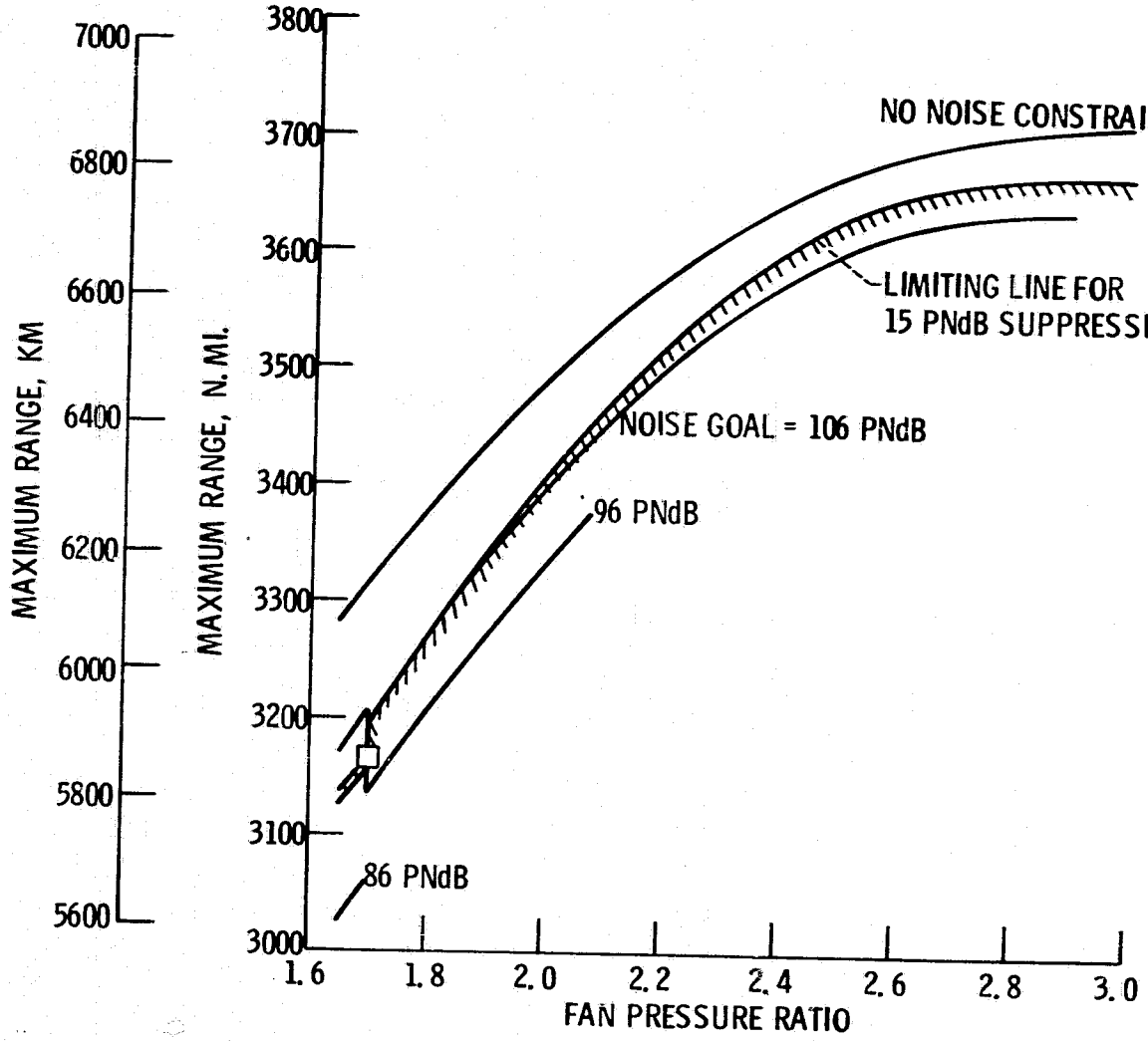

Figure 7. - Maximum total range versus fan pressure ratio for several noise goals. Suppression weight penalty included. Takeoff $T_4 = 1260^0$ C, cruise $T_4 = 1050^0$ C MN = 0.98, $\beta_{HPT} = 7.5$ percent, $\beta_{LPT} = 0$ percent, L/D varies with engine diameter.

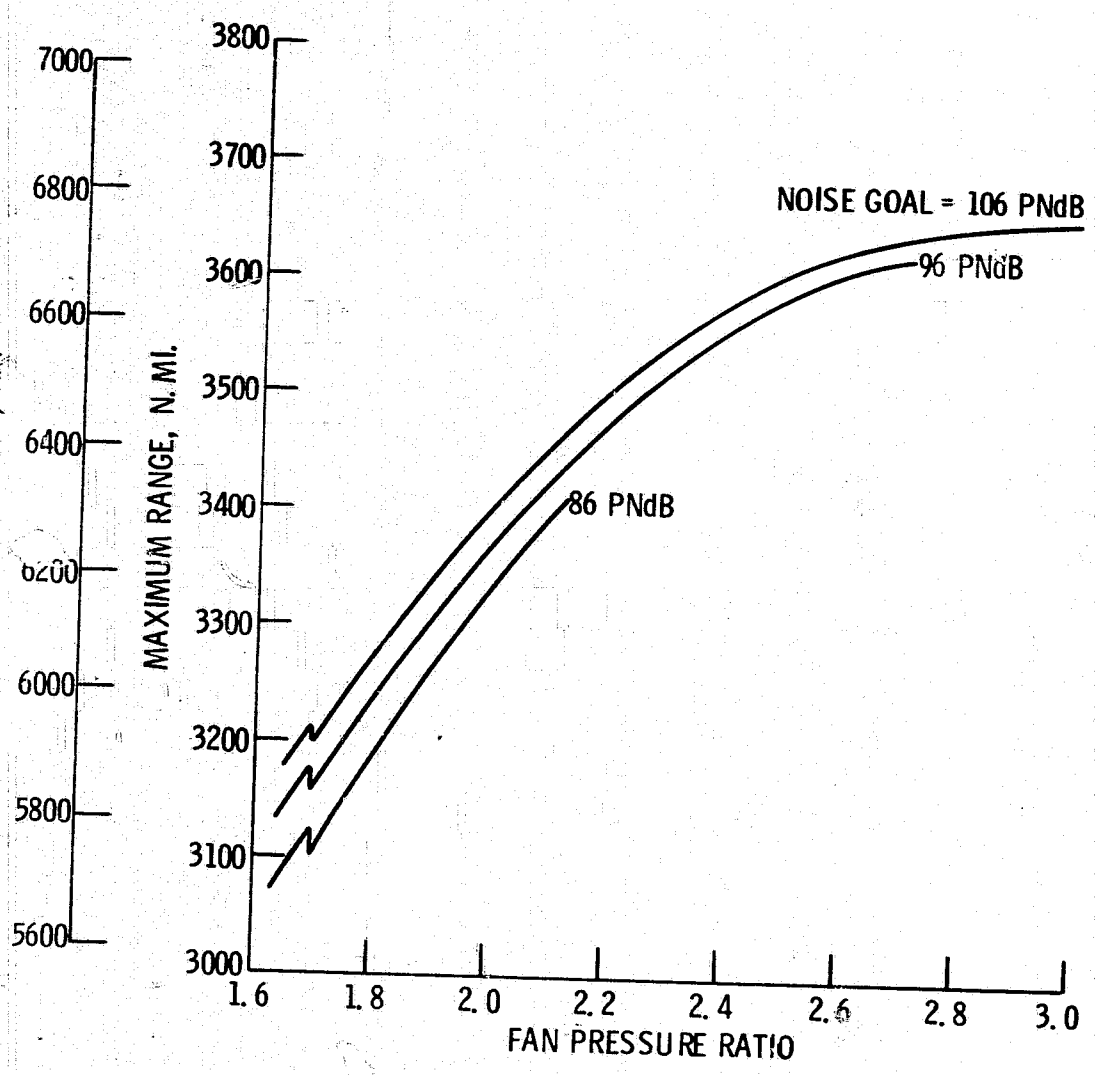

Figure 8. - Maximum total range versus fan pressure ratio for several noise goals. Takeoff T_4 = 1260° C, cruise T_4 = 1050° C, cruise MN = 0.98, β_{HPT} = 7.5 percent, β_{LPT} = 0 percent, L/D varies with engine diameter, 10 PNdB jet noise suppressor assumed without weight penalty. Machinery noise suppression up to 40 PNdB assumed as necessary.

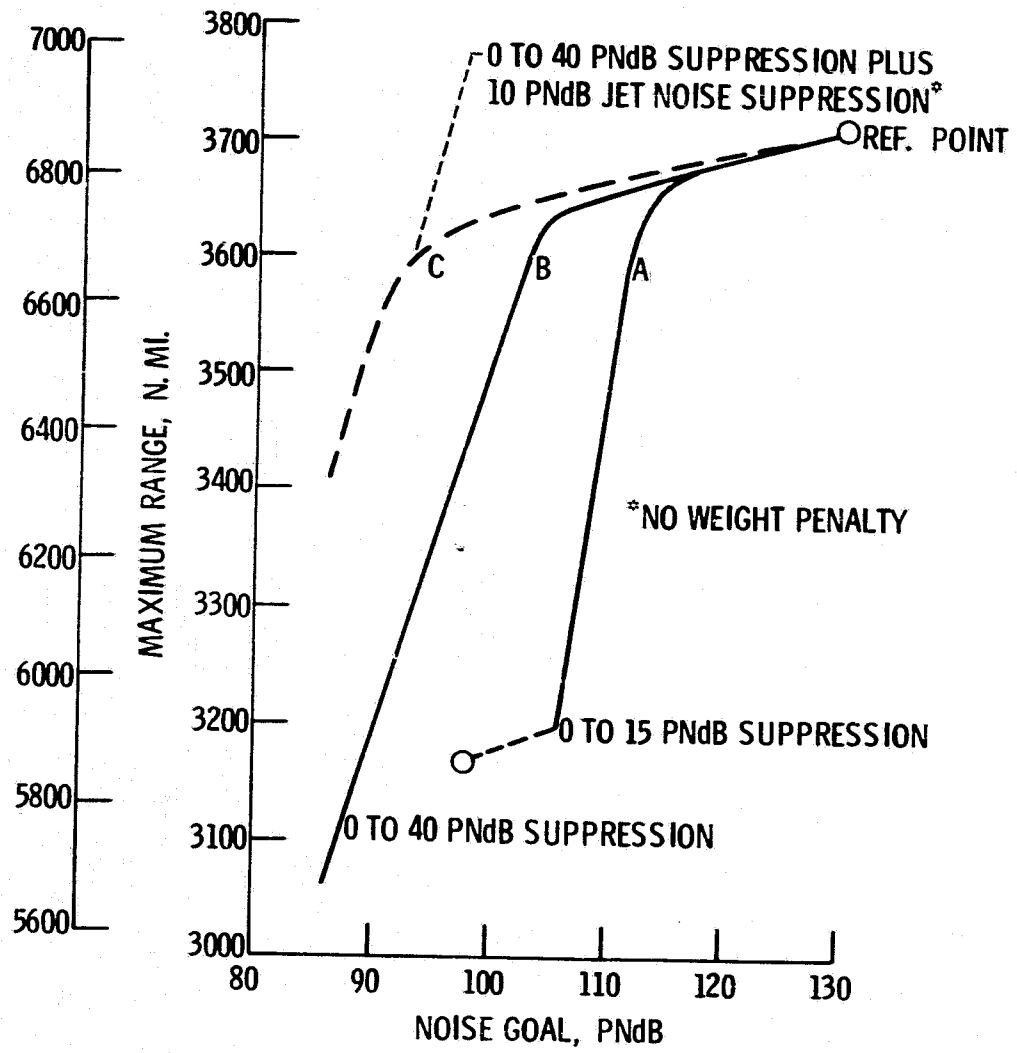

Figure 9. - Range versus noise tradeoff. Takeoff T_4 = 1260° C, cruise T_4 = 1050° C, cruise MN = 0.98, β_{HPT} = 7.5 percent, β_{LPT} = 0 percent, L/D varies with engine diameter.

CURVE	REFERENCE POINT	A		B			C		
NOISE GOAL, PNdB	NONE	106	98	106	96	86	106	96	86
MAXIMUM RANGE, KM	6880	5950	5880	6740	6260	5670	6760	6700	6310
RANGE PENALTY, KM	0	930	1000	139	611	1210	102	167	556
OPTIMUM FPR	3.0	1.7	1.7	2.9	2.08	1.7	3.0	2.72	2.16
OPTIMUM OPR	30.5	31.8	31.1	30.6	31.0	31.0	30.5	30.7	30.9
OPTIMUM BPR	2.4	4.8	5.5	2.45	4.1	6.5	2.4	2.7	3.9
JET NOISE SUPP.	0	0	0	0	0	0	10	10	10
MACHINERY NOISE SUPP.	0	7	15	34	28	40	25	38	40
NO. OF FAN STAGES	2 OR 3	1	1	2 OR 3	2	1	2 OR 3	2 OR 3	2
APPROACH NOISE, PNdB	130	106	98	106	96	78	106	96	86
SIDELINE NOISE, PNdB	120	106	98	106	96	86	99	94	86

E-6783

Figure 10. - Range-noise tradeoff, turbine rotor-inlet temperature = 1260° C.

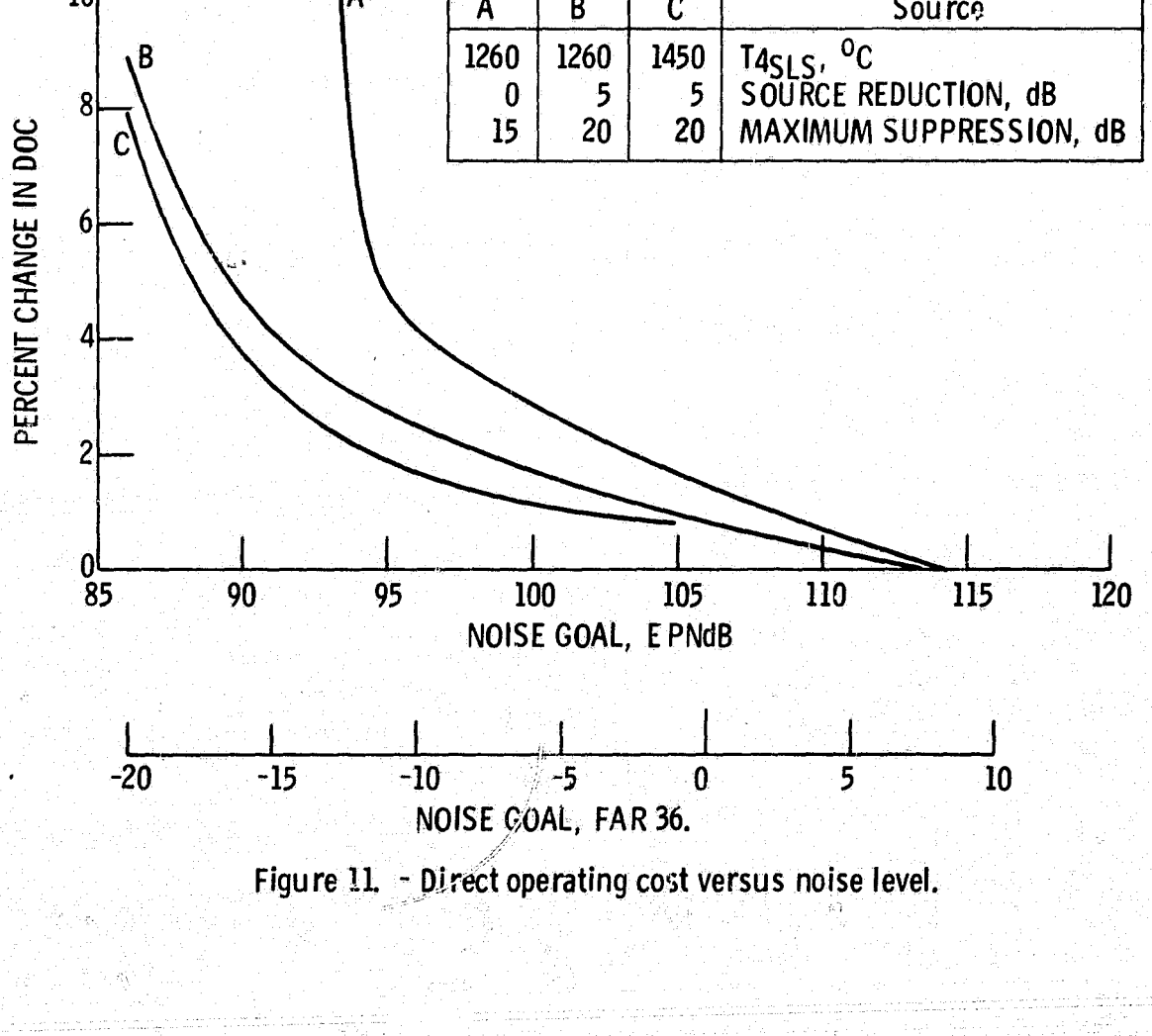

Figure 11. - Direct operating cost versus noise level.

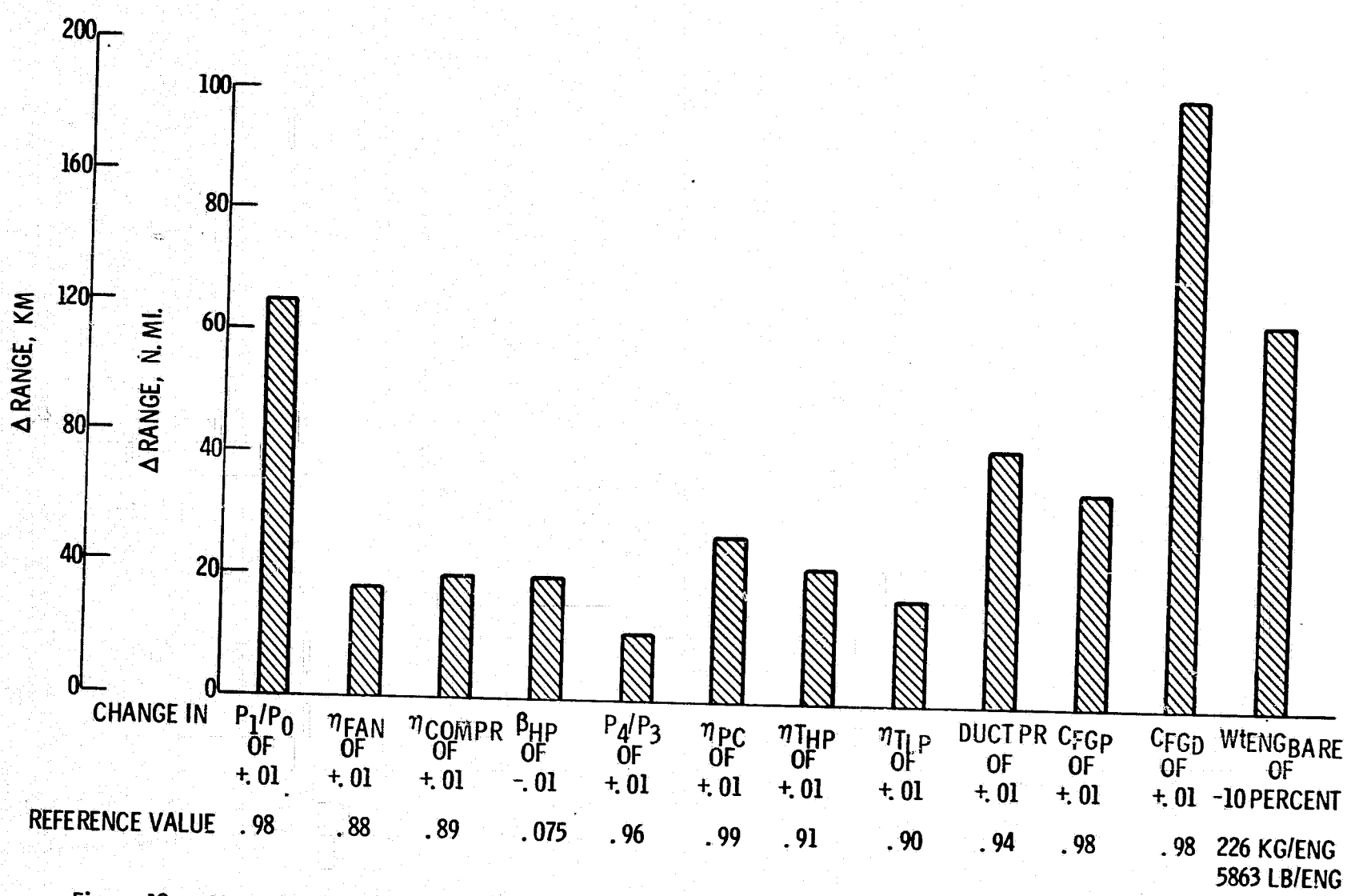

Figure 12. - Change in range for a change in engine design parameter. Reference engine, takeoff $T_4 = 1260^0$ C, cruise $T_4 = 1050^0$ C, FPR = 1.70, OPR = 31.0, BPR = 4.8, cruise MN = 0.98.

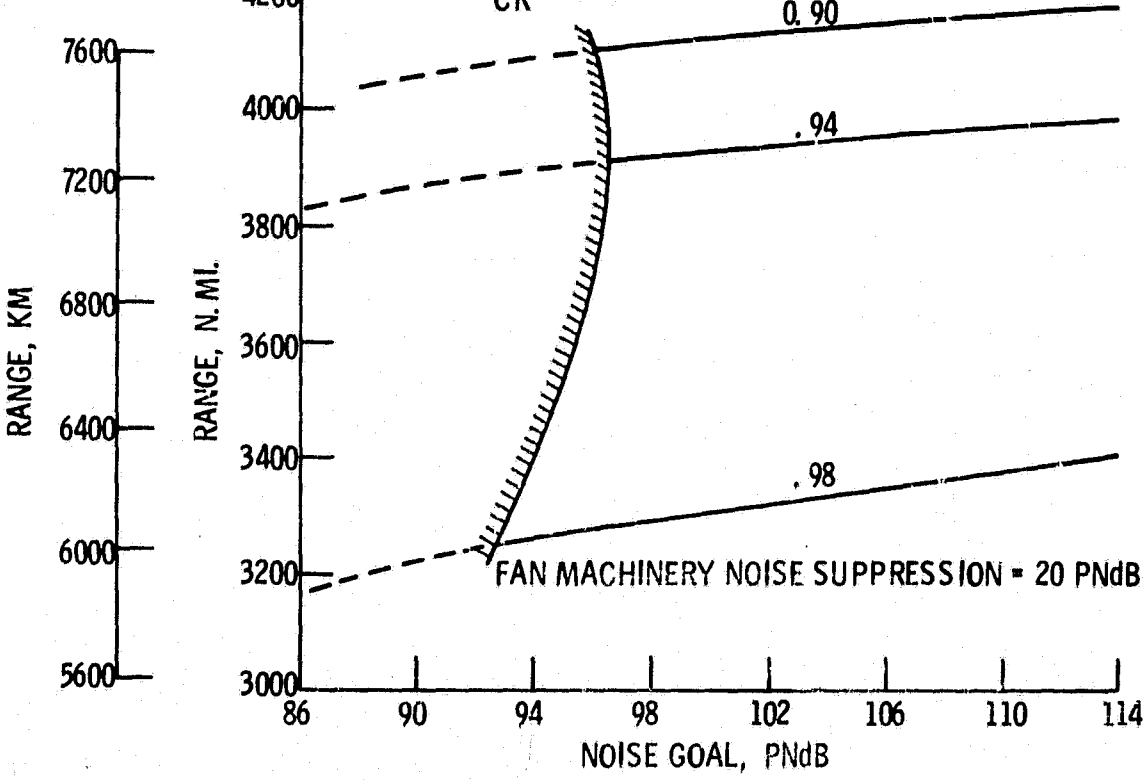

Figure 13. - Range of acoustically-treated optimum airplanes as a function of desired noise goal for various design cruise Mach numbers. Takeoff gross weight, 175 000 kg; payload, 300 passengers. $T_{4_{SLS}}$, 1260° C.

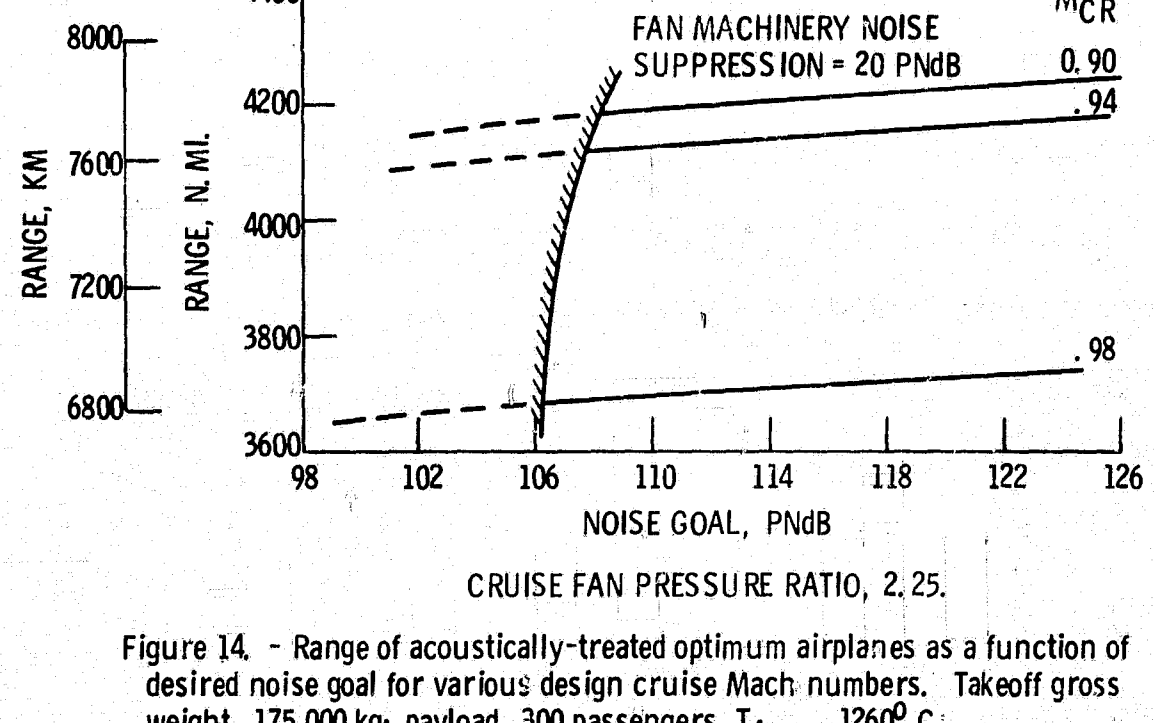

Figure 14. - Range of acoustically-treated optimum airplanes as a function of desired noise goal for various design cruise Mach numbers. Takeoff gross weight, 175 000 kg; payload, 300 passengers $T_{4_{SLS}}$, 1260° C.

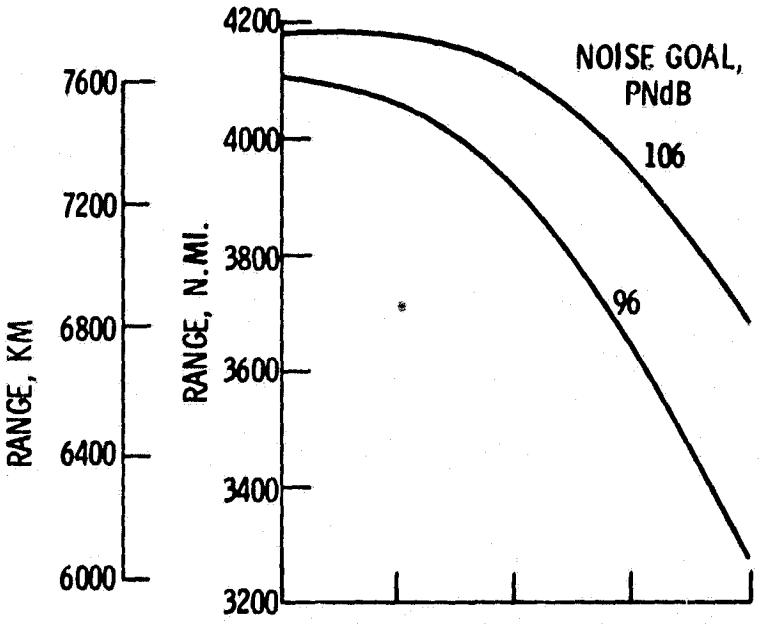

(a) TOTAL RANGE WITH ACOUSTIC TREATMENT.

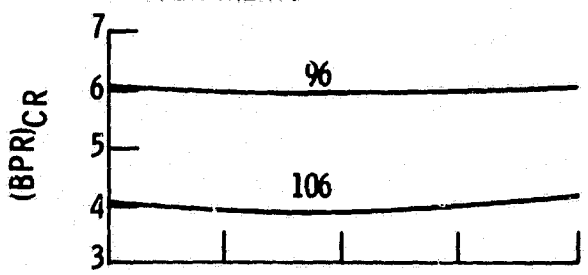

(b) CRUISE BYPASS RATIO.

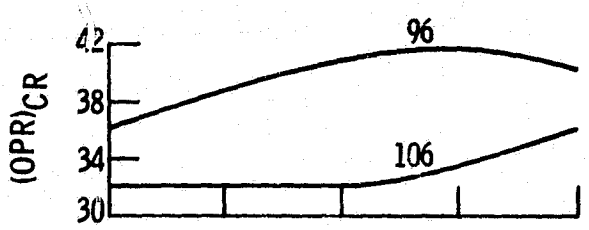

(c) CRUISE OVERALL FAN AND COMPRESSOR PRESSURE RATIO.

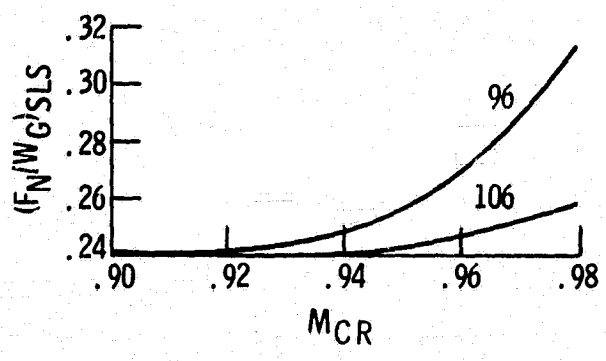

(d) SEA-LEVEL-STATIC THRUST-TO-GROSS-WEIGHT RATIO.

Figure 15. - Characteristics of range-optimized cycles related to design cruise Mach number at noise goals of 106 and 96 PNdB. Takeoff gross weight, 175 000 kg; payload, 300 passengers; T_{4SLS}, 1260° C.

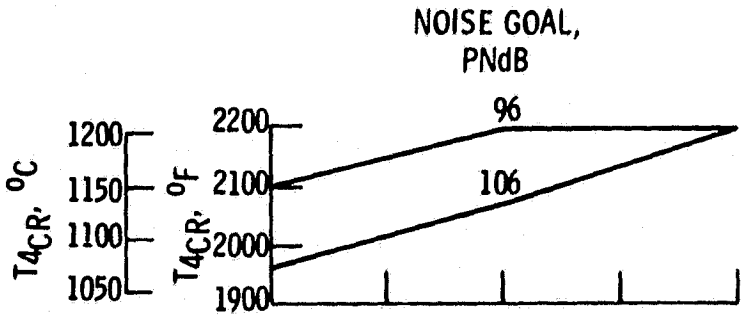

(e) CRUISE TURBINE-ROTOR-INLET TEMPERATURE.

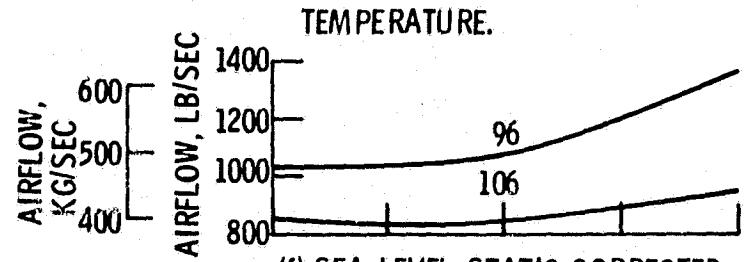

(f) SEA-LEVEL-STATIC CORRECTED AIRFLOW AT FAN FACE.

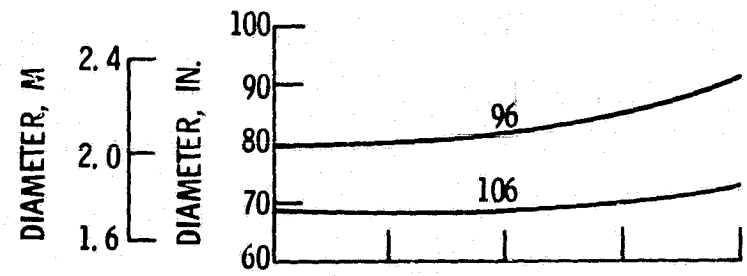

(g) ENGINE MAXIMUM DIAMETER.

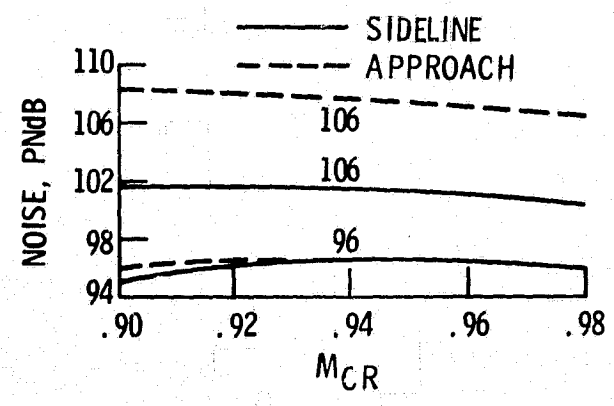

(h) SIDELINE AND APPROACH TOTAL PERCEIVED NOISE.

Figure 15. - Concluded.

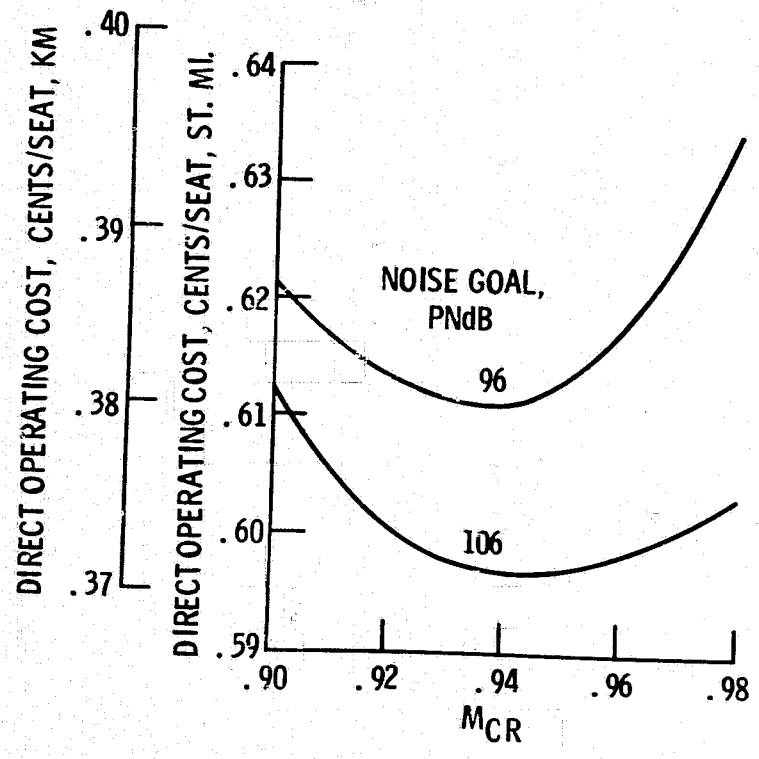

Figure 16. - Direct operating cost of range-optimized cycles related to design cruise Mach number at noise goals of 106 and 96 PNdB. Takeoff gross weight, 175 000 kg; payload, 300 passengers. $T_{4_{SLS}}$, 1260^0 C.

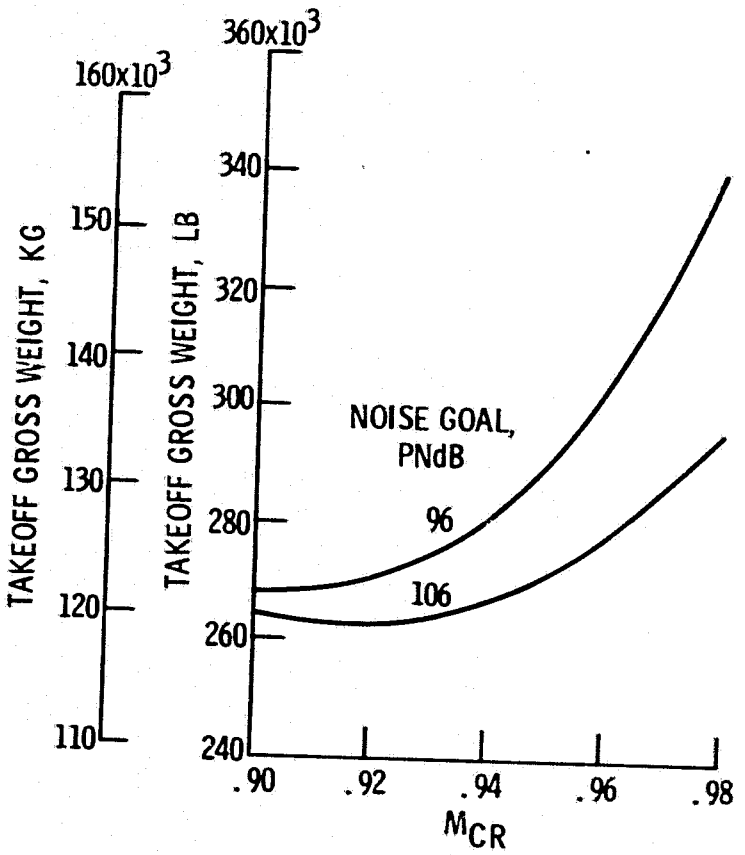

Figure 17. - Characteristics of optimized cycles related to design cruise Mach number at noise goals of 106 and 96 PNdB. Total range, 5560 km; payload, 300 passengers; $T_{4_{SLS}}$, 1260^0 C.

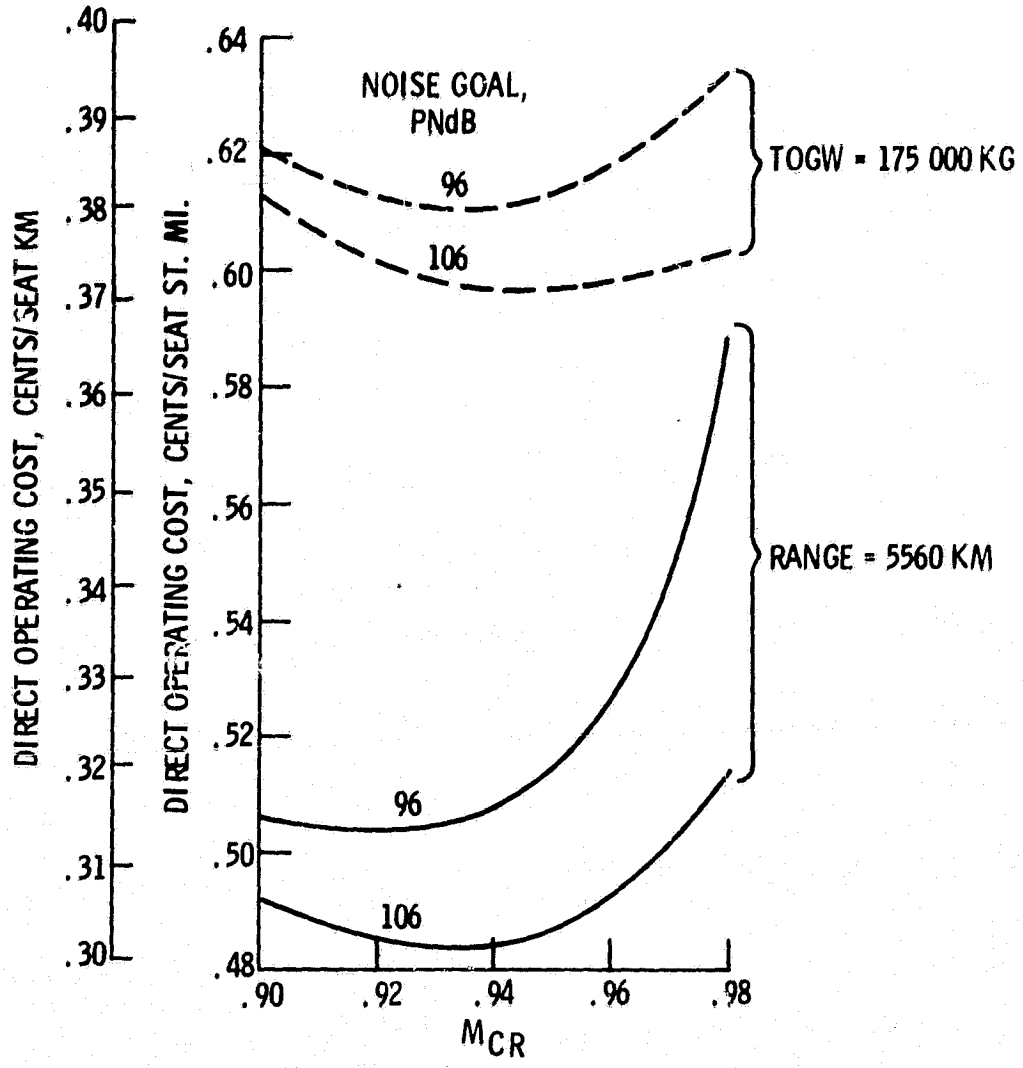

(a) AIRPLANE COST ESTIMATES BASED ON CURRENT AIRPLANES.

Figure 18. - Direct operating cost of optimized cycles related to design cruise Mach number at noise goals of 106 and 96 PNdB. Payload, 300 passengers; $T_{4_{SLS}}$, 1260^{0} C.

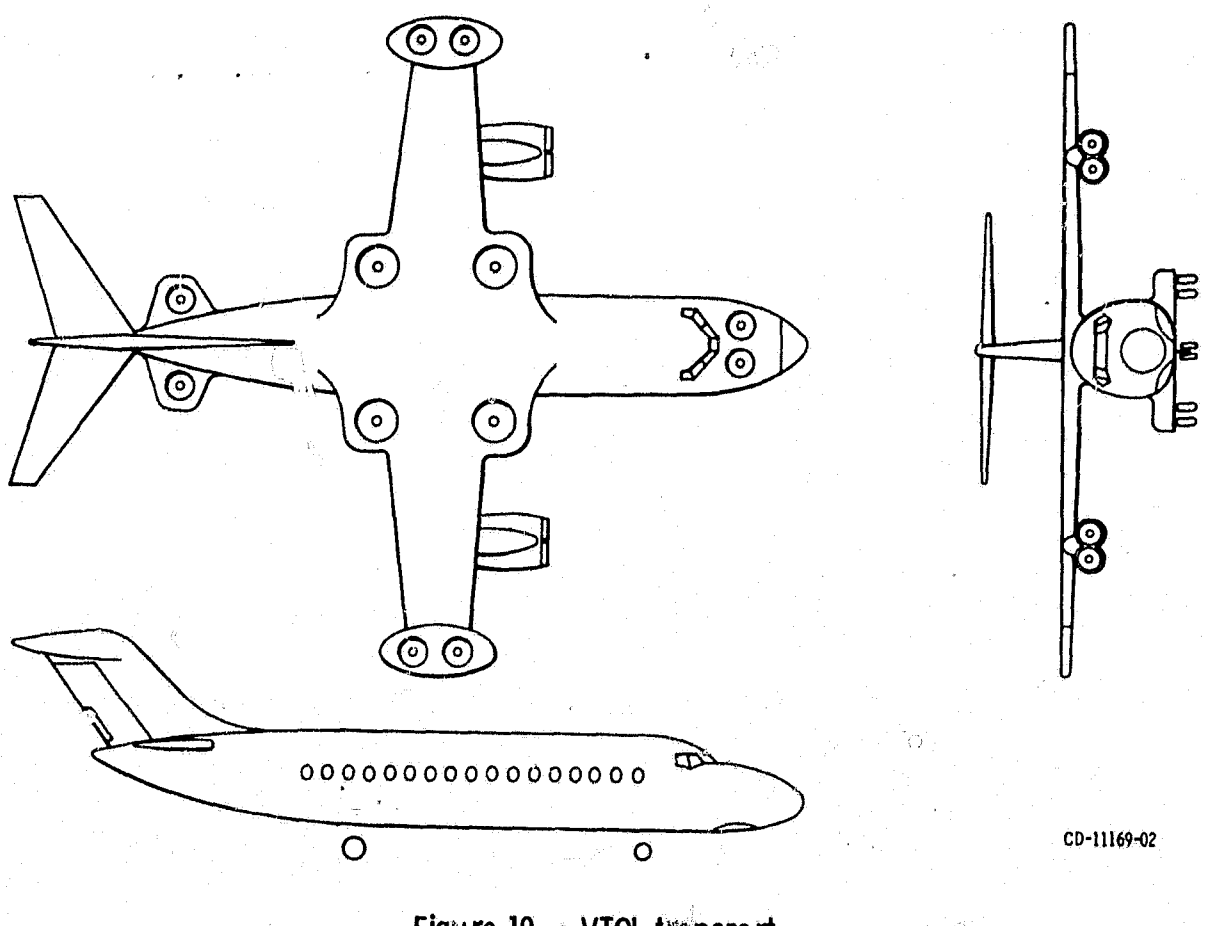

CD-11169-02

Figure 19. - VTOL transport.

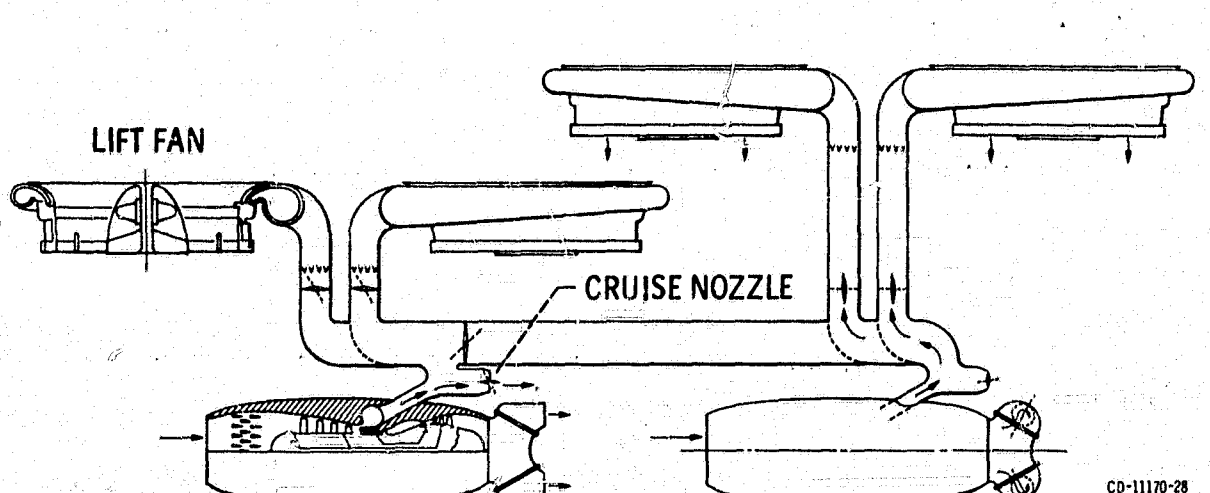

Figure 20. - Air generator remote drive lift fan propulsion system.

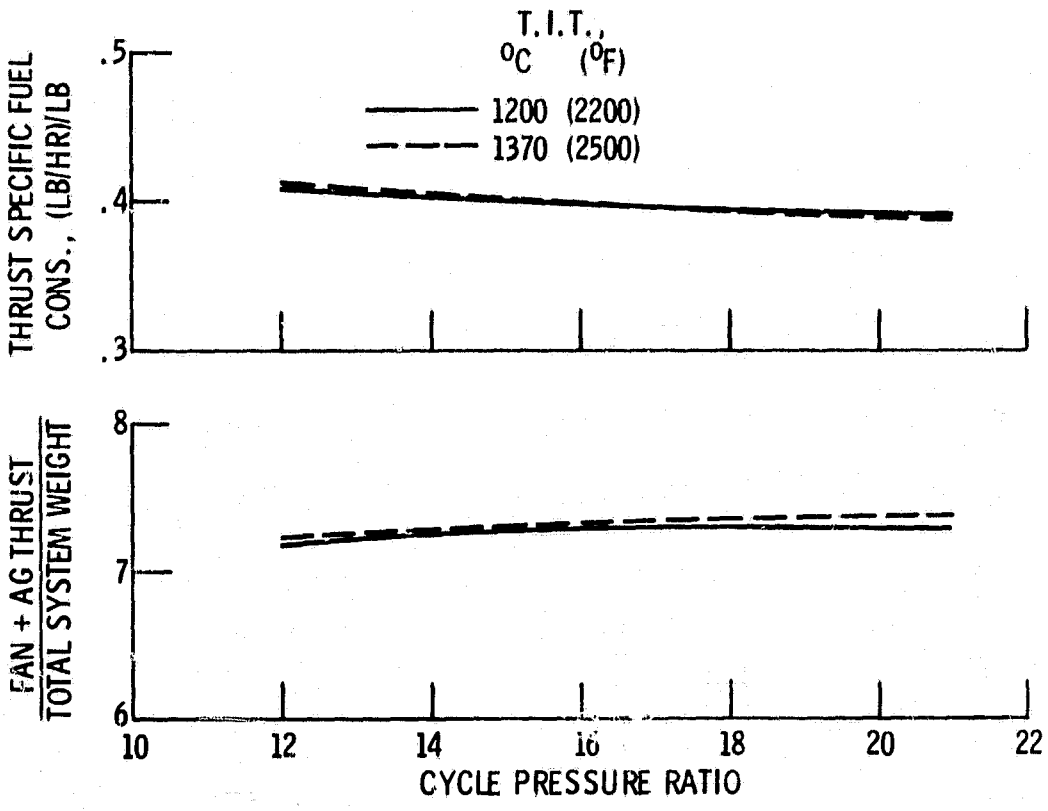

(a) EFFECTS OF OVERALL PRESSURE RATIO ON PERFORMANCE AND WEIGHT.

Figure 21. - Effects of air generator parameters on propulsion system performance, weight, and size. Lift fan pressure ratio is 1.20.

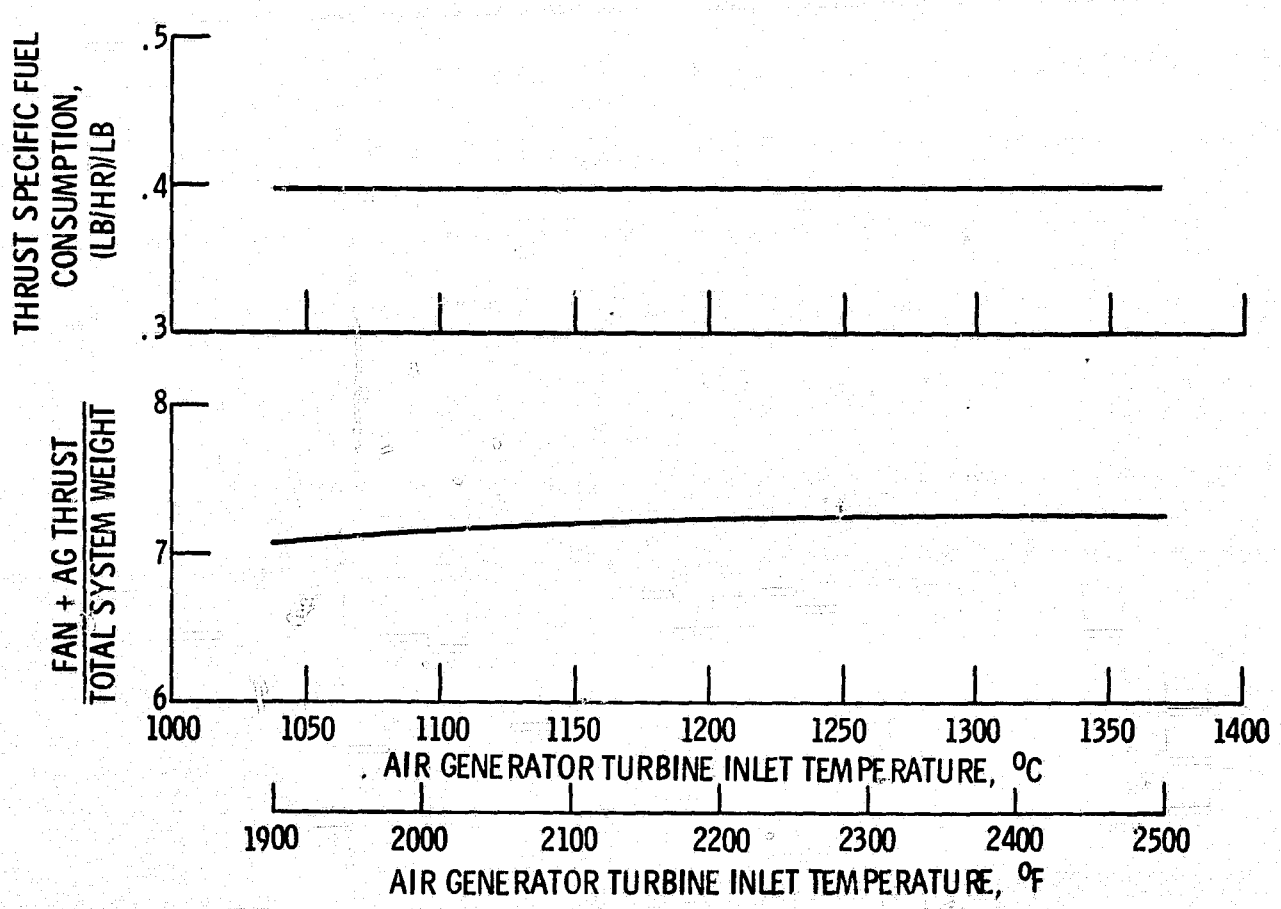

(b) EFFECTS OF TURBINE TEMPERATURE ON PERFORMANCE AND WEIGHT. OVERALL PRESSURE RATIO IS 15.

Figure 21. - Concluded

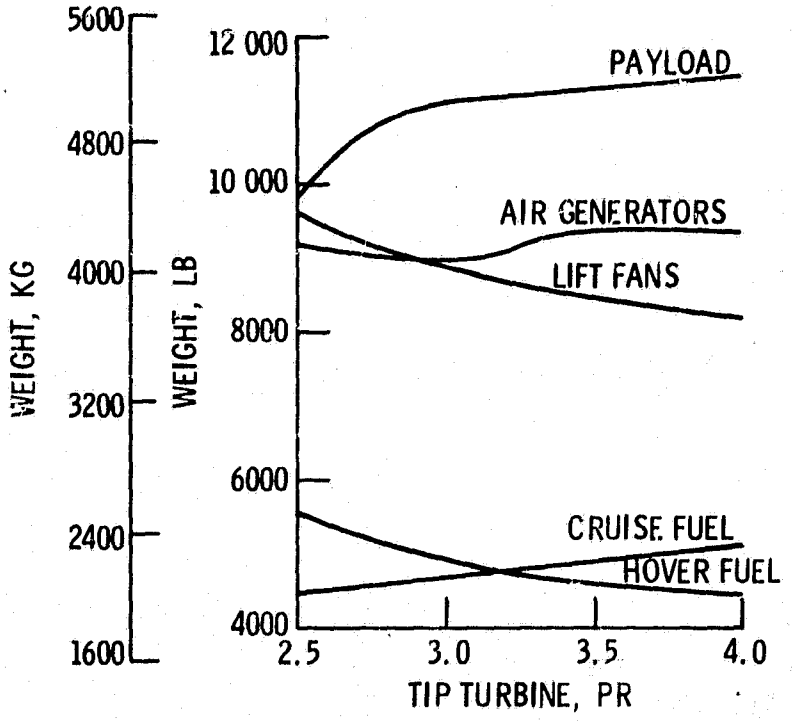

Figure 22. - Weight trends. Lift fan PR = 1.25, L/D = 10.

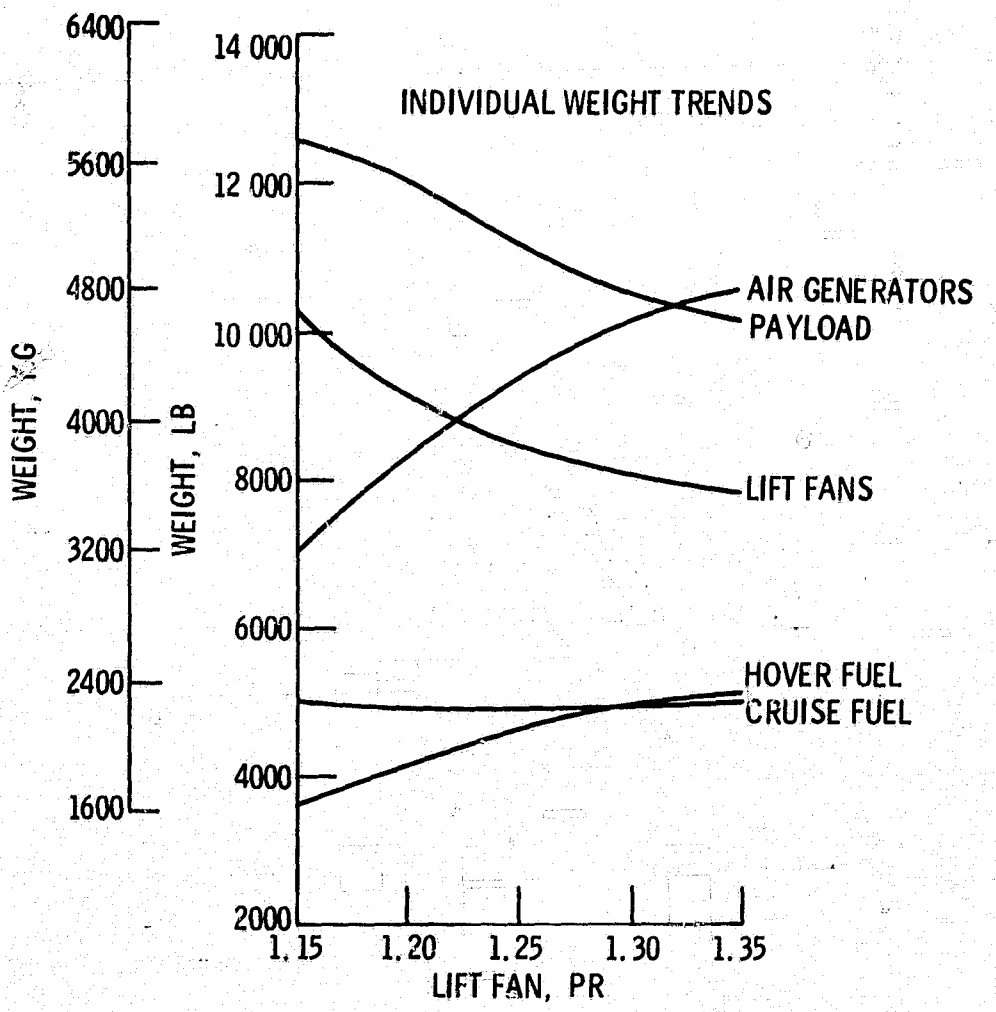

Figure 23. - Weight trends. Tip turbine PR = 3.5, $(L/D)_{CR}$ = 10.

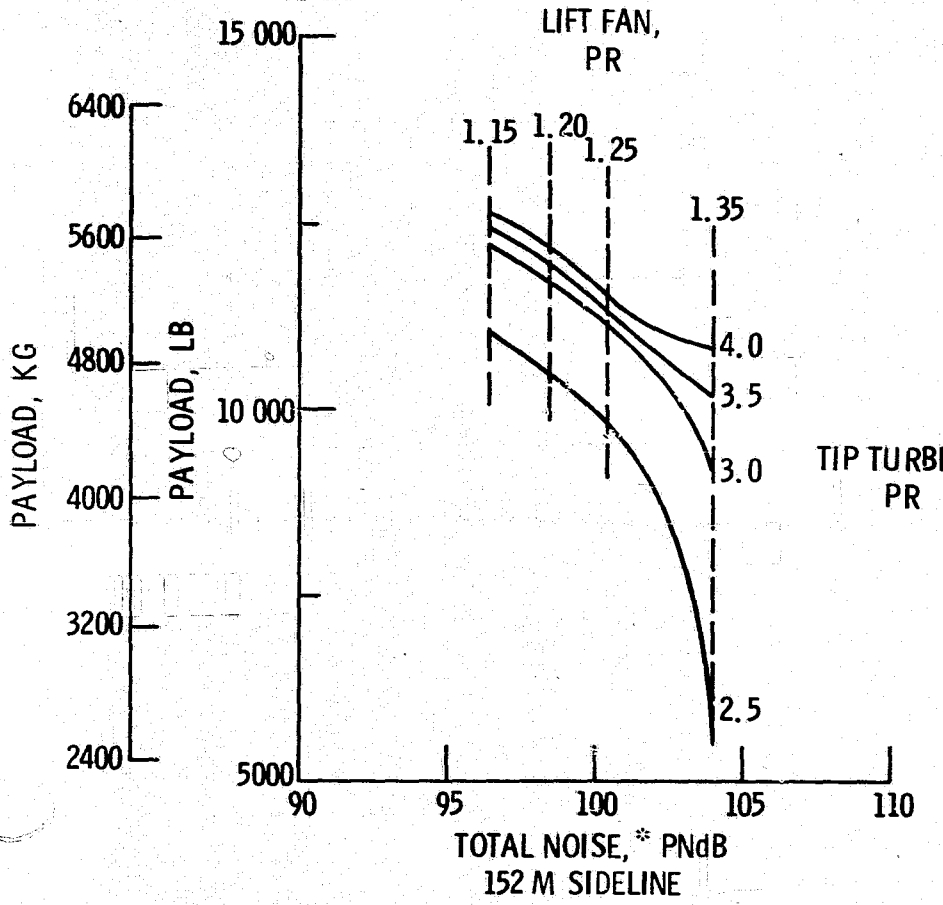

Figure 24. - Performance-noise tradeoff. $(L/D)_{CR} = 10$.

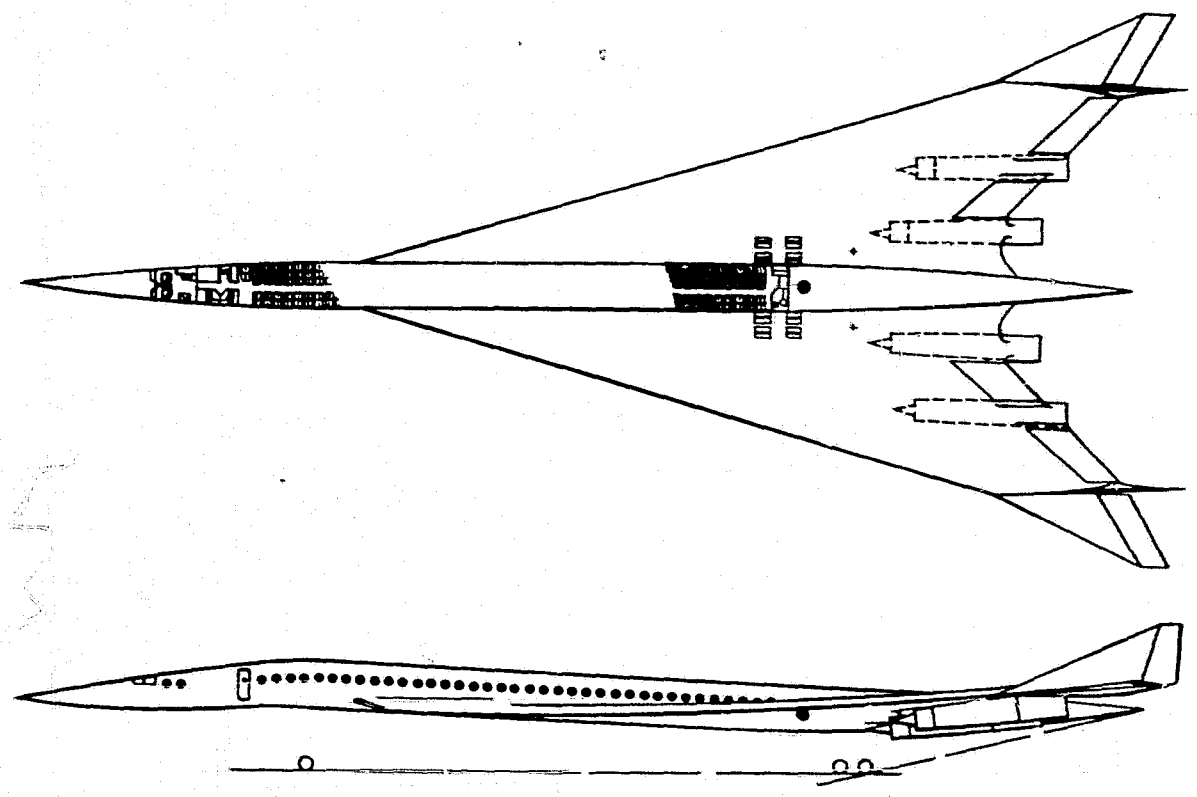

Figure 25. - Supersonic transport.

TURBINE TEMPERATURE, ^{o}C	1200 TO 1700
OVERALL PRESSURE RATIO	7 TO 19
FAN PRESSURE RATIO	1.5 TO 3.5
BYPASS RATIO	1.0 TO 3.1
MAXIMUM AUGMENTATION TEMPERATURE, ^{o}C	1700

Figure 26. - Range of engine variables.

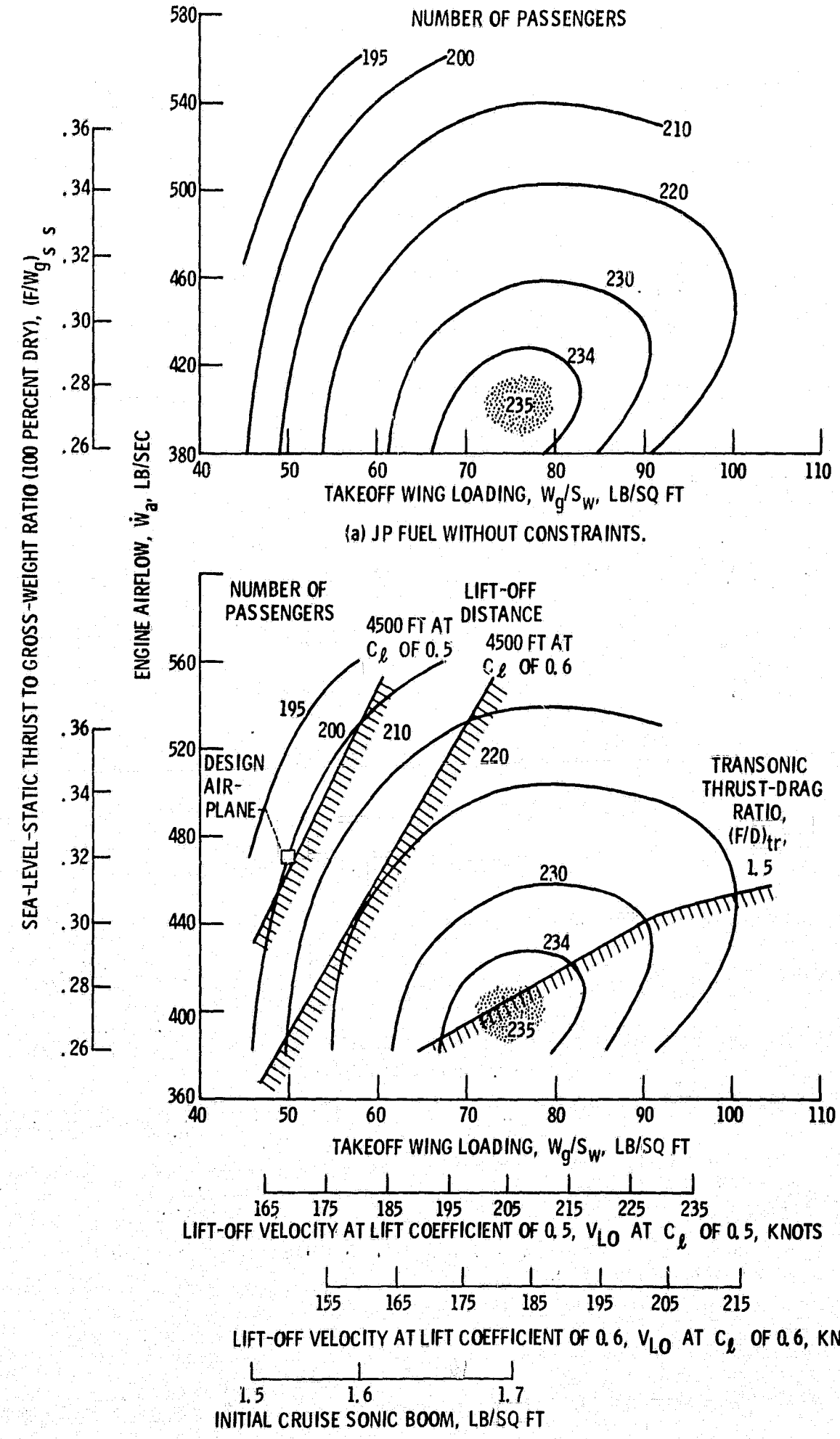

Figure 27. - Wing and engine sizing. Turbine inlet temperature, 2100° F.

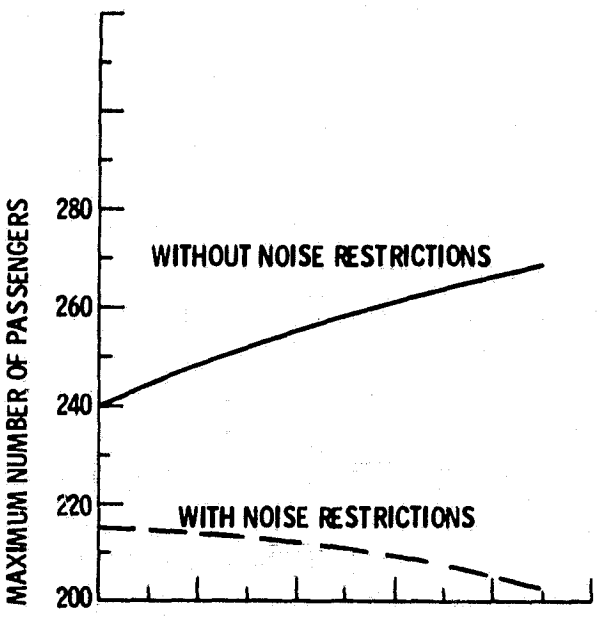

(a) MAXIMUM NUMBER OF PASSENGERS.

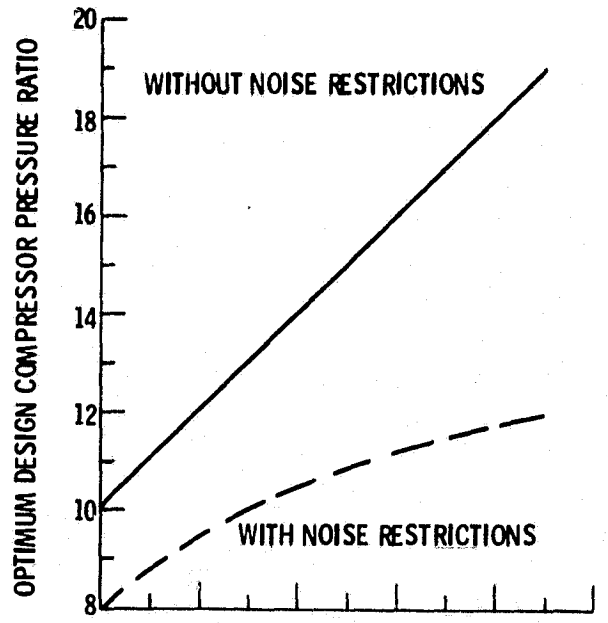

(b) OPTIMUM DESIGN COMPRESSOR PRESSURE RATIO.

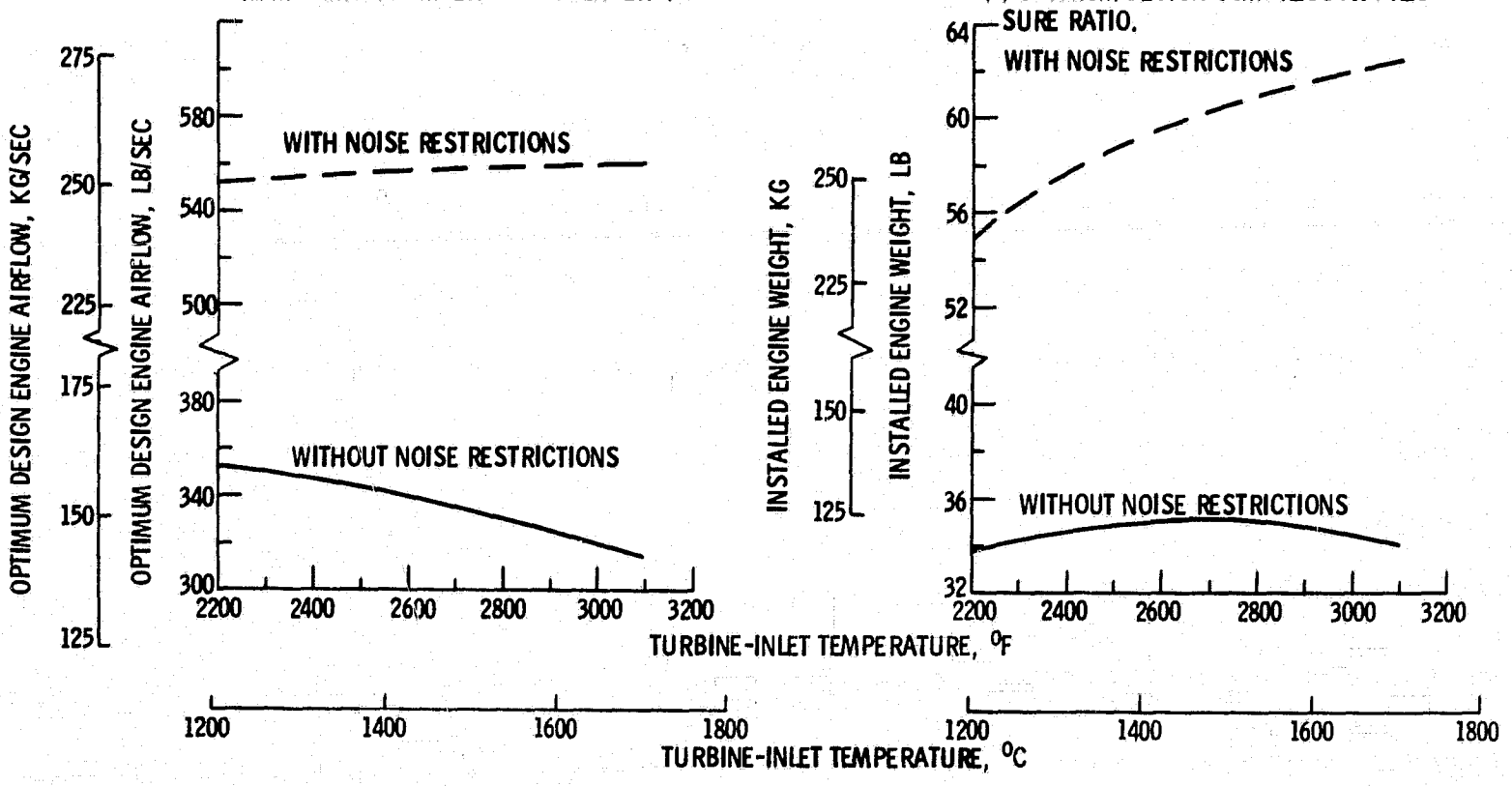

(c) OPTIMUM DESIGN ENGINE AIRFLOW PER ENGINE.

(d) INSTALLED WEIGHT OF FOUR AFTERBURNING TURBOJET ENGINES.

Figure 28. - Effect of design turbine-inlet temperature for afterburning turbojets; ramp gross weight, 460 000 pounds (208 652 kg); Mach 3.0 cruise.

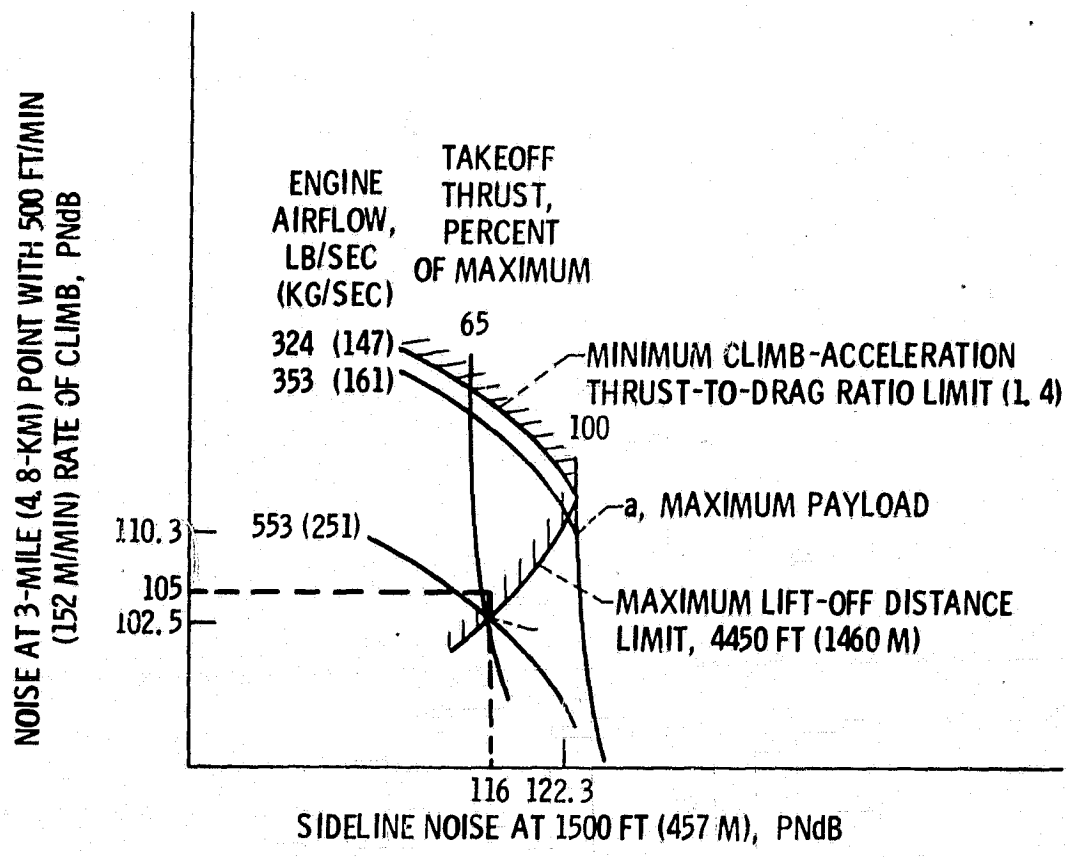

Figure 29. - Effect of engine noise goals on aircraft and engine parameters with four afterburning turbojet engines. Design turbine-inlet temperature, 2200° F (1204° C).

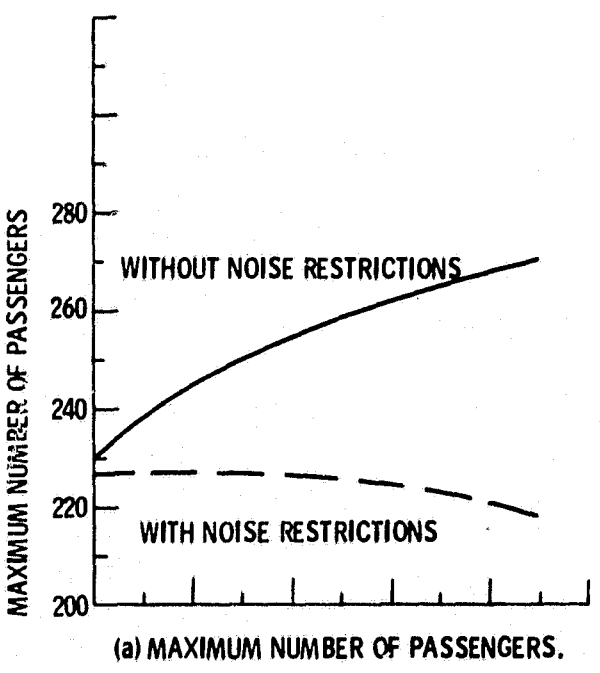

(a) MAXIMUM NUMBER OF PASSENGERS.

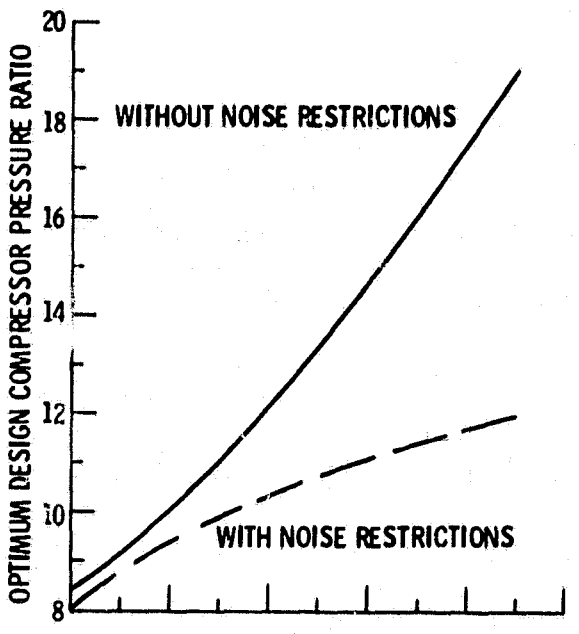

(b) OPTIMUM DESIGN COMPRESSOR PRESSURE RATIO.

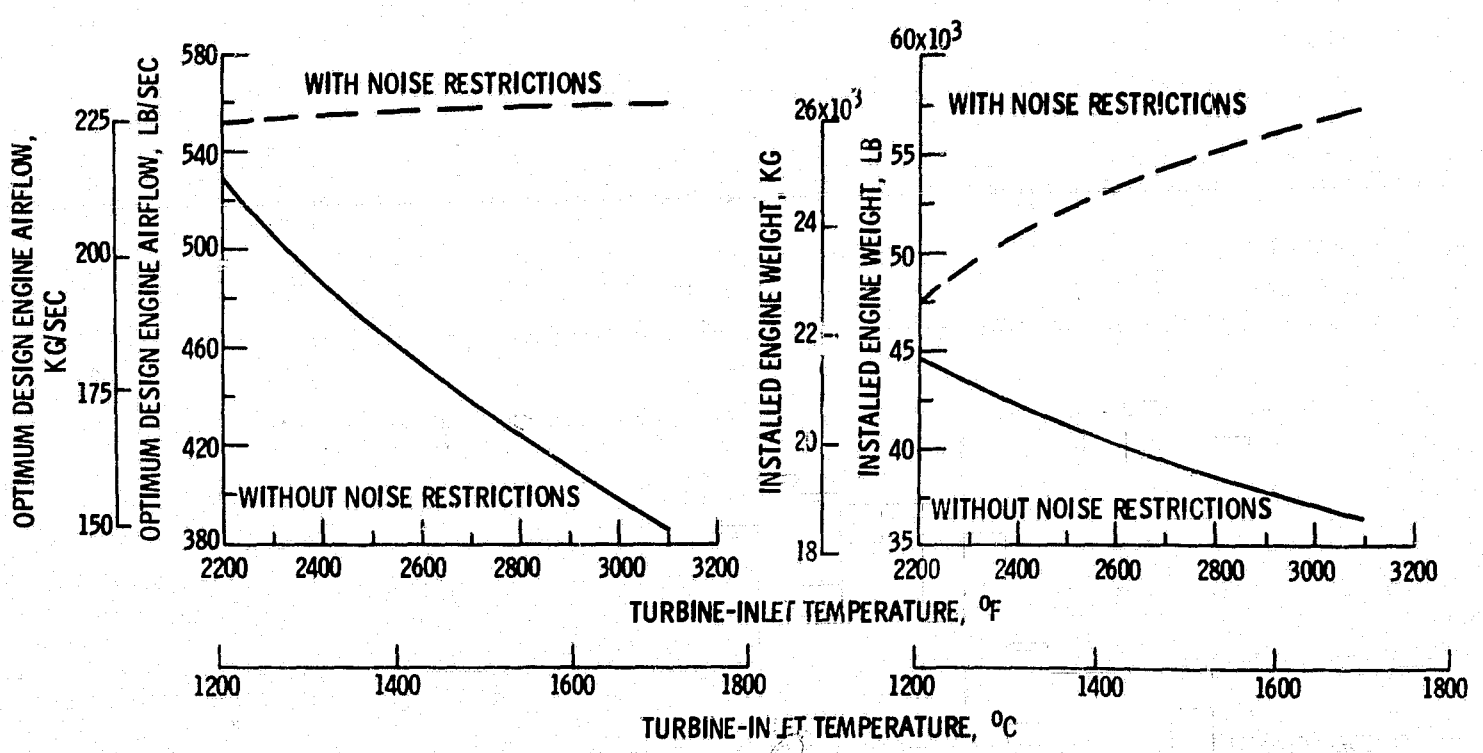

(c) OPTIMUM DESIGN ENGINE AIRFLOW PER ENGINE.

(d) INSTALLED WEIGHT OF FOUR NONAFTERBURNING TURBOJET ENGINES

Figure 30. - Effect of design turbine-inlet temperature for nonafterburning turbojets. Ramp gross weight, 460 000 pounds (208 652 kg); Mach 3.0 cruise.

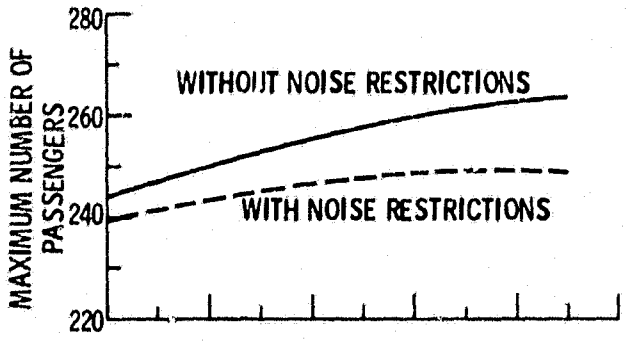

(a) MAXIMUM NUMBER OF PASSENGERS.

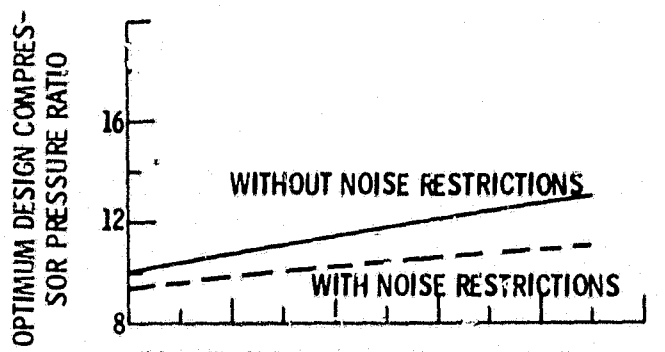

(b) OPTIMUM DESIGN COMPRESSOR PRESSURE RATIO.

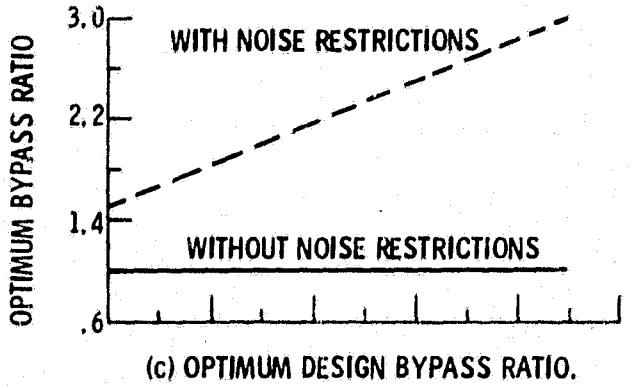

(c) OPTIMUM DESIGN BYPASS RATIO.

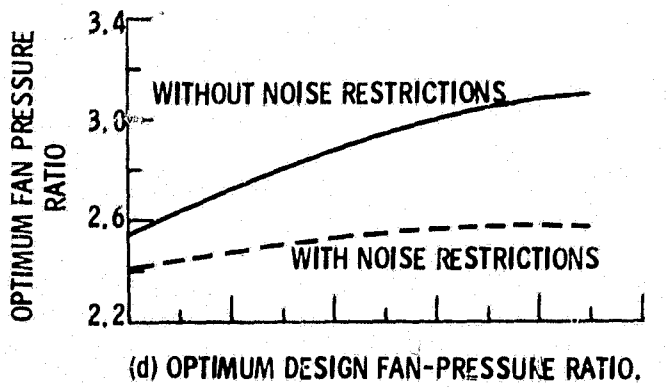

(d) OPTIMUM DESIGN FAN-PRESSURE RATIO.

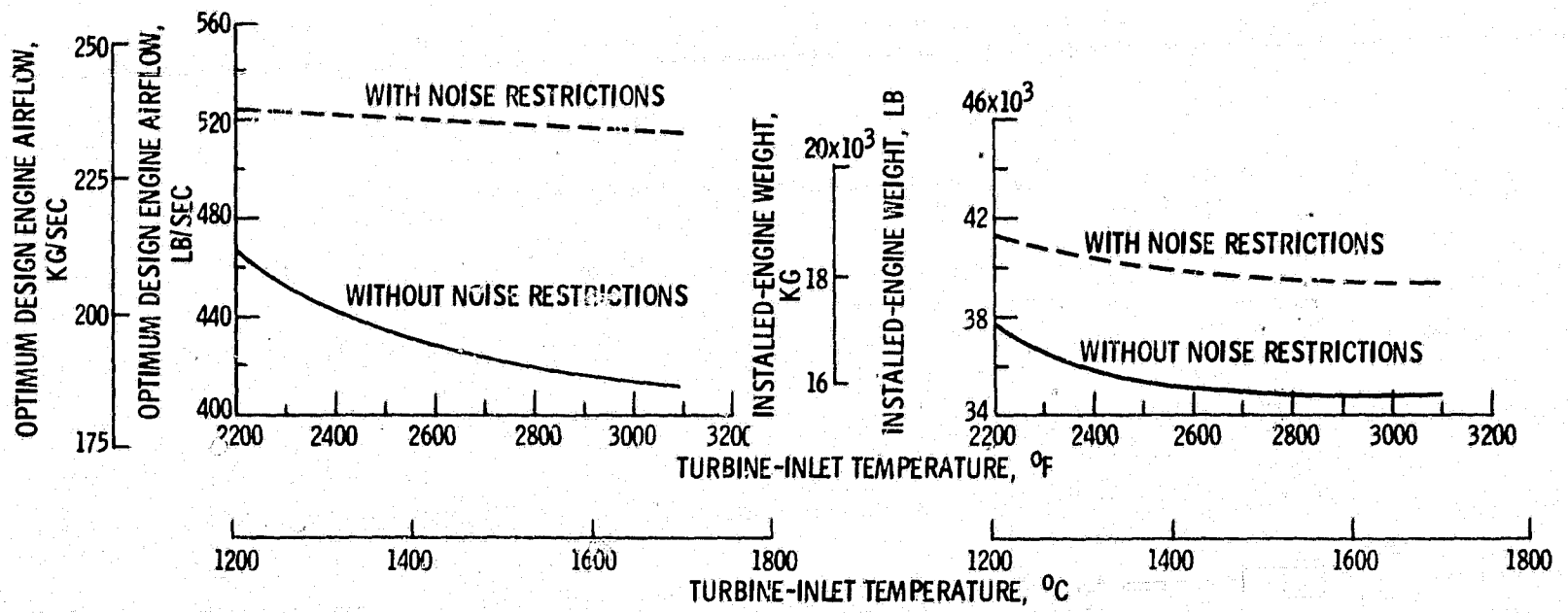

(e) OPTIMUM DESIGN ENGINE AIRFLOW PER ENGINE.

(f) INSTALLED-ENGINE WEIGHT OF FOUR DUCT-BURNING TURBOFAN ENGINES.

Figure 31. - Effect of design turbine-inlet temperature for duct-burning engines. Ramp gross weight, 460 000 pounds (208 652 kg); Mach 3.0 cruise.

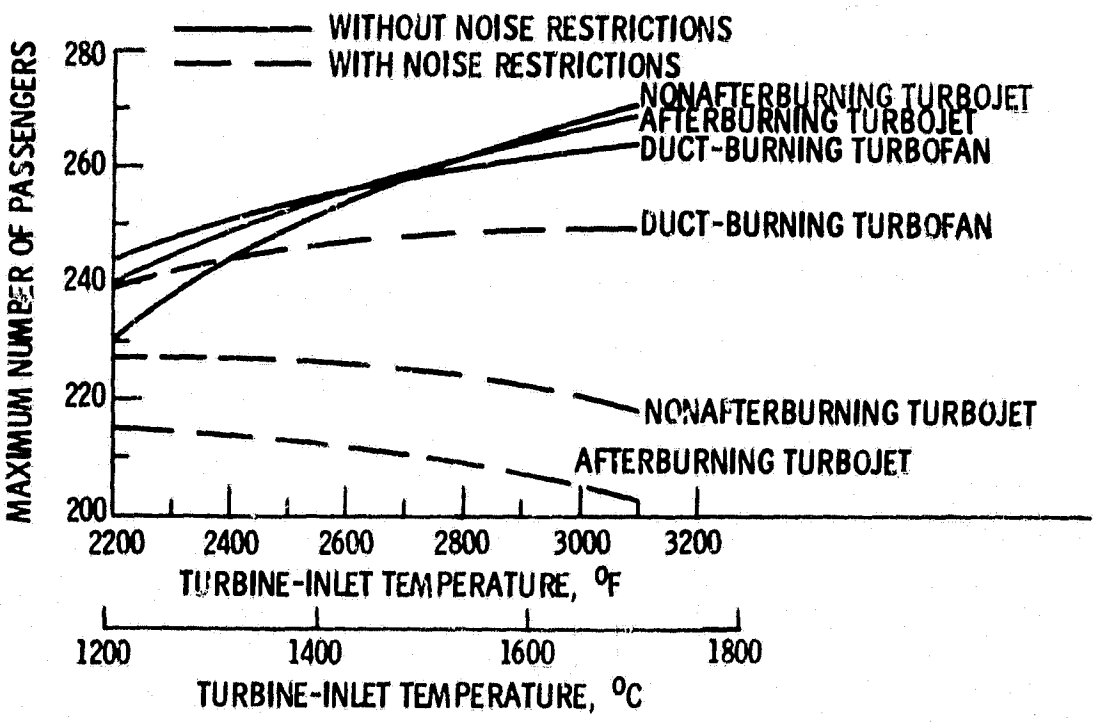

Figure 32. - Payload carrying comparison for various turbine-inlet temperatures. Ramp gross weight, 460 000 pounds (208 652 kg); minimum sea-level-static thrust to gross weight ratio, 0.32; Mach 3.0 cruise.

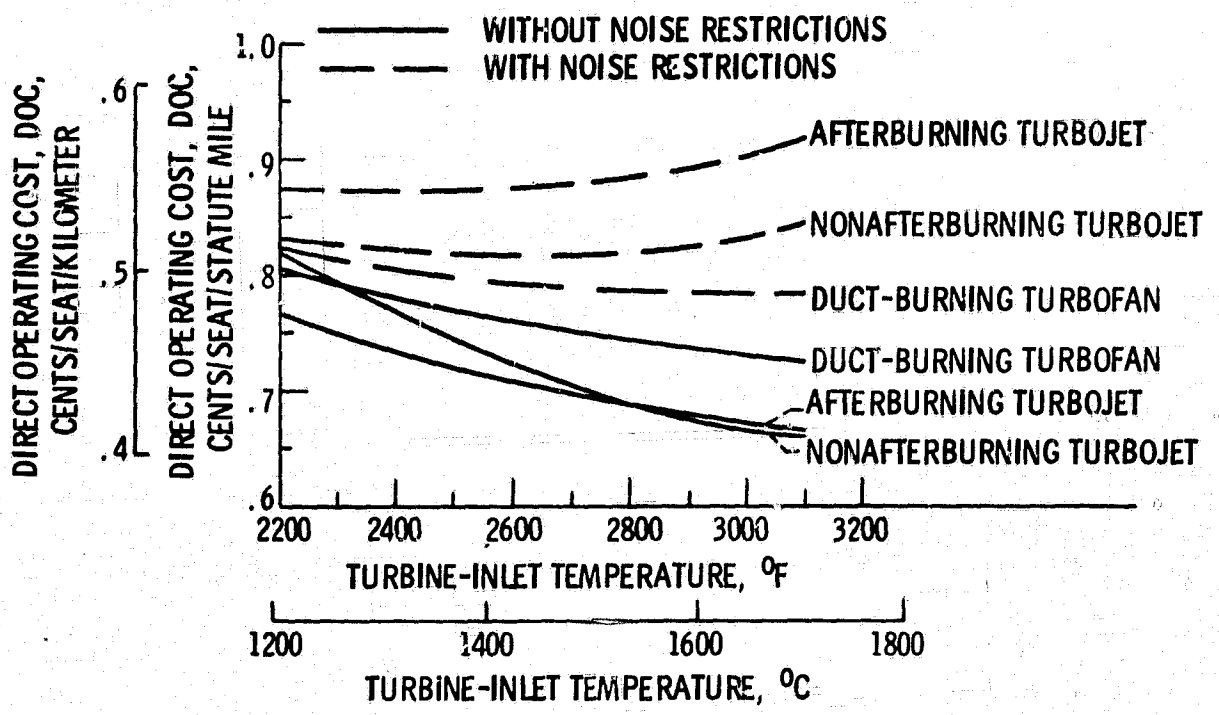

Figure 33. - Direct operating cost comparison for various turbine-inlet temperatures. Ramp gross weight, 460 000 pounds (208 652 kg); Mach 3.0 cruise.

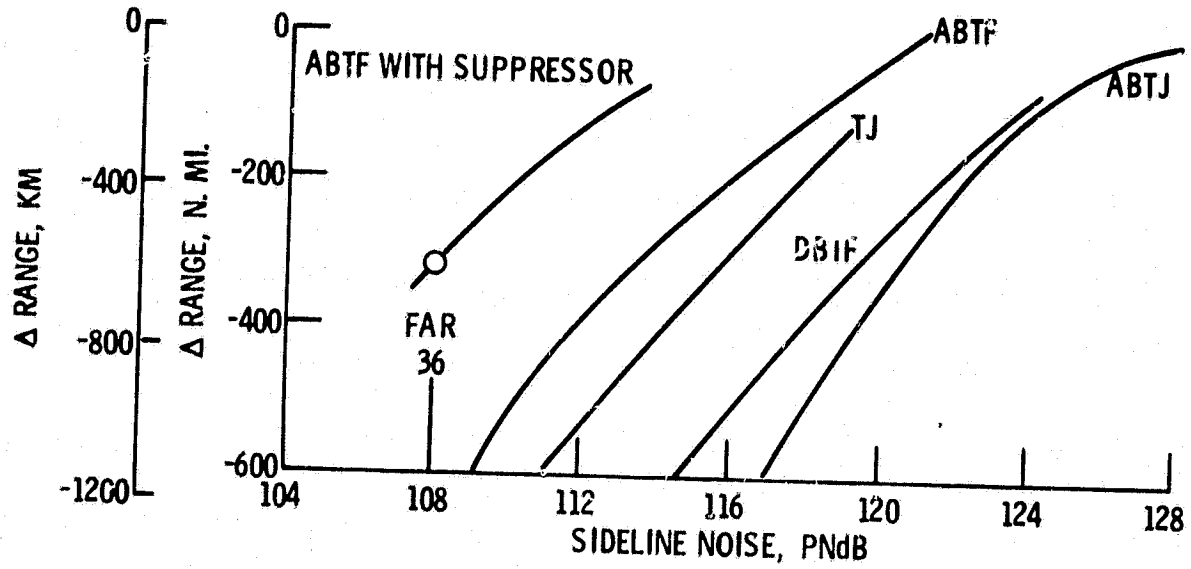

Figure 34. - Range-noise tradeoff; TOGW, 340 000 kg; Mach 2.7; payload, 22 200 kg; design turbine temperature, 1200° C.

$$\Sigma F = ma \qquad E = Wh + \frac{1}{2}mV^2$$

$$T - D - W\sin\gamma = m\dot{V} \qquad E_S = \frac{E}{W} = h + \frac{V^2}{2g}$$

$$\frac{V(T-D)}{W} = V\sin\gamma + \frac{V\dot{V}}{g} \qquad \frac{d}{dt}(E_S) = \dot{h} + \frac{V\dot{V}}{g} = P_S$$

$$\frac{V(T-D)}{W} = \dot{h} + \frac{V\dot{V}}{g} \qquad P_S = \frac{V(T-D)}{W}$$

Figure 35. - Derivation of specific excess power (P_S).

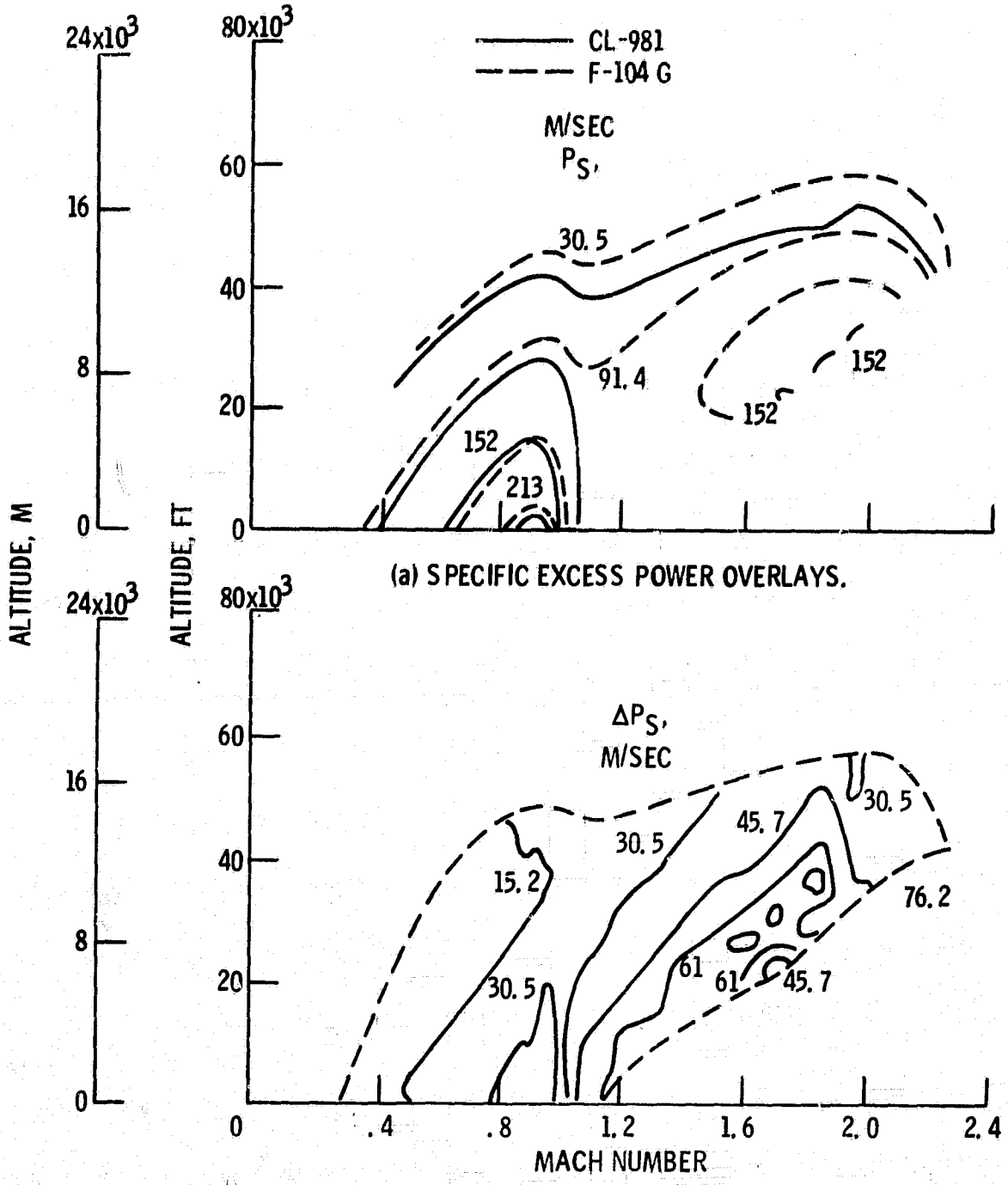

Figure 36. - Fighter performance comparison.

E-6783

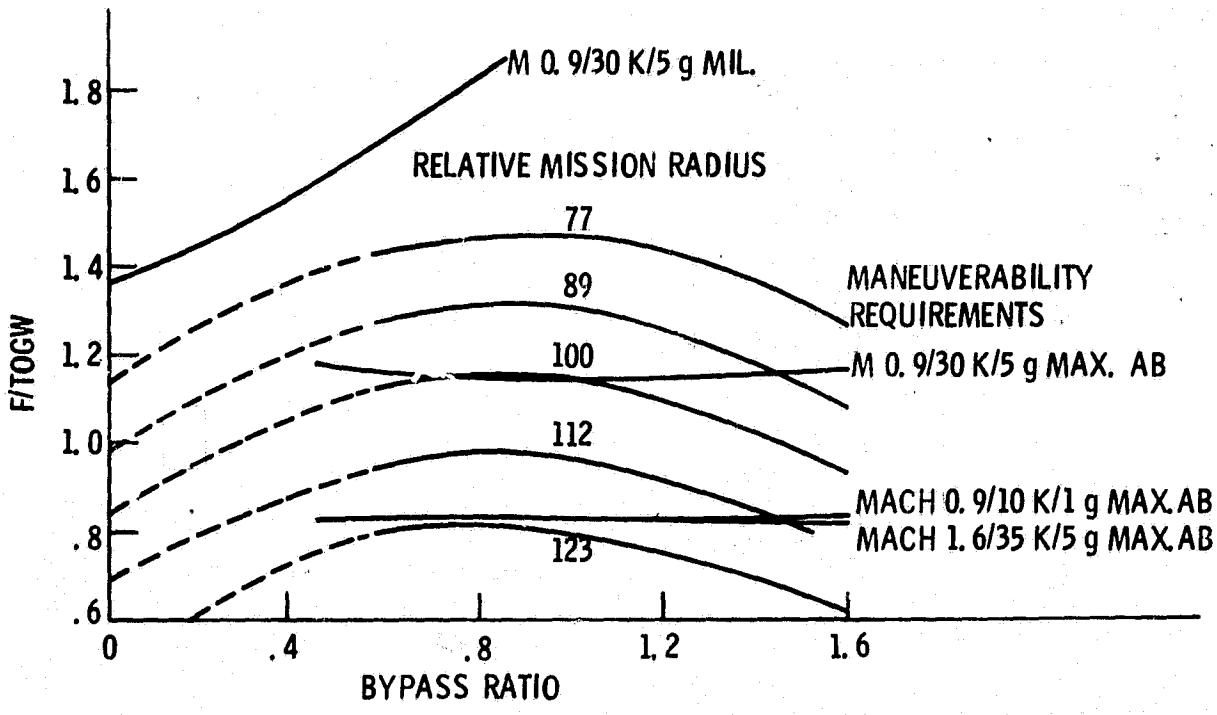

Figure 37. - Selection of bypass ratio and engine size.

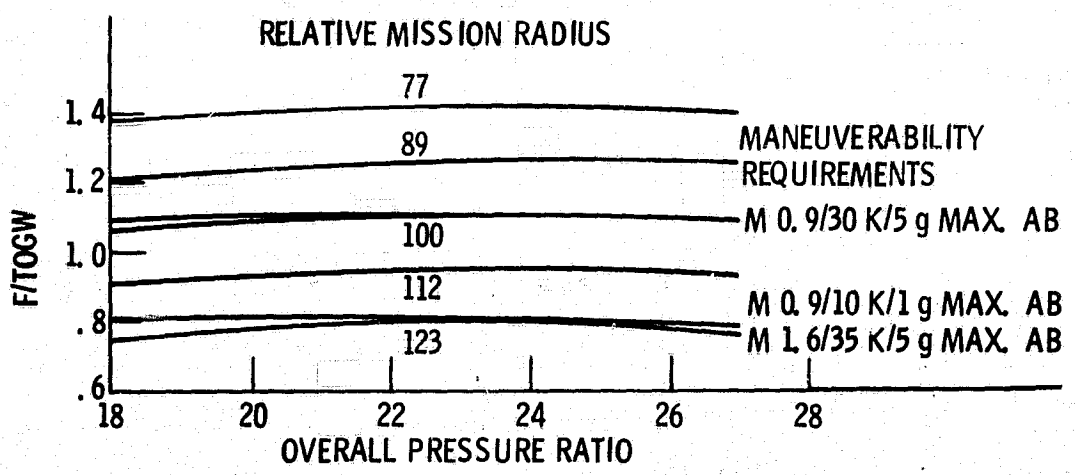

Figure 38. - Selection of overall pressure ratio; BPR = 0. 8.

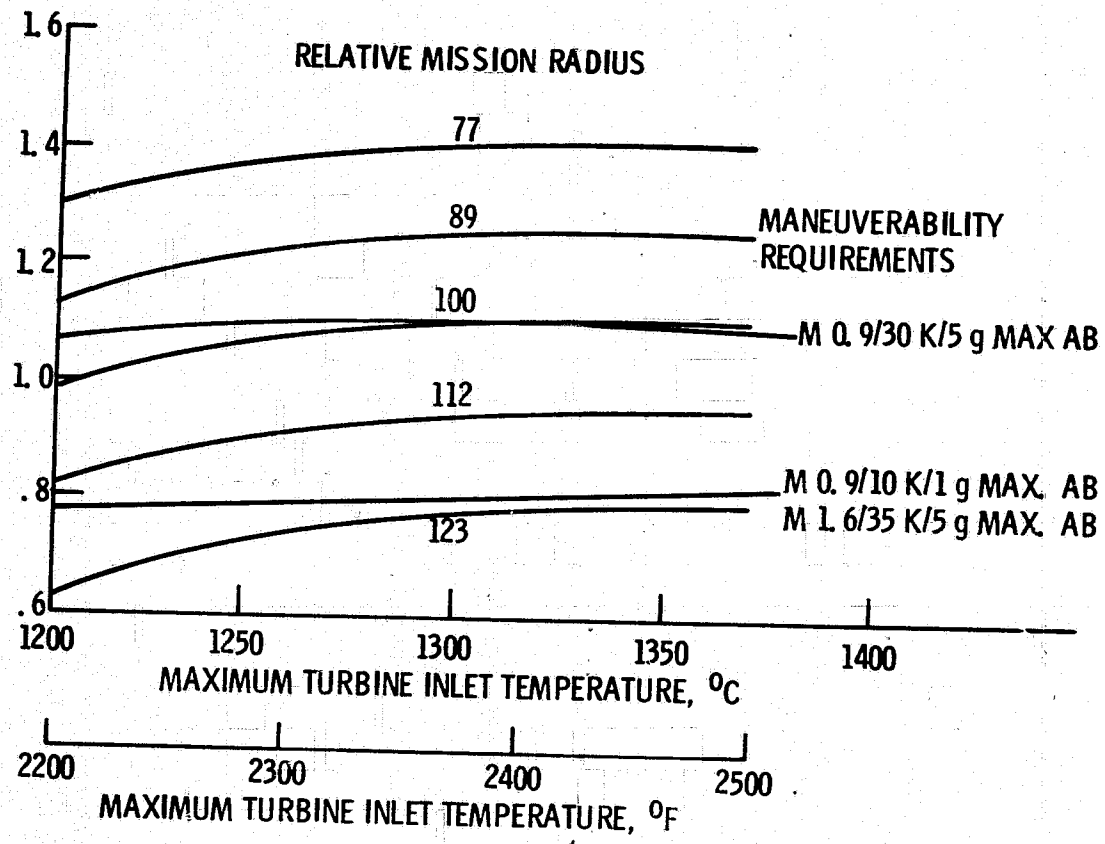

Figure 39. - Selection of turbine inlet temperature. BPR = 0.8; OPR = 23.

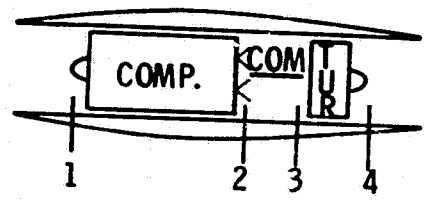

Figure B1. - Turbojet engine.

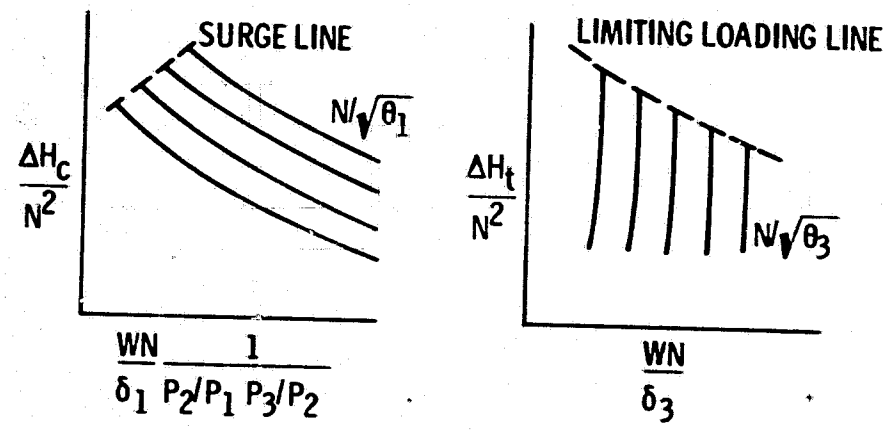

Figure B2. - Compressor and turbine matching maps.

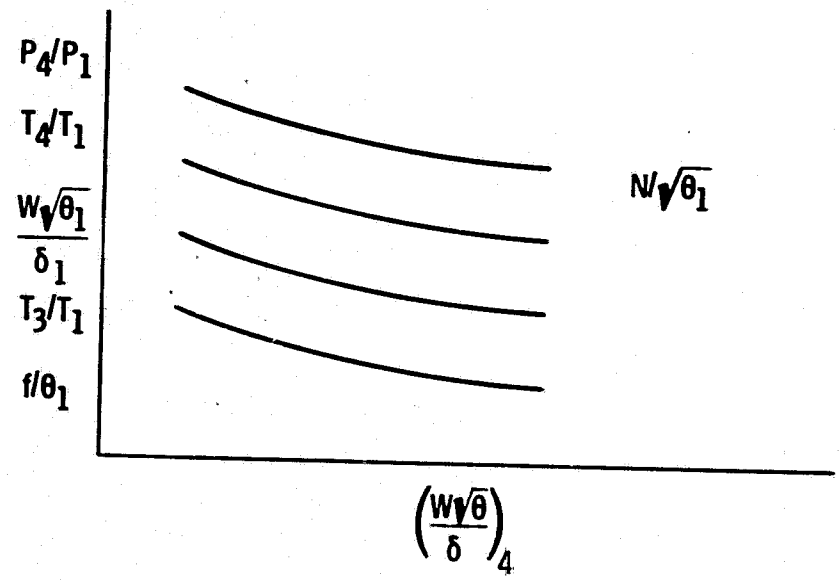

Figure B3. - Pumping characteristics.

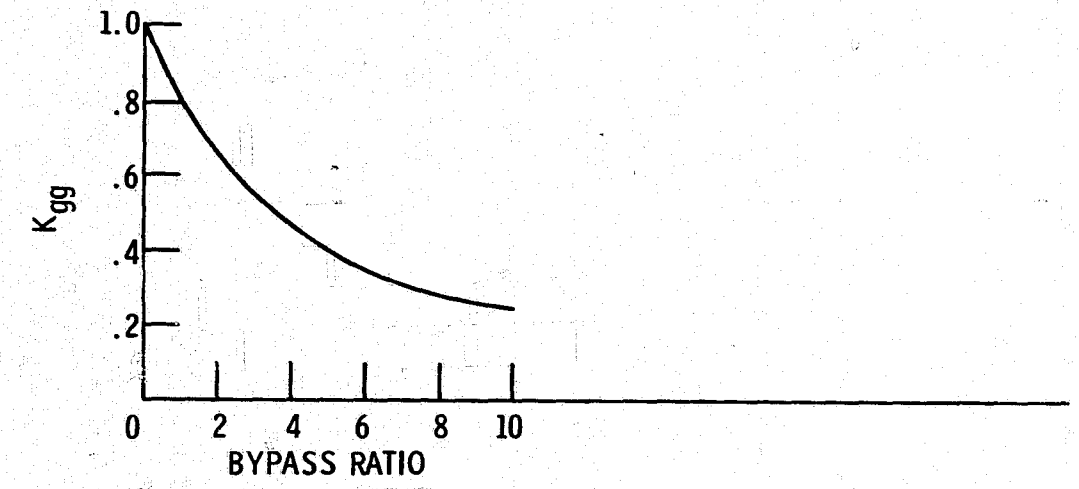

Figure C1. - Ratio of gas generator weight to total weight, K_{gg}

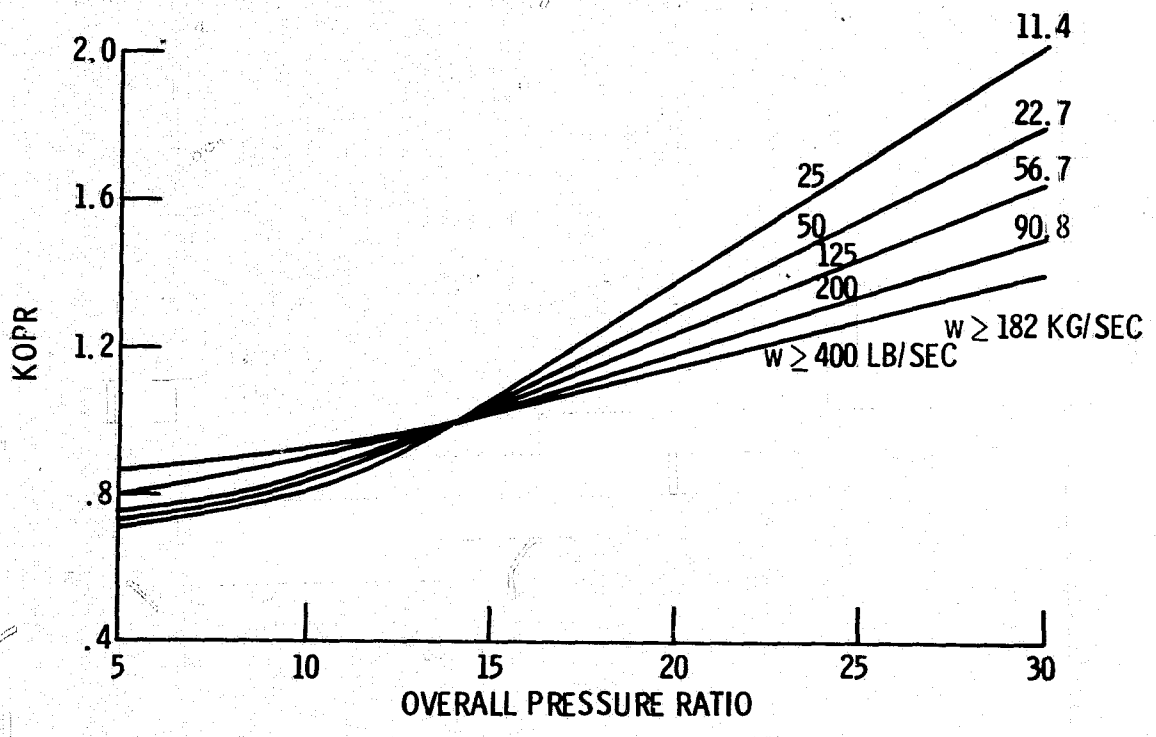

Figure C2. - Correction for overall pressure ratio, KOPR.

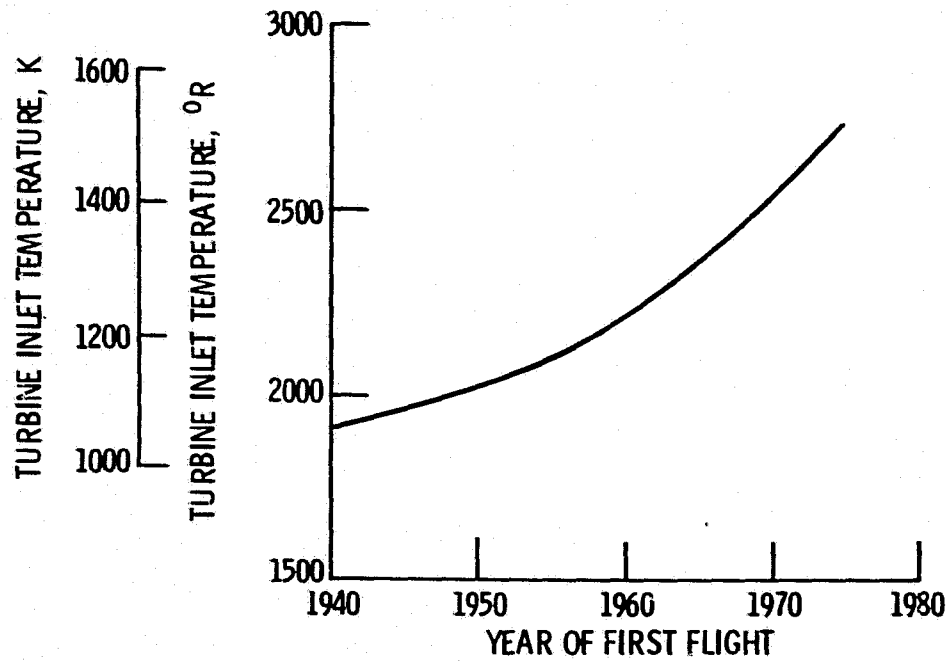

Figure C3. - Trend in turbine inlet temperature.

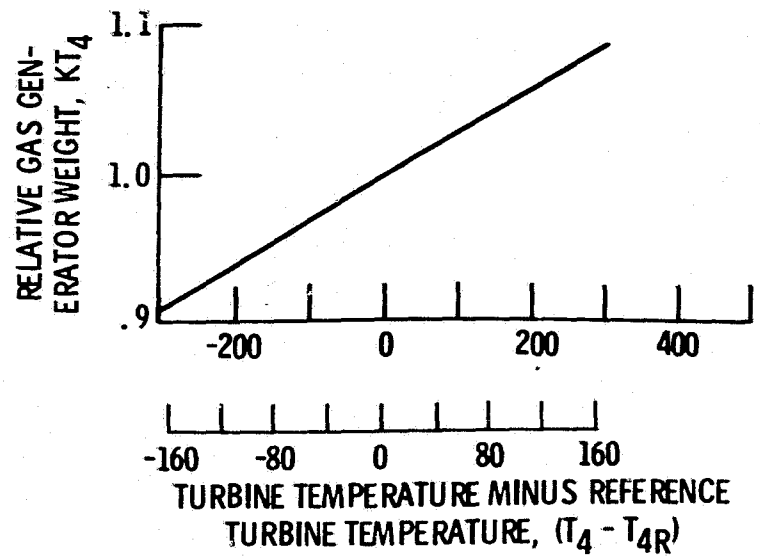

Figure C4. - Correction for turbine inlet temperature, KT_4.

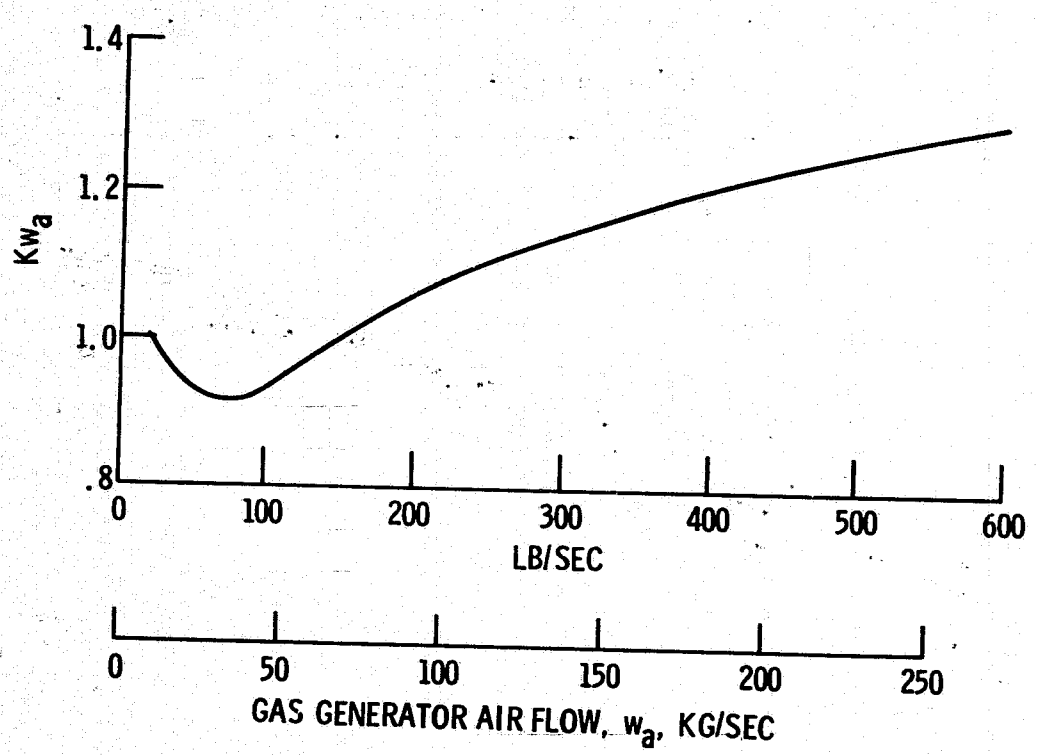

Figure C5. - Correction for gas generator airflow, Kw_a

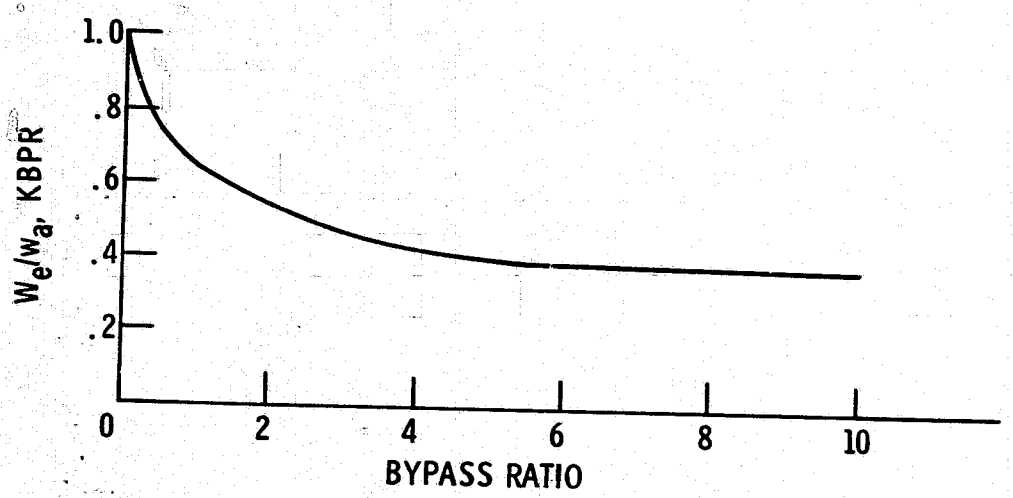

Figure C6. - Correction for bypass ratio, KBPR

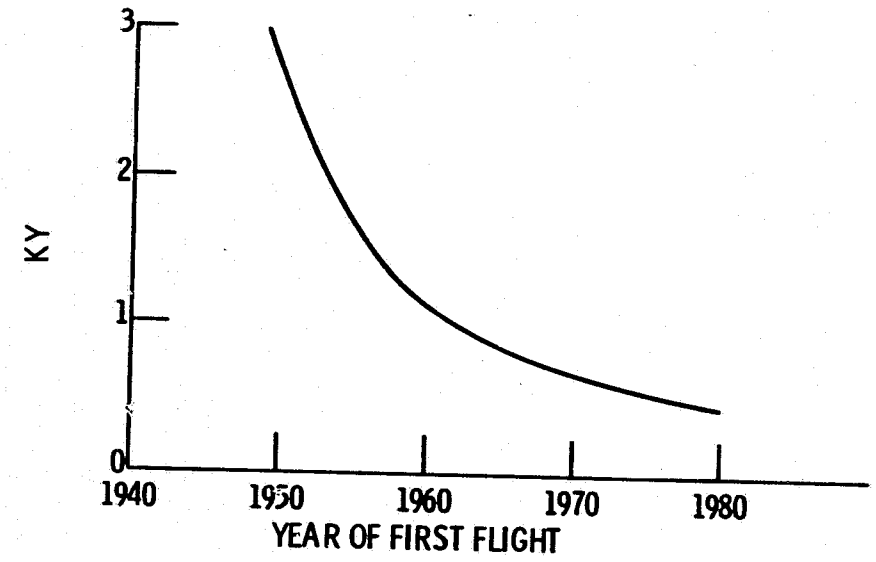

Figure C7. - Correction for year, KY

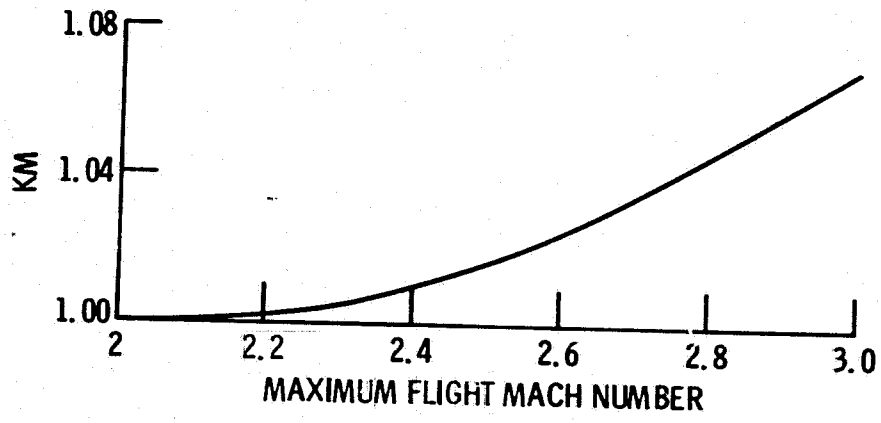

Figure C8. - Correction for Mach number, KM

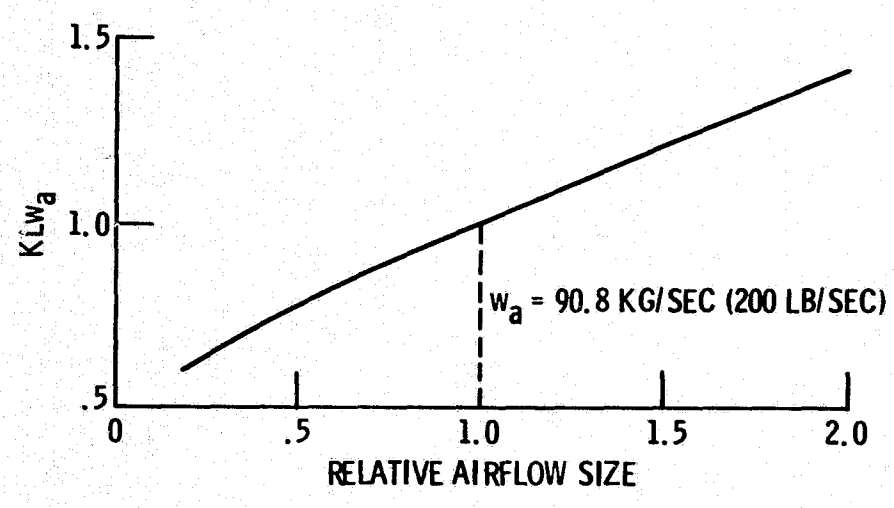

Figure C9. - Primary airflow size scaling factors for engine length.

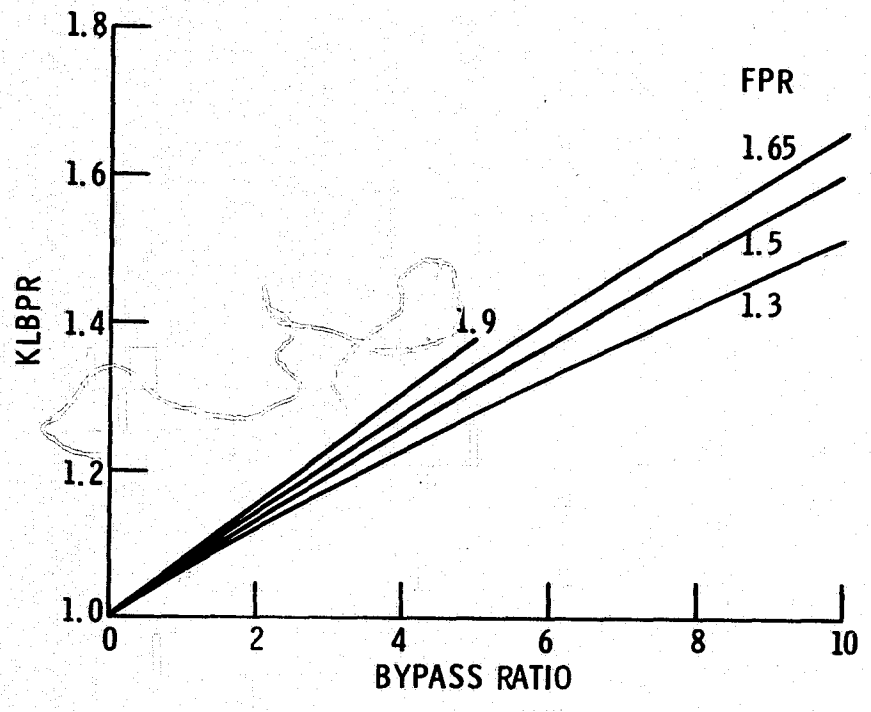

Figure C10. - Bypass ratio-fan pressure ratio correction factor.

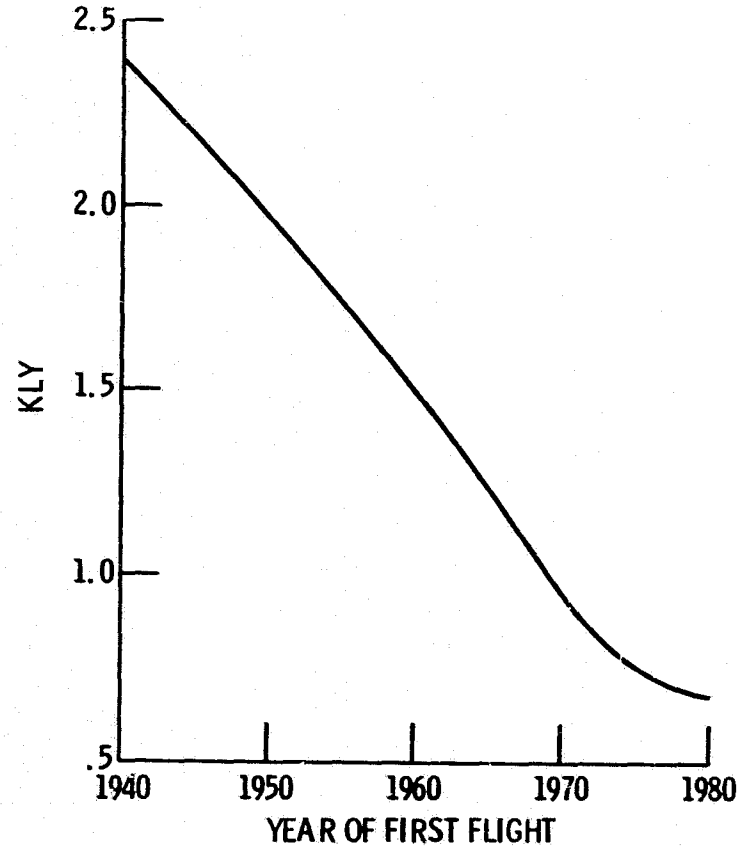

Figure C11. - Results of length correlation.

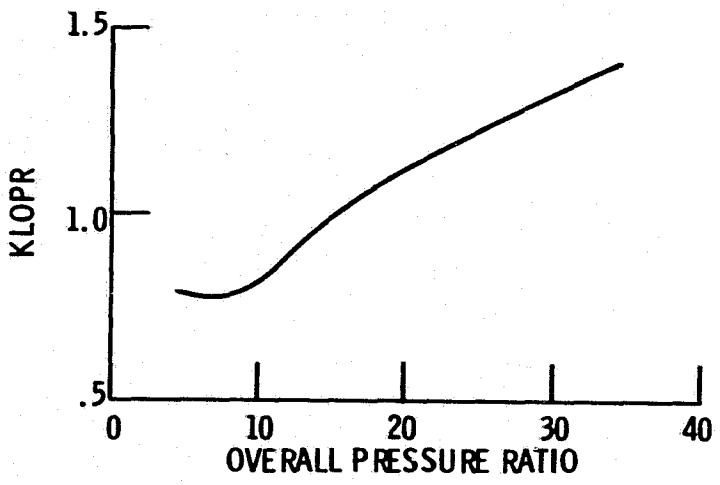

Figure C12. - Correction for overall pressure ratio.

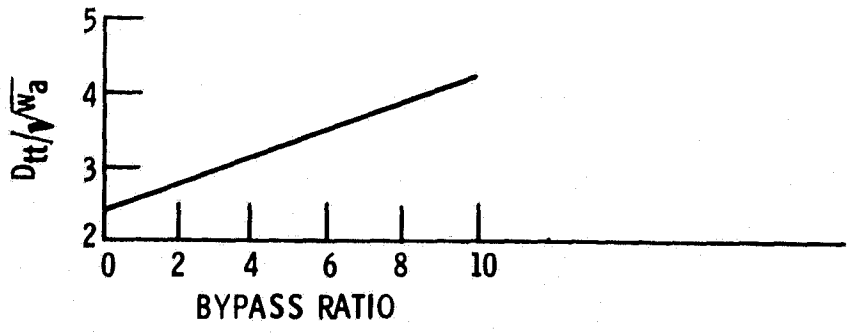

Figure C13. - Turbine tip diameter variation with bypass ratio.

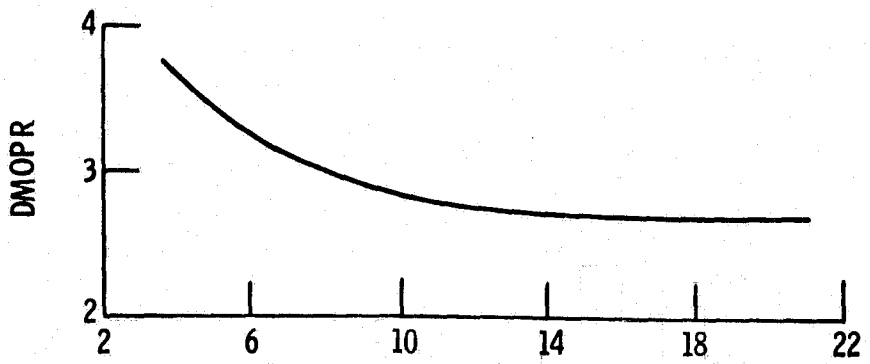

Figure C14. - Trend of normalized turbojet maximum diameter with pressure ratio.

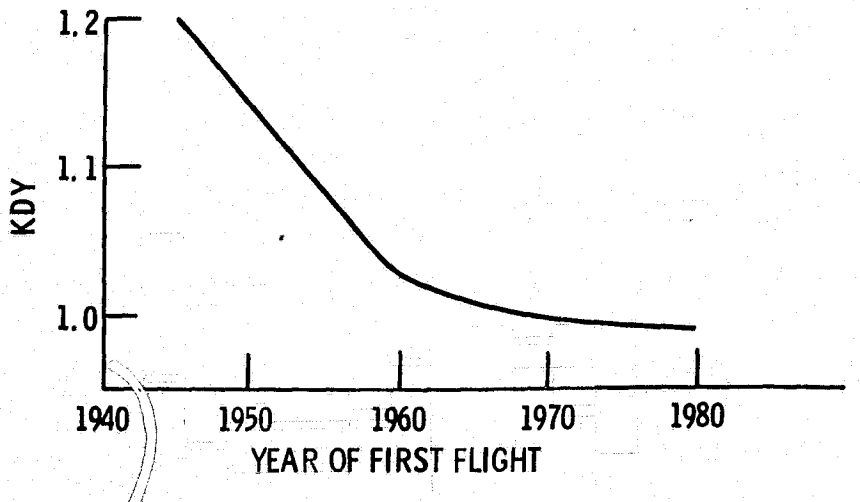

Figure C15. - Technology level (year) correction factor on turbojet maximum diameter.